Measuring Perceived Gloss of Rough Surfaces

Lin Qi

Submitted for the degree of Doctor of Philosophy

Heriot-Watt University

School of Mathematical and Computer Sciences

July 2012

Abstract

This thesis is concerned with the visual perception of glossy rough surfaces, specifically those characterised by $1/f^{\beta}$ noise.

Computer graphics were used to model these natural looking surfaces, which were generated and animated to provide realistic stimuli for observers. Different methods were employed to investigate the effects of varying surface roughness and reflection model parameters on perceived gloss.

We first investigated how the perceived gloss of a matte Lambertian surface varies with RMS roughness. Then we estimated the perceived gloss of moderate RMS height surfaces rendered using a gloss reflection model. We found that adjusting parameters of the gloss reflection model on the moderate RMS height surfaces produces similar levels of gloss to the high RMS height Lambertian surfaces.

More realistic stimuli were modelled using improvements in the reflection model, rendering technique, illumination and viewing conditions. In contrast with previous research, a non-monotonic relationship was found between perceived gloss and mesoscale roughness when microscale parameters were held constant. Finally, the joint effect of variations in mesoscale roughness (surface geometry) and microscale roughness (reflection model) on perceived gloss was investigated and tested against conjoint measurement models. It was concluded that perceived gloss of rough surfaces is significantly affected by surface roughness in both mesoscale and microscale and can be described by a full conjoint measurement model.

TO MY FAMILY

Acknowledgements

First and foremost I offer my sincerest gratitude to my supervisor, Professor Mike J. Chantler, who has supported me throughout my thesis with his patience and knowledge whilst allowing me the room to work in my own way. I also offer it to my SICSA supervisor Dr. J. Paul Siebert, thanks for the discussion and advice. Thanks to Professor Junyu Dong, for his guidance on my first academic steps.

I would like to thank Professor Patrick R. Green for his comments and suggestions on my experiments. Thanks to my colleagues in the Texture Lab for their discussions and help: Dr. Jiri Filip, Dr. Andy Spence, Dr. Stefano Padilla, Dr. Alasdair Clarke, Dr. Pratik Shah, Dr. Khemraj Emrith, Dr. Fraser Halley, Thomas Methven, Pawel Orzechowski, Xinghui Dong and David Robb. Thanks to all the participants in my experiments.

Last but not the least, I wish to thank my parents and all my families, for supporting me spiritually throughout my life. My wife, Lina, whose love and encouragement allowed me to finish this journey. I will give her a heartfelt "thanks".

Table of Contents

List of Figures

List of Tables

Glossary

$1/f^{\beta}$ **noise surface** Simulated surface with a random phase spectrum and a magnitude spectrum proportional to $1/f^{\beta}$.

assumption of sphericity Equality of variances of the differences between parameter (condition) levels.

Durbin-Waston statistic Statistic to detect the presence of autocorrelation.

Greenhouse-Geisser An estimation method to correct degrees of freedom when the sphericity assumption is violated.

half-angle Angle direction that bisects (divides into halves) the angle between the incoming light and the viewer.

height map Greyscale image that defines the height of the individual pixels of a surface.

isotropic Surface that has no directional preference in its optical behaviour.

Kolmogorov-Smirnov test Test for the normality of a distribution.

linear regression Mathematical fitting to data using a linear function.

magnitude estimation Psychophysical method that requires subjects to assign numbers in proportion to the magnitude of the stimulus they perceive.

Mauchly's test A test to assess the sphericity.

mesoscale roughness The roughness induced by surface height map in pixel level.

method of adjustment Psychophysical method that requires subjects to alter the level of stimulus.

microscale roughness The roughness induced by the distribution of microfacets in a microfacet model in sub-pixel level.

multi-bounce rendering The rendering method that incorporates inter-reflections.

polynomial contrast Type of contrast analysis.

stimulus Visual sample used in psychophysical experiments.

surface The three dimensional (length, breadth and height) outside part or uppermost layer.

trend analysis Technique for extracting an underlying pattern of behaviour.

Acronyms

2AFC Two-Alternative Forced Choice.

ANOVA ANalysis Of VAriance.

BRDF Bidirectional Reflectance Distribution Function.

BSSRDF Bidirectional Scattering-Surface Reflectance Distribution Function.

CIE International Commission on Illumination.

cm centimetre.

cpd cycles per degree.

cpi cycles per image width.

DOI gloss Distinctness of Image gloss.

dpi dots per inch.

FFT Fast Fourier Transform.

HDR High Dynamic Range.

MDS Multidimensional Scaling.

mm millimetre.

nm nanometre.

PBRT Physically Based Rendering Toolkit.

RMS Root Mean Square.

Symbols

α Roughness parameter in BRDF models.

β Magnitude roll-off factor of $1/f^{\beta}$ noise surface.

E_{ls} Binary image of environment map after luminance threshold.

ε Observer's precision in judgement.

ϵ Residual term in linear regression.

ε_{g} Greenhouse-Geisser estimate of sphericity.

f_{r} BRDF.

G Perceived gloss.

G^{A} Additive conjoint measurement model for perceived gloss.

G^{F} Full conjoint measurement model for perceived gloss.

G^{I} Independent conjoint measurement model for perceived gloss.

$\boldsymbol{H}$ Unit halfway vector pointing to the half-angle.

χ^2 chi-square statistic.

k_{d} Diffuse component parameter in BRDF models.

k_{s} Specular component parameter in BRDF models.

$\boldsymbol{L}$ Unit vector of incoming light direction $\boldsymbol{\omega_{\mathrm{i}}}$.

$\boldsymbol{N}$ Unit vector of surface normal.

$\boldsymbol{n}$ Unit local normal vector on textured surface.

$\boldsymbol{\omega_{\mathrm{i}}}$ Incoming light direction in BRDF.

$\boldsymbol{\omega_{\mathrm{o}}}$ Outgoing light direction in BRDF.

p Surface gradient in horizontal direction.

$P_{\mathrm{e}}(\theta_{\mathrm{i}})$ Percentage of strong light source pixels in environment for incident zenith angle θ_{i}.

ϕ_{i} Azimuth angle of illumination direction.

ϕ_{o} Azimuth angle of viewing direction.

P_{hp} Estimated percentage of highlight pixels.

P^{*}_{hp} Predicted percentage of highlight pixels.

π Ratio of circumference of circle to its diameter.

P_{s} Distribution of surface absolute slope angle.

q Surface gradient in vertical direction.

R' Physical gloss reflectometer value.

$\boldsymbol{R}$ Unit vector of specular light reflect direction.

ρ Pearson correlation coefficient.

σ Root mean square of surface height.

σ_{g} Standard deviation of Gaussian distribution.

S_{ij} Surface with microscale roughness level i and mesoscale roughness level j.

S_{σ_i} Surface with RMS height σ_i.

Θ Random phase.

θ_{i} Zenith angle of illumination direction.

θ_{o} Zenith angle of viewing direction.

$\boldsymbol{V}$ Unit vector of viewing direction or outgoing light direction $\boldsymbol{\omega_{\mathrm{o}}}$.

Chapter 1

INTRODUCTION

This thesis reports the investigation of the perceptions of observers on glossy, rough, textured surfaces. The motivation and goals behind the research will be explained in Section 1.1, the scope of work will be described in Section 1.2, followed by the main contributions in Section 1.3 and finally the organization of this thesis is described in Section 1.4.

1.1 Motivation and Goals

Humans see thousands of objects daily, which are comprised of many kinds of surfaces and materials. While the perception of objects has been extensively studied in biological vision in terms of object shape and contour, the perception of material has been studied much less [Adelson, 2001] [CIE Publication 175, 2006] [Maloney and Brainard, 2010]. However, the perception of material is very important in people's daily life. For example, when people see a spherical object without any context information (e.g. environment and reference objects), it can be assumed to be a football or an orange, or other objects. The ambiguity is resolved by surface properties such as colour, texture, surface geometry, which help people recognise the material and judge what the object is (see surface varieties in Figure 1.1).

Surfaces exhibit a wide range of appearance characteristics. Some properties are related to surface mechanical characteristics, such as roughness, coarseness, directionality, regularity, randomness, waviness, and granularity; while others are related to surface optical characteristics, such as colour, texture, glossiness, translucency.

Surface properties can be measured both physically and perceptually. The former involves methods using physical instruments, and it is usually assumed to be equivalent to a perceptual counterpart. However, the association between these two forms of measurement has not been extensively studied. Therefore, the motivation of this thesis is to investigate how the human visual system characterises one of the surface properties.

The goal of the work reported in the thesis was to measure the effect of variations in surface mesoscale and microscale parameters on perceived gloss. We begin by explaining why we chose to study perceived gloss, and then describe the models and the model parameters that comprise the space to be investigated. Then it will be possible to address the author's main goal: discovering the effect of these factors on the chosen characteristic: perceived gloss.

Figure 1.1: Different objects in the scene show surface varieties. Many characteristics can be interpreted from these surfaces, in terms of e.g. colour, gloss, and texture. The image is from the Bonn OBJECTS2011 Datasets [Schwartz et al., 2011].

Once a knowledge of the relationship between the surface parameters and perceived gloss has been developed then it will be possible to exploit this knowledge in many areas where material characteristics are important [Adelson, 2001], such as those listed by Padilla [2008] for example:

- "quality control,

- 'human like' sample retrieval,
- perceptual scaling or morphing,
- visualizations,
- product evaluation, and
- and product development."

In addition, such knowledge can be applied in the computer graphics field, for example in perceptual-based material modelling, and computer aided design and manufacturing.

1.2 Scope of Work

It would be impossible to research every single surface characteristic within a single PhD. Therefore, this thesis will be limited to investigating the visual perception of surface glossiness; the argument for choosing this surface characteristic is presented in Chapter 2. Furthermore, we will use computer generated stimuli to provide parametric control of the stimuli and only use surfaces that are isotropic, in particular $1/f^{\beta}$ noise surfaces.

It has been found that perceived gloss is affected by a combination of intrinsic and extrinsic factors. This thesis focuses on the effect of surface geometry and reflection on perceived gloss, and in particular, the effects of surface roughness in both the meso- and the microscale. The argument for choosing these properties and corresponding physical models is provided in Chapter 2 and the models are detailed in Chapter 3. Other factors (reviewed in Chapter 2) are inevitably involved in the experimental stimuli modelling, and they will be discussed and examined in order to develop more realistic stimuli. These will be discussed in each of the chapters as they appear.

1.3 Original Contributions

The author believes that this thesis describes three main contributions to the field of surface visual perception. They are:

1. that the use of multi-bounce rendering and realistic lighting environments have a significant impact on the perception of gloss of rough surfaces,
2. that perceived gloss is a non-monotonic function of mesoscale roughness, and
3. that the joint effect of mesoscale roughness and microscale roughness on perceived gloss can only be described by a full conjoint model.

1.4 Thesis Organization

This thesis is divided into nine chapters. The next two chapters describe related work and detail the models used. Chapter 3 also provides a description of the investigation strategy employed in the rest of the thesis which is divided into two main phases according to the sophistication of the rendering environment and associated stimuli. In more detail:

Chapter 2 reviews related literature and describes why we chose glossiness as the research topic. We discuss how physical gloss is measured and review related work on perceived gloss which is structured in terms of influencing factors. Since this thesis focuses on textured surfaces, previous work concerning gloss perception on non-planar surfaces is discussed in detail and the candidate surface geometry model is selected. From this review, the factors and corresponding models to be investigated are specified.

Chapter 3 describes the surface geometry model and reflection model, whose parameters will be varied and investigated in this study. The investigation strategy is also presented.

Chapter 4 investigates the apparent gloss of 'matte' surfaces reported by Wijntjes and Pont [2010]. It also describes how the experiments were set up and explains the tools used to realise them.

Chapter 5 investigates how perceived gloss is affected by variation of gloss reflection model parameters, and we investigate whether or not such gloss reflection models can be used with moderate RMS height surfaces to provide similar levels of gloss to those perceived for the high RMS height, matte surfaces, investigated in Chapter 4.

Chapter 6 is a linking chapter. This chapter discusses the constraints of the sim-

ple rendering system used in previous chapters. A more sophisticated rendering system is developed to model more realistic stimuli that are used in the following experiments.

Chapter 7 describes the gloss measurement of $1/f^{\beta}$ noise surfaces as a function of mesoscale roughness.

Chapter 8 investigates the joint effect of variations in mesoscale roughness (surface geometry) and microscale roughness (reflection) on perceived gloss.

Chapter 9 concludes the thesis as a whole.

Chapter 2

LITERATURE SURVEY

The goal of the work described in this thesis was to measure the effect of variations in surface mesoscale and microscale parameters on perceived gloss. The previous chapter introduced the thesis goal and described the overall approach.

The aim of the work reported in this chapter was to investigate and survey relevant literature to propose candidate surface and reflection models and highlight useful methodologies.

We review previous work in four areas. Section 2.1 briefly introduces research on material perception and explains why we chose to study the gloss characteristic. We discuss the physical measurement of gloss in Section 2.2 to demonstrate the importance of studying the perception of gloss. Section 2.3 reviews the factors that influence gloss perception. Manipulations of surface geometry reported in the literature concerning gloss perception are discussed in detail in Section 2.4, including those that report the effects of changing surface roughness, and the criteria for selecting an appropriate surface geometry model are examined. This chapter is summarized and concluded in Section 2.5.

2.1 Material Perception and Surface Gloss

The aim of this section is to review research on material perception of object surfaces and select a perceptual characteristic to investigate.

2.1.1 Review of Material Perception

Material perception is a multi-sensory experience. Sight, hearing, touch, smell and taste can all contribute to learning a new material or recognising familiar materials. The two main senses involved provide visual and tactile cues. It has been found that visual cues have cross-validation with tactile cues [Picard, 2006]. This thesis concentrates on the visual perceptions of textured surfaces.

Humans can easily recognise surface materials from visual information and can infer surface properties from the complex interactions that occur between light and the material surface, based on their experience and memory of seeing thousands of materials daily [Adelson, 2001]. The exact mechanism of material perception in the vision system is still unknown.

In the field of material perception, Hutchings [1999], Pointer [2003] and CIE Publication 175 [2006] have proposed four classes of material attributes used by the vision system to characterise surface optical properties: colour, gloss, translucency and texture. Gloss is reported to be the second most relevant attribute after colour [Hanson, 2006] [Obein et al., 2004a]. Colour measurement has been extensively researched and colour appearance models have been proposed [CIE Publication 175, 2006]. Perceived translucency has been primarily studied by Fleming et al. [2004a]. Colour, gloss and translucency are all related with texture, they cause spatial variation in appearance in terms of non-uniformity of colourant and this category of texture is named optical texture [Pointer, 2003]. Another category of texture is induced by surface relief and is named as physical texture [Pointer, 2003], or surface texture which is more commonly used [Chantler, 1994]. A surface with variation in height relief is often called a textured surface. This thesis is concerned with the perception of gloss on textured surfaces under this taxonomy, and thus the following review is focused on the perception of such surfaces.

There are many features that have been used to describe surfaces, and researchers have investigated the perceptual dimensions of textured surfaces, e.g. Maloney and Brainard [2010]. The earliest study of mapping physical features to human perception was performed by Tamura et al. [1978]. They proposed six features: coarseness, contrast, directionality, line/blob likeness, regularity and roughness. A potential problem is that these features may not have the same meaning for the

subjects of their experiment. This work is the earliest research into perceptual dimensions of surface texture.

Rao and Lohse [1993] used a free sorting method in their experiment, where the subjects could choose any properties they wanted in the grouping task. A Multi-dimensional Scaling (MDS) method was applied to the resulting similarity matrix to derive a perceptual space. They found three orthogonal dimensions of the visual properties: (i) repetitive vs. non-repetitive; (ii) high-contrast and non-directional vs. low-contrast and directional; and (iii) granular, coarse and low complexity vs. non-granular, fine and high-complexity. Long and Leow [2001] found a four-dimensional space but did not name the dimensions.

As has been reviewed by Padilla [2008], roughness, directionality and coarseness are the first three properties in the perception of textured surfaces. Padilla [2008] studied how people perceive roughness of $1/f^{\beta}$ noise surfaces and proposed a model in the frequency domain which fits human behaviour well [Padilla et al., 2008]. Shah [2010] investigated the perceived directionality of $1/f^{\beta}$ noise surfaces in a similar framework. These studies share a common characteristic which is that the parameters investigated control the surface mesoscale geometric pattern, whereas the surface optical microscale property was assumed to be Lambertian. They made this simplification under the assumption that the surface optical property does not affect these characteristics significantly. However, the Lambertian reflection model is just one approximation of one type of the real-world material. Most real-world surfaces exhibit complex reflecting and scattering characteristics [Adelson, 2001] [CIE Publication 175, 2006]. This problem also exists in those studies in which photographs of surfaces have been used to investigate surface and material perception [Tamura et al., 1978] [Long and Leow, 2001].

2.1.2 Surface Appearance from Reflection

As suggested by Adelson [2001], the image of a surface is determined by three properties: shape, intrinsic optics and extrinsic optics. The characteristic of shape (surface geometry) is mainly determined by the mechanical properties of a surface and some related perceptual characteristics have been studied [Tamura et al., 1978] [Rao and Lohse, 1993] [Padilla, 2008] [Shah, 2010]. The extrinsic optics are from the illumi-

nation and scene context. The intrinsic optics characterise how the surface interacts with incident light. As visual perception is derived from optical information, we should study surface optical properties when studying perceived surface properties.

In this thesis, only non-luminous materials are considered. The self-luminous and stimulated emission materials are out of the scope of this thesis. However, given this restriction, the interaction between surface and light is still complicated. When light irradiates the surface, the light can do four things: it can be absorbed by the material; it can pass through the material; it can be reflected off the material; and it can be scattered. It can also do combinations of these. Absorbtion, reflection and refraction are the relevant optical properties of the material. Absorbtion and refraction can bring the properties of translucency. These properties involve very complex aspects of light propagation and human perception [Fleming et al., 2004a] [Fulvio et al., 2006], and are not studied in this thesis. This thesis is only concerned with reflection on opaque surfaces.

Figure 2.1 illustrates three basic reflection types widely used in the computer graphics field. Diffuse reflection is common and most surfaces reflect this category of light. Specular reflection is observed on mirrors and very smooth surfaces. The perfect specular reflection is visible only when the surface normal bisects the light vector and the viewing vector. It is called the half-angle direction because it divides into halves the angle between the light direction and the viewing direction. Thus, a perfectly specular reflecting surface would show a specular highlight as a sharply reflected image of a light source. However, there are no perfect diffuse or perfect mirror reflectors, but a combination of the two. Glossy reflection implies that some light is reflected in a mirror-like manner from the light source to the viewing direction. These reflection types are just three types of simulation of real-world light reflection used in the computer graphics field. In the real world, reflected light is usually a mixture of reflections, and can include other reflections such as the Fresnel phenomenon. More discussion concerning reflection modelling will be conducted in later sections and chapters.

There are several terms used for describing reflection appearance, such as matte, shininess, glossiness, mirror, lustre, gleam, glow, and metallic [Adelson, 2001]. The latter four are not commonly used for simulating surfaces and only exist for some specific materials such as crystal, metals and heated objects [Adelson, 2001]. Some

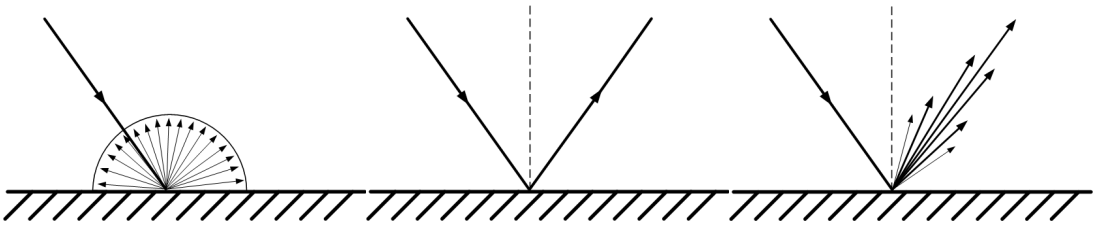

(a) diffuse (b) specular/mirror (c) glossy

Figure 2.1: The three basic reflection types used in the computer graphics field. (a) diffuse reflection, where the incident light is scattered in every direction of the hemisphere. (b) specular/mirror reflection, where the incident ray is reflected as a single ray. The angle between the reflected ray and the surface normal is the same as the angle between incident ray and surface normal. (c) "glossy" reflection, which preserves the directionality of light rays, but has some scattering or softening.

of these phenomena involve refraction and luminance (lustre and glow). The other characteristics can be encompassed by the term glossiness. The changing of reflectance appearance from matte to mirror can be characterised by glossiness, where matte relates to low glossiness and mirror to high glossiness [Pellacini et al., 2000]. Other researchers argue that gloss is a mirror-like front surface reflection but that such reflection is not regarded as being "glossy" [Hanson, 2006].

2.1.3 Summary

From the above review, we will choose surface glossiness as the characteristic to be investigated concerning human perception of textured surfaces. Many methods have been developed to model and simulate the complicated interaction between light and a surface. On the other hand surface appearance has been studied and measured both physically and psychophysically.

Hunter and Harold [1987] named six types of gloss from natural surface appearance (see Table 2.1). The last type "surface uniformity gloss" is not a function of reflectance, but concerns surface albedo textures. This thesis will not consider this type of gloss. The other five types of gloss are mainly determined by the surface reflection properties, while the "Distinctness-of-image" gloss has strong relationship with the illumination environment. The following sections will discuss literature on both the physical and perceptual measurement of gloss.

Table 2.1: Six gloss types named by Hunter and Harold [1987].

Types of Gloss	Visual Evaluation	Types of Surfaces
Specular gloss	Shininess, brilliance of highlights	Medium gloss surfaces of book paper, paint, plastics, etc.
Sheen	Shininess at grazing angles	Low gloss surfaces of paint, paper, etc.
Contrast gloss or lustre	Contrast between specularly reflecting areas and other areas	Low gloss surfaces of textile fiber, yarn and cloth, newsprint, bond paper, diffuse-finish metals, hair, fur, etc.
Absence-of-bloom gloss	absence of haze, or milky appearance, adjacent to reflected highlights	High and semigloss surfaces in which reflected highlights may be seen
Distinctness of Image gloss (DOI gloss)	Distinctness and sharpness of mirror images	High gloss surfaces of all types in which mirror images may be seen
Surface-uniformity gloss	Surface uniformity, freedom from visible nonuniformities such as texture	Medium to high gloss surfaces of all types

2.2 Physical Measurement of Gloss

Although the perceived gloss is the focus of this thesis, this section will briefly review the physical measurement of gloss. We do this not only to demonstrate the difference between physical gloss and perceived gloss but also to show the necessity of investigating the perceived gloss of textured surfaces.

The physical measurement of gloss originates from measuring and standardising the reflectance property of products, such as paper, paints, plastics, etc. A complete evaluation of gloss is dependent on several factors, such as the refractive index of the material, the angle of incident light and the surface topography (surface texture). Gloss can also be affected by environmental factors, like weathering and surface abrasion. Thus gloss can be useful as a criterion to evaluate the quality of a product in development, process development, and end-use performance testing [Keyf and Etikan, 2004].

Physical gloss is an optical phenomenon of the surface, which is based on the interaction of light with the physical characteristics of a surface. As Leloup et al. [2011] quoted, "Gloss results from the directionally selective reflectance properties of a surface, with a preference toward the specular reflection direction" [CIE Publication 017.4, 1987].

Since the 1930's, instruments have been used to measure reflection behaviour [Pfund, 1930]. Many methods, standards and devices have been developed for measuring characteristics of physical gloss [Smith, 1999] [Kigle-Boeckler, 1995]. The most commonly used device is the gloss metre, which is an electronic optical device that measures the ability of the surface to reflect light. It has a built-in illuminator and receptor to measure the strength of reflected light at particular incident angles. International standards specify incident angles for different gloss level materials and different types of gloss. Examples are listed in Table 2.2.

More details about physical gloss measurement can be found in international standards [ASTM D2457, 2008] [ASTM C346, 2009] [ASTM D3134, 2008] [ASTM D523, 2008] [ASTM D5767, 2004] [ASTM E284, 2009] [ASTM E430, 2011] [ISO 2813:1994, 1994] [DIN 67530, 1982] [TAPPI T 480 om-09, 2009].

The measurement from a gloss metre is the reflectometer value R', which is a relative

Table 2.2: Commonly used angles in industry standards for physical measurement of gloss.

Incident angle	Reflected angle	Description
20°	20°	High gloss surface [ASTM D523, 2008]
60°	60°	Medium gloss surface [ASTM D523, 2008]
85°	85°	Shininess at grazing angle [ASTM D523, 2008]
45°	45°	Ceramic industry [ASTM C346, 2009]
75°	75°	Paper industry [TAPPI T 480 om-09, 2009]
30°	30.3°	Distinctness of image (DOI) [ASTM E430, 2011]
30°	32°	Bloom [ASTM E430, 2011]
30°	35°	Haze [ASTM E430, 2011]

value. The results are related to a highly polished black glass with a refractive index of 1.567 for the wavelength 589.26 nanometre (nm) for all angles [ASTM D523, 2008] [ISO 2813:1994, 1994]. The glass has an assigned specular gloss value of 100 for each configuration of incident and reflected angle. To achieve highly accurate and repeatable results, the test specimen should be:

- flat
- free of structure
- similar in colour and lightness

Goniophotometry is the most precise and informative technique for measuring the gloss of surfaces: it measures the intensity of the reflected light over different viewing angles [Pointer, 2003]. Surface gloss was evaluated by both specular reflection and diffuse reflection [Harrison and Poulter, 1951] [Tighe, 1978].

From the above review of the physical measurement of gloss, it can be seen that physical gloss is based on the ability of surfaces to reflect light under specified conditions. The biggest shortcoming is that the surface should be flat and without mesoscale structure. Curved or textured surfaces cannot be measured with conventional gloss meters. However, real-world surfaces exhibit many kinds of shapes and relief. These surfaces cannot be measured by conventional gloss metres, but humans can easily infer their glossiness. The subject of how perceived gloss is re-

lated to particular measurements of physical gloss has been primarily studied by Billmeyer and O'Donnell [1987], Obein et al. [2004a], Ji et al. [2006], and Leloup et al. [2011]. They have noted that there are potential problems in assuming that physical measurements correlate directly with perceptual scales.

2.3 Perceived Gloss

In 1987, the International Commission on Illumination (CIE) updated the definition of gloss: gloss is "the mode of appearance by which reflected highlights of objects are perceived as superimposed on the surface due to the directionally selective properties of that surface" [CIE Publication 017.4, 1987]. As argued by Obein et al. [2004a]: "gloss is no longer considered as a purely physical property of the material and is clearly defined as a visual percept, a visual quantity associated with surfaces consequent to their geometrical properties".

In contrast with the physical measurement of gloss, biological vision researchers found perceived gloss is affected by many factors [Adelson, 2001] [Hanson, 2006]. This section will review this work and in particular will investigate the influencing factors. These factors will be summarised in the end of this section, and the ones to be investigated further in this thesis will be identified.

2.3.1 Early Work and Work Using Real Materials

Early work focused on an important cue for gloss perception – specular highlights [Beck and Prazdny, 1981] [Blake and Bülthoff, 1990] [Berzhanskaya et al., 2002] [Berzhanskaya et al., 2005]. They found highlights on a curved surface are essential for observers to judge surface gloss and curvature. Specular highlights contain very rich information about light sources, surface shape, and surface material. Beck and Prazdny [1981] studied how the size, brightness, orientation, placement of highlights and surface intensity gradient affect the perception of gloss. Blake and Bülthoff [1990] reported some of the earliest investigations into the human perception of specular reflection from binocular vision and stated that the vision system employs a physical model based on ray optics and differential geometry.

A number of studies have investigated perceived gloss with real materials. Ng et al. [2003] used printed samples as the stimuli and found that gloss perception follows Weber's Law within the gloss range measured with gloss metres. Obein et al. [2004a] and Ji et al. [2006] found that physical measurement of gloss is not always linearly related to its perceptual correlate but follows a sigmoidal relationship. Obein et al. [2004a] found gloss constancy under changing illumination direction, whereas Leloup et al. [2011] provided a metric for both surface and illumination properties. Ged et al. [2010] found observers can recognise real surfaces from gloss appearance. These studies used real material as stimuli together with gloss measurement devices. They exposed the limitations of such devices. They experimentally verified that physical gloss measurements do not represent perceived gloss and stated the necessity of separately measuring perceived gloss. Wills et al. [2009] performed a comprehensive study by associating real material measurements and psychophysical scales, from which they extracted nine gloss dimensions.

In the study of human visual perception, using real materials is not convenient because it is difficult to incrementally vary their properties. The investigation of gloss perception in this thesis requires a flexible experimental framework in which selected factors can be easily controlled. Simulations of material appearance make it easy to control such variables and conditions using parametric models. Therefore, digital images of synthetic surfaces are a compelling candidate for use as the visual stimuli, and have been utilized in this thesis.

2.3.2 Work Using Synthetic Stimuli

A major part of studies concerning gloss perception employ computer simulation. This allows researchers to easily change the surface appearance to study how people respond to variations in surface parameters. Moreover, the conditions and constraints can be manipulated to study how these factors influence gloss perception. The following literature review is structured by intrinsic and extrinsic factors.

When simulating material appearance in computer graphics, reflectance functions are used to model surface optical properties. The reflectance function is usually termed "material" in the computer graphics field. The reflectance function characterises how light is transmitted back into space, which involves as many as 12

parameters [Müller et al., 2004]. After simplifications of light transport, assumed wavelength and surface invariance, an eight dimensional Bidirectional Scattering-Surface Reflectance Distribution Function (BSSRDF) can be derived. This describes not only reflection but also refraction. As gloss concerns only reflection from the surface, further simplifications can be made: the surface is assumed to be made of homogeneous material without subsurface scattering, and reflectance is position invariant. This means that a Bidirectional Reflectance Distribution Function (BRDF) can be employed as the model. Uniformity of reflectance is often assumed in gloss perception studies, leading to an isotropic BRDF. Because of the parsimoniousness (few parameters) and computation efficiency, analytical BRDF models are widely used in simulating materials such as metal, plastic, paint etc [Kurt and Edwards, 2009].

Spheres have been widely used to investigate the effect of variations in reflectance functions on perceived gloss [Pellacini et al., 2000] [Ferwerda et al., 2001] [Fleming et al., 2001] [Xiao and Brainard, 2008]. The advantage is that spheres are simple to render and present all possible surface orientations to the viewer.

Pellacini et al. [2000] and Ferwerda et al. [2001] rewrote the isotropic Ward BRDF model to provide a psychophysically-based gloss model with two perceptually meaningful dimensions derived from psychophysical experiments using synthetic spheres as the stimuli.

The limitation of using spherical objects is that the influence of surface geometry is neglected. Vangorp et al. [2007] experimentally examined the perceived appearance of different 3D objects with stimuli generated using the reflection model proposed by Pellacini et al. [2000] and Ferwerda et al. [2001]. They found that the associated perceptual space does not produce constant material and gloss perception for different objects. The difference is due to the variation of surface geometry. Olkkonen and Brainard [2011] studied the joint effect of illumination and object shape on perceived gloss and found large interactions.

Surface geometry was found to significantly affect gloss perception [Nishida and Shinya, 1998] [Ho et al., 2008] [Wendt et al., 2008] [Wijntjes and Pont, 2010]. Nishida and Shinya [1998] found that gloss constancy is not guaranteed when surface geometry is varied, and contextual information is important for reflection judge-

ment. The limitations of their work are the unrealistic and unnatural appearance of the stimuli. Ho et al. [2008] studied how observers judge perceived "bumpiness" and glossiness of artificial 3D textures rendered using a complex reflection model. They modelled how these two properties affected the perception of each other. Their additive conjoint measurement model showed that increasing physical bumpiness increases perceived gloss. However, the shape of the "bumpy" meso-structure limited the manipulation of surface geometry. Wijntjes and Pont [2010] found that high RMS height Lambertian surfaces can introduce an appearance of illusory gloss. We were inspired by the work of Wijntjes and Pont [2010] and initiated experiments on textured surfaces under the same conditions. Details are provided in Chapter 4. In these studies, the surfaces either comprised limited frequencies (except [Wijntjes and Pont, 2010]) or were synthesized by simple structures on a planar surface, which are not sufficient to cover a wide range of natural and realistic surfaces. Furthermore, the illumination used in these studies was simplified to area light or collimated light.

The above work focused on surface intrinsic factors, such as surface reflection properties and surface geometry. In addition to studying the intrinsic factors, researchers have explored the extrinsic factors that influence gloss perception, such as illumination, binocular viewing, head motion and surface motion.

Illumination is an important factor for material perception. Early studies found that the direction of collimated illumination can dramatically change the appearance of Lambertian surface textures [Chantler, 1994] [Nefs et al., 2005], and observers can estimate illumination direction from the shading and shadowing information on these surfaces [Koenderink et al., 2004]. Studies on gloss perception normally use simple lighting conditions, such as collimated light [Wijntjes and Pont, 2010], point light [Nishida and Shinya, 1998] [Wendt et al., 2008], and area light [Ho et al., 2008] [Pellacini et al., 2000] [Ferwerda et al., 2001]. Other researchers have used more complex illumination, and real-world illumination environments [Dror et al., 2001a] [Dror et al., 2001b] [Dror et al., 2004]. It was found that the environments that observers are familiar with affect the accuracy and reliability of the perception of materials [Fleming et al., 2001] [Fleming et al., 2003].

The state of motion of the object can also affect gloss perception. Hartung and Kersten [2002] found a glossy 3D object looks shiny in a complex environment when it is still, but looks like a painted matte object when it is rotating without changing

its environment reflection on the object surface. They concluded that the relative motion can help visual system see materials.

Nagata et al. [2007] found that increasing stimulus duration decreases the perception of image glossiness. But their stimuli were unrealistic (they comprised lateral images of a cylindrical object).

Viewing conditions also affect gloss perception. Binocular viewing and lateral head motion can contribute to more sensitive gloss perception [Obein et al., 2004b] [Wendt et al., 2007] [Wendt et al., 2008] [Sakano and Ando, 2008a] [Sakano and Ando, 2008b] [Sakano and Ando, 2010]. Binocular viewing provides a disparity of specular highlight in addition to surface geometry disparity. The head motion produces better perception of surface shape and view-dependent specular reflections. These factors can provide richer information for gloss perception, analogous to that provided by object motion.

Further more, Doerschner et al. [2010b] found that the spatial pattern of the object, viewing background, and dynamic range of background affect gloss perception. Ferwerda and Phillips [2010], Phillips and Ferwerda [2009] found the appearance of a synthetic object was perceived as being glossier on a high dynamic range display (higher attainable luminance) compared to when viewed on a low dynamic range display.

All of the above research investigated perceived gloss from the aspect of generating a glossy appearance. But there are some studies that focused on particular cues in two-dimensional images.

Since digital images are widely used in studying gloss perception, image intensity and manipulations of images using digital image processing techniques were investigated by researchers. The early hypothesis formed by Barrow and Tenenbaum [1978] argues that people employ an inverse optical procedure using shading and highlights on a curved surface when judging surface gloss and curvature. This is in keeping with a large body of research [Blake and Bülthoff, 1990] [Beck and Prazdny, 1981] [Norman et al., 2004] [Todd et al., 2004]. But a hypothesis suggesting that people can use simple image histogram statistics in gloss perception was proposed recently. Motoyoshi et al. [2007] suggested that skewness of the luminance histogram and sub-band filter outputs are correlated with perceived gloss and inversely correlated

with surface albedo. They showed that under certain circumstances, "skewness" is highly correlated with judgements of gloss and lightness. They also found an after-effect of skewness adaption. Sharan et al. [2008] replaced direct rating of lightness or glossiness with comparison to a physical Munsell scale and tested additional image statistics. All the stimuli used in their work consisted of photographs of surfaces with medium-scale structures. Landy [2007] commented on the work of Motoyoshi et al. [2007] and concluded that "for a surface to appear glossy, not only must it include a specular reflectance, but the surroundings must result in a pattern of illumination consistent with the statistics of natural scenes", "for an image to appear glossy, it has to first look like a surface". The hypothesis concerning simple image histogram statistics was challenged by Anderson and Kim [2009]. Counterpart evidence was presented to suggest that image histogram skewness provides no diagnostic information about surface reflection. They raised a hypothesis that the visual system computes the consistency between position and orientation of highlights and the geometric shape. This hypothesis was tested by Kim et al. [2011] and Marlow et al. [2011] who examined the congruence of brightness and highlights with surface curvature.

2.3.3 Summary

As a summary of this section, the perceived gloss is found to be affected by a large number of factors including:

- surface reflectance properties,
- surface geometry,
- illumination,
- surface motion,
- observation duration,
- monocular/binocular viewing,
- head motion,
- spatial configuration of the object,
- viewing background,

- dynamic range of background,
- dynamic range of display, and
- image intensity statistics (e.g. skew).

Having investigated the literature concerning the above factors and considering the fact that very little work has been published on the effect of the surface mesoscale geometry and the reflection property on the perception of gloss, we have chosen to investigate the properties of surface reflectance and surface geometry. Factors such as binocular viewing, observation duration, head motion, dynamic range of background and display, viewing background and image based information will not be investigated. Factors such as illumination and surface motion will be examined in Chapter 6 in order to provide a more realistic environment for accurately measuring the perception of gloss on rough surfaces.

All of the literature reviewed in this section concerned with synthetic stimuli used a BRDF model to characterise surface optical properties. Three analytical BRDF models were utilized in this thesis, the details will be described in the next chapter.

The surface reflection property characterises surfaces at the pixel level and therefore we term this a "microscale" parameter. Correspondingly, surface geometry can be inferred from surface shape/depth and shading, and we consider this to be a "mesoscale" parameter. However, choosing a model of surface geometry needs further discussion as different surfaces have been used in the literature. We will extend the review concerning surface geometry to select a suitable surface model. This is described in the next section.

2.4 Manipulations of Surface Geometry

As mesoscale surface geometry is one of the important factors to be investigated in this study, manipulations of synthetic surface geometry in the literature will be reviewed in more detail with the aim of selecting a suitable model.

Motivated by Occam's razor we prefer models with low numbers of parameters as this simplifies exploration of the parametric space. In addition, this thesis is concerned with rough surfaces, and so the candidate model should be able to generate

a wide range of perceived roughness. Most importantly, candidate surfaces need to be natural in appearance, so that observers can interpret them more consistently. Therefore, the surface geometry model should meet the following criteria, it should be:

- parsimonious (contain few parameters),
- provide controllable geometry, and
- be of natural appearance.

As reviewed in Section 2.3, investigations into perceived gloss using synthetic stimuli was initially studied using spheres. Although Nishida and Shinya [1998] found that surface geometry greatly affects perceived surface appearance, the advantages of using spheres still make them the first choice when studying gloss related factors such as illumination [Fleming et al., 2003] [Fleming et al., 2001] [Doerschner et al., 2010a] and dynamic range [Doerschner et al., 2010b]. Since only the curvature of the overall surface plane can be manipulated, they are not suited to our study.

Later studies mapped three dimensional textures onto spheres [te Pas and Pont, 2005] [Ramanarayanan et al., 2007]. te Pas and Pont [2005] used real spherical objects with obvious meso-structures such as golf balls and candles. Ramanarayanan et al. [2007] used synthetic spherical objects whose surfaces were disturbed by Perlin noise [Perlin, 2002]. They found that surface geometry affects the perception of material and illumination. Real surfaces were excluded from consideration because of the shortcomings described in Section 2.3. The global curvature of a rough surface may influence gloss perception, so the chosen surface will not be from or applied to any 3D object.

Surfaces used by Nishida and Shinya [1998] were generated using a random Fourier phase spectrum and a Gaussian magnitude spectrum $H(f_x, f_y) = a \exp[-(f_x^2 + f_y^2)/s^2]$. Surface geometry was varied by varying the amplitude and variance of the Gaussian function, which control the surface height amplitude and the spatial frequency respectively. Their surface model is similar to that used by Padilla et al. [2008], but the surface appearance is 'wavy' and far from realistic.

Wendt et al. [2008] generated smooth and curved surfaces by summing 15 randomly oriented sine-wave gratings. Therefore, these surfaces have similar general shape.

Their surface model can be seen as a set of band limited Fourier components, which cannot model surface roughness except via height variance.

Ho et al. [2008] built three dimensional textured surfaces by randomly adding semi-ellipsoidal structures to a planar surface and using position jittering. The surface geometry was changed by manipulating the surface "bumpiness" in terms of stretching the z radii of the ellipsoidal meso-structures. This surface model is intuitive parsimonious and specified at the mesoscale.

Wijntjes and Pont [2010] used Brownian surfaces which have a power spectrum of $1/f^2$ and a random phase spectrum. They changed surface geometry by altering RMS height. Their surface model is more realistic in appearance than those described in the literature referenced above.

Manipulations of surface geometry fall into two categories related to surface roughness: Root Mean Square (RMS) height and height spatial frequency [Padilla, 2008]. Changing surface RMS height cannot vary the scaling behaviour of surface gradients. Surfaces with very large RMS height appear more like a three dimensional object rather than a textured surface, and the high slope areas cannot be modelled to produce realistic surfaces [Padilla, 2008]. Other manipulations change the relative surface spatial frequency characteristics [Ramanarayanan et al., 2007] [Nishida and Shinya, 1998], but these surface models are not parsimonious and the surface appearance is not natural-looking. Natural surfaces include not only curved, smooth ones but those of rough textures as well.

The $1/f^\beta$ noise surface model is attractive, as it has a low number of parameters (two) and has been found to provide realistic looking stimuli with a wide range of easily controlled roughness [Padilla et al., 2008] [Voss, 1988] [Mandelbrot, 1983]. These characteristics make the $1/f^\beta$ noise surface a good candidate for our stimuli and it was selected as the surface geometry model to be used in this study.

2.5 Summary

The goal of this thesis is to investigate the effect of surface mesoscale and microscale model parameters on perceived gloss. This chapter first desribes why we chose gloss as the characteristic to investigate by reviewing literature concerning material

perception. Surface colour has been extensively studied for material perception [CIE Publication 175, 2006], and glossiness is found to be the second most important property for material perception after colour [Hanson, 2006] [Obein et al., 2004a]. Hence, glossiness has been chosen as the research topic for this thesis.

We showed that there are many standards for measuring physical gloss. However, perceived gloss does not always correlate well with its physical counterpart [Obein et al., 2004a] [Ji et al., 2006] [Leloup et al., 2011], as perceived gloss is a more complex psychological phenomenon that is a result of many different factors [Adelson, 2001] [Hanson, 2006].

The literature concerning perceived gloss was reviewed in terms of intrinsic and extrinsic factors. It has received only limited study concerning rough surfaces. Ho et al. [2008] studied perceived gloss on bumpy surfaces and described the results using a conjoint measurement model. Wijntjes and Pont [2010] reported that observers perceived high RMS height Lambertian surfaces as being "glossy".

Hence, two factors, surface geometry and surface reflection (mesoscale and microscale parameters respectively) were chosen to be investigated in this work.

The BRDF model was selected to characterise surface reflection properties because of its flexibility and popularity in the literature.

After a further review of the literature concerning gloss perception with complex surfaces, the $1/f^{\beta}$ noise surface model was chosen to represent surface geometry in this thesis [Padilla, 2008] [Voss, 1988].

In the next chapter, the surface geometry ($1/f^{\beta}$ noise) and reflection (BRDF) models will be discussed in detail.

Chapter 3

SURFACE GEOMETRY AND REFLECTION MODELS

From the literature survey presented in the last chapter, we concluded that perceived gloss is affected by several factors, of which surface geometry and reflection were chosen to be investigated in the research reported here. $1/f^{\beta}$ noise and the BRDF were chosen as mesoscale and microscale models respectively.

The purpose of the work reported in this chapter therefore was to examine the advantages and disadvantages of the most popular BRDF models and choose candidates for investigation in later chapters (Section 3.2). This chapter also presents the $1/f^{\beta}$ surface model and the two parameters that affect surface mesoscale roughness (Section 3.1). The way in which the models will be used to investigate perceived gloss is addressed in Section 3.3.

3.1 $1/f^{\beta}$ Noise Surface and Mesoscale Roughness

$1/f^{\beta}$ noise surfaces are generated by producing height maps with magnitude spectrum $H(f)$ scaled with spatial frequency as shown in Equation 3.1:

$$H(f) = \frac{\sigma}{N(\beta)} f^{-\beta} \tag{3.1}$$

where β is the roll-off factor of the surface height magnitude spectrum or the inverse slope in $\log H$-$\log f$ space as shown in Figure 3.1. σ is the RMS height of the surface. In this thesis we use zero mean height surfaces; the RMS height is always

therefore equal to the standard deviation and denoted by the symbol σ. $N(\beta)$ is the normalising factor. This surface model is commonly termed as $1/f^{\beta}$, which is a simplification of Equation 3.1.

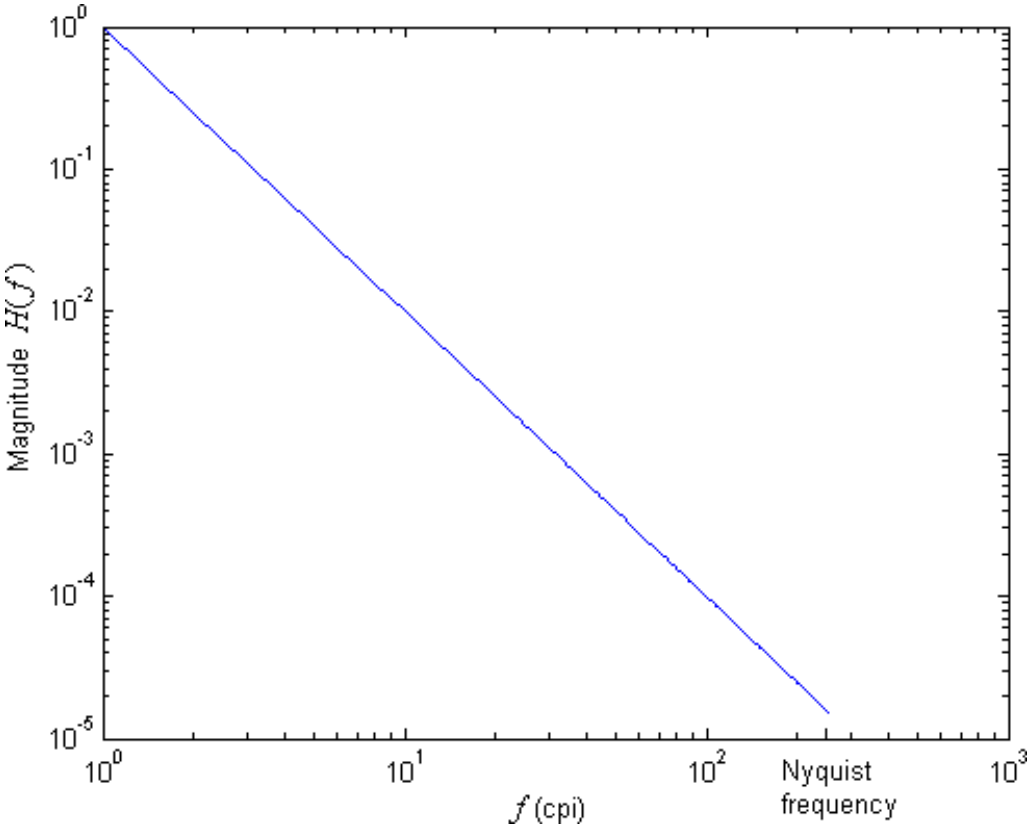

Figure 3.1: Graphical plot of magnitude spectrum $H(f)$ against frequency f in log-log space with roll-off factor $\beta = 2$. Note that $\beta = 2$ means that for every decade change in frequency the height variance changes by 2 decades.

The height map has a random phase complex conjugate spectrum. The phase generation algorithm is based on a pseudo random number generator. It generates a sequence of numbers that approximates the properties of random numbers. The sequence is not truly random in that it is completely determined by the random seed. Pseudo-random numbers are important in practice for their speed in number generation and their reproducibility. For this study, they make our stimuli repeatable.

The symbol Θ will denote the phase of the stimuli. The number next to it will denote the random seed used to initialise the random number generator. Padilla [2008] has shown that changing the random phase seed does not change perceived roughness.

The height maps are obtained using an inverse discrete Fast Fourier Transform (FFT). In the implementation, the imaginary part of the inverse FFT of the above noise model is zero due to the complex conjugate symmetry and is ignored [Padilla, 2008].

$1/f^{\beta}$ noise surfaces can be varied using two parameters: surface RMS height (σ) and roll-off factor (β). The roll-off factor can be varied when the surface magnitude spectrum is generated; while the RMS height can be varied either before or after applying the inverse FFT [Shah, 2010]. Before a surface is rendered, its height map is first standardised to unit RMS height and then scaled to the desired RMS height (σ). In the rest of this thesis, the term "RMS" is used to refer to surface RMS height.

Both parameters (β and σ) have been used to study perceived roughness, and it was found that they compensate for each other perceptually [Padilla et al., 2008]. We name this kind of roughness "mesoscale roughness" in this thesis to differentiate from roughness at the subpixel (or micro) scale which will be introduced in the next section. Figure 3.2 shows a graphical illustration of changing mesoscale roughness using β and σ, and Figure 3.3 shows example surfaces.

The height maps were generated at a maximum frequency of 256 cycles per image width (cpi), resulting in an image resolution of 512×512 pixels. Note that the $1/f^{\beta}$ noise surface is band limited and the frequencies are discrete. The height maps were used to render the surface images. The rendering of surfaces uses a reflectance model which characterises surface optical microscale properties. These will be introduced in the next section.

To summarize this section, we have defined the surface geometry model (Equation 3.1), and will use its two parameters (β and σ) to investigate the effect of surface mesoscale roughness on perceived gloss.

3.2 BRDF Model and Microscale Roughness

In order to obtain stimuli images, the mesoscale surface geometry generated using the $1/f^{\beta}$ model must be rendered using a microscale reflectance model and an illumination model. The illumination, which is not a research topic in this thesis,

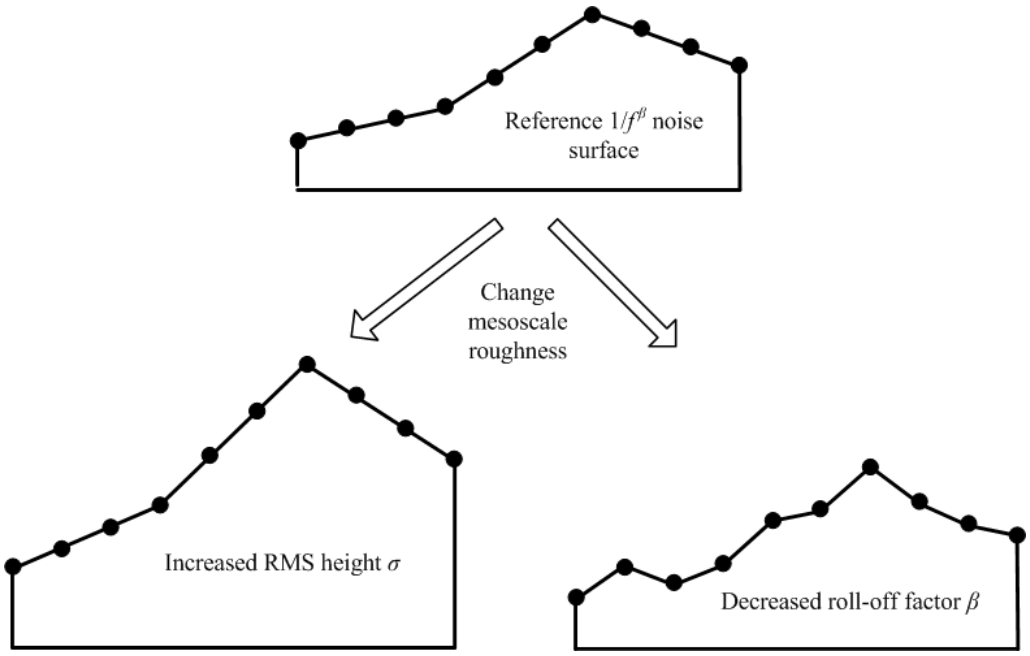

Figure 3.2: Sketch to illustrate the effects of changing mesoscale roughness of a $1/f^{\beta}$ noise surface in terms of RMS height (σ) and roll-off factor (β). The three graphs are three line profiles of a surface, and the black dots represent sample surface locations. The top graph is the reference surface; the bottom left has increased RMS height; the bottom right has decreased roll-off factor β. Notice the two different ways of changing surface mesoscale geometry.

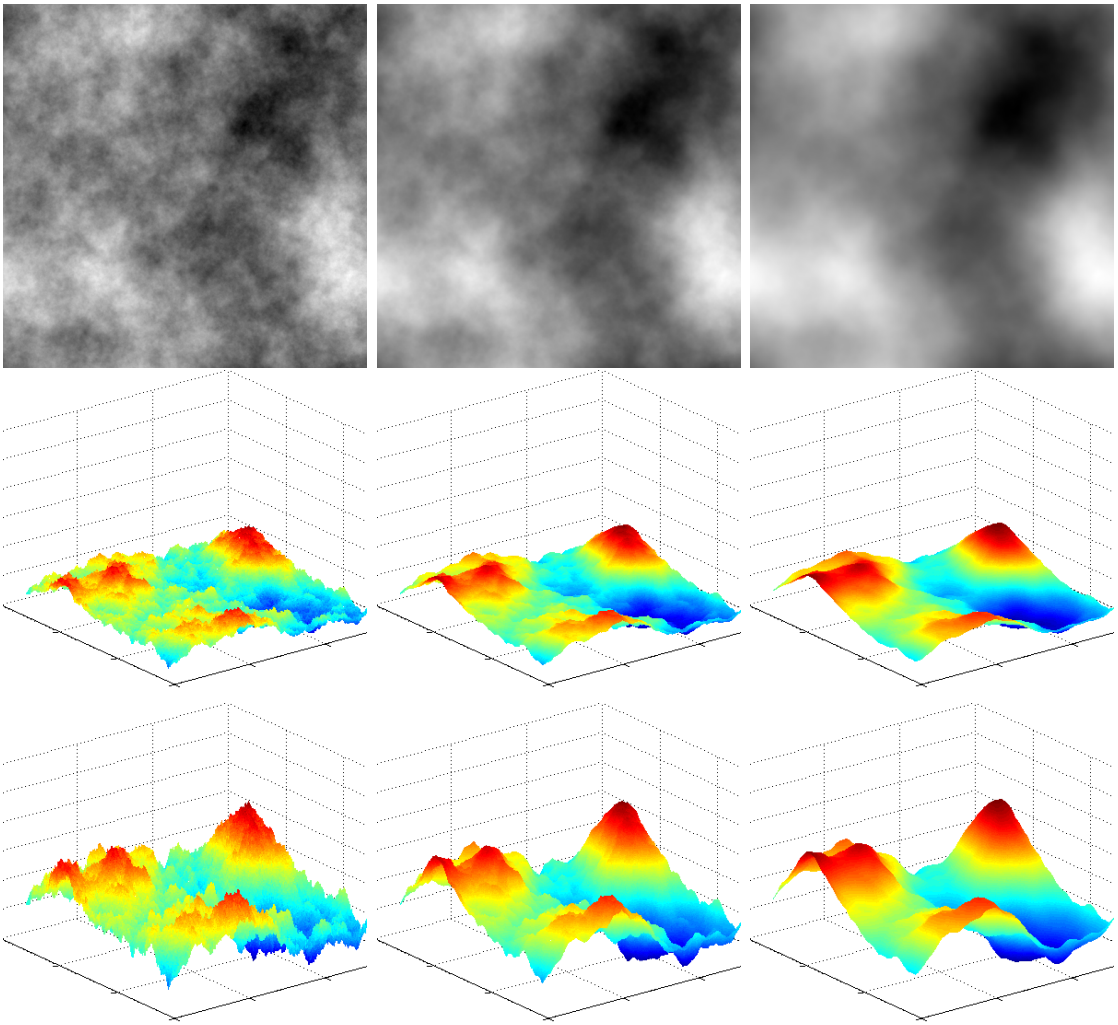

Figure 3.3: Height maps that demonstrate the change of surface geometry due to varying roll-off factor (β) and RMS height (σ). The first row shows three $1/f^{\beta}$ noise surface height maps coded by image intensity with different roll-off factors β ($\beta = 1.6, 2.0, 2.4$). The second row shows their 3D plots with RMS height $\sigma = 10.7$. The third row shows the same surfaces scaled to provide a larger RMS height $\sigma = 64.5$. The phase spectrum is held constant in these height maps ($\Theta = 0$), giving them a similar general shape in order to make comparisons easier.

will be discussed in Chapter 6. This section surveys reflectance models, and selects three for later use.

3.2.1 BRDF Models

In this thesis, only light reflection on opaque surfaces is considered, while refraction and subsurface scattering are not. The reflectance model can therefore be restricted to Bidirectional Reflectance Distribution Functions (BRDF).

The BRDF is a four-dimensional function that defines how light is reflected at an opaque surface. If the configuration is as shown in Figure 3.4, the mathematical definition will be Equation 3.2:

$$f_{\mathrm{r}}(\boldsymbol{\omega_{\mathbf{i}}}, \boldsymbol{\omega_{\mathbf{o}}}) = \frac{\mathrm{d}L_{\mathrm{r}}(\boldsymbol{\omega_{\mathbf{o}}})}{\mathrm{d}E_{\mathrm{i}}(\boldsymbol{\omega_{\mathbf{i}}})} \tag{3.2}$$

where f_{r} is the BRDF, L_{r} is the radiance, E_{i} is the irradiance. $\boldsymbol{\omega_{\mathbf{i}}}$ is incoming light direction, $\boldsymbol{\omega_{\mathbf{o}}}$ is outgoing direction, both defined with respect to the surface normal $\boldsymbol{N}$. In the analytical models described later, the directions $\boldsymbol{\omega_{\mathbf{i}}}$ and $\boldsymbol{\omega_{\mathbf{o}}}$ are denoted by unit vectors $\boldsymbol{L}$ and $\boldsymbol{V}$ pointing to lighting and viewing directions respectively. The BRDF returns the ratio of reflected radiance exiting along $\boldsymbol{\omega_{\mathbf{o}}}$ to the irradiance incident on the surface from direction $\boldsymbol{\omega_{\mathbf{i}}}$. Note that each direction $\boldsymbol{\omega}$ is itself parameterised by azimuth angle ϕ and zenith angle θ, therefore the BRDF is four-dimensional.

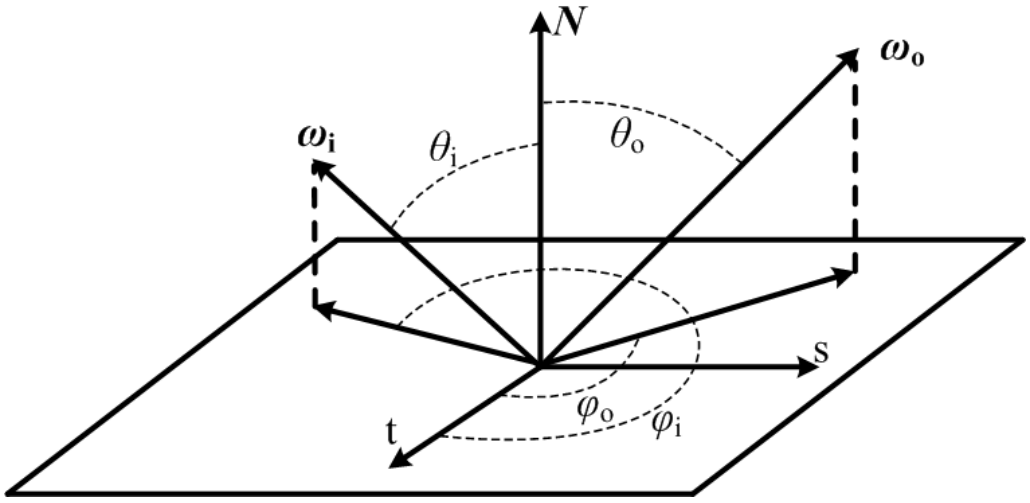

Figure 3.4: BRDF variables.

The direct way to obtain the BRDF of a real material is to measure f_r for every combination of $\boldsymbol{\omega_{\mathbf{i}}}$ and $\boldsymbol{\omega_{\mathbf{o}}}$, which is impractical. A more practical way is to use dense

samples and interpolation, which still results in a large data set. Instead, many analytical BRDF models have been proposed to approximate real material appearance. These models can be mathematically expressed using a small number of parameters. Users can tune these parameters to generate different surface appearances.

There are a large number of analytical BRDF models. We will introduce selected models which meet the following criteria: that they should be

- computationally attractive,
- have a low number of parameters (be parsimonious),
- produce surfaces of realistic appearance, and
- be well cited in the literature.

All the models discussed below are isotropic (they have no directional preference in optical behaviour) and the incident light is of unit intensity. More details concerning BRDF models can be found in a survey by Kurt and Edwards [2009].

The Lambertian Model

The Lambertian model [Lambert, 1760] is an empirical model that describes diffuse reflection using a cosine law. The mathematical formula is shown in Equation 3.3, where k_d is the albedo of the surface, $\boldsymbol{N}$ is the unit vector representing the surface normal and $\boldsymbol{L}$ is the unit light vector.

$$f_\mathrm{Lamb} = k_\mathrm{d}\ \boldsymbol{N} \cdot \boldsymbol{L} \tag{3.3}$$

Lambertian surfaces rarely exist in the real world, and reflections on most real-world surfaces are complicated mixtures of reflectance as described in Section 2.1. In computer graphics, the term 'specular reflection' is normally used for both glossy reflection and perfect specular (mirror) reflection as illustrated in Figure 2.1.

The Phong and Blinn-Phong Models

The Phong model and the Blinn-Phong model are two simple, early, empirical models that describe the specular reflection by considering the viewing direction [Phong,

1975] [Blinn, 1977]. The specular terms of these two models are formulated in Equation 3.4 and Equation 3.5 respectively:

$$f_{\text{Phong}} = k_{\text{s}} \, (\boldsymbol{R} \cdot \boldsymbol{V})^{\alpha} \tag{3.4}$$

$$f_{\text{Blinn}} = k_{\text{s}} \, (\boldsymbol{N} \cdot \boldsymbol{H})^{\alpha} \tag{3.5}$$

where f_{Phong} and f_{Blinn} denote the specular reflectance intensity for the two models; k_{s} is the specular reflection component; $\boldsymbol{R}$ is the unit reflection vector of light vector $\boldsymbol{L}$ (or $\boldsymbol{\omega_{\text{i}}}$) about the surface normal $\boldsymbol{N}$, which can be calculated as $\boldsymbol{R} = 2(\boldsymbol{L} \cdot \boldsymbol{N})\boldsymbol{N} - \boldsymbol{L}$; $\boldsymbol{V}$ denotes the unit viewing vector ($\boldsymbol{\omega_{\text{o}}}$); $\boldsymbol{H}$ is the unit halfway vector and is pointing to the half-angle between $\boldsymbol{L}$ and $\boldsymbol{V}$, which can be calculated as $\boldsymbol{H} = (\boldsymbol{L} + \boldsymbol{V})/|\boldsymbol{L} + \boldsymbol{V}|$. The difference between the Phong model and the Blinn-Phong model lies in the vectors chosen for the dot product.

These two models are mathematically simple and as a result, are very commonly used and often combined with Lambert's law.

The Ward Model

Psychophysical studies using more realistic synthetic stimuli used more complicated BRDF models, such as the Ward model [Ward, 1992] due to its combination of reasonable complexity and use of physically meaningful parameters. In comparison with other empirical reflectance models (e.g. Phong and Blinn), this model obeys the physical laws of Helmholtz reciprocity and energy conservation. The formula of the Ward model is shown in Equation 3.6.

$$f_{\text{Ward}}(\theta_{\text{i}}, \phi_{\text{i}}, \theta_{\text{o}}, \phi_{\text{o}}) = \frac{k_{\text{d}}}{\pi} + k_{\text{s}} \cdot \frac{\exp(-\frac{\tan^2 \delta}{\alpha^2})}{4\pi\alpha^2 \sqrt{\cos\theta_{\text{i}} \cos\theta_{\text{o}}}} \tag{3.6}$$

where $f_{\text{Ward}}(\theta_{\text{i}}, \phi_{\text{i}}, \theta_{\text{o}}, \phi_{\text{o}})$ is the surface BRDF; θ_{i}, ϕ_{i} and θ_{o}, ϕ_{o} are zenith and azimuth angles of illumination and viewing directions respectively; k_{d} is the diffuse reflection component; k_{s} is the specular reflection component; α is the standard deviation of the local surface slope; and δ is angle between surface normal $\boldsymbol{N}$ and halfway vector $\boldsymbol{H}$.

The Ward model has been used in several studies as it is the native reflectance model of the rendering software RADIANCE [Ward, 1994].

The Ashikhmin-Shirley Model

More complicated reflectance models consider the surface microscale geometry and in particular the microfacet theory proposed by Torrance and Sparrow [1967]. These models are based on the assumption that surfaces are made up of tiny microfacets, which will be discussed in more detail in the next subsection. We used the Ashikhmin-Shirley model to render more realistic surfaces in this thesis. This model considers the microfacet assumption and the Fresnel effect. The Fresnel effect is the phenomenon that surfaces reflect most of the incident light at the grazing angle ($\theta_{\mathrm{i}} \approx 90°$). Analogous to the above models, the Ashikhmin-Shirley model is also in the classic form of a sum of a diffuse term and a specular term (Equation 3.7):

$$f_{\mathrm{A-S}}(\boldsymbol{\omega_{\mathbf{i}}}, \boldsymbol{\omega_{\mathbf{o}}}) = f^{\mathrm{D}}_{\mathrm{A-S}}(\boldsymbol{\omega_{\mathbf{i}}}, \boldsymbol{\omega_{\mathbf{o}}}) + f^{\mathrm{S}}_{\mathrm{A-S}}(\boldsymbol{\omega_{\mathbf{i}}}, \boldsymbol{\omega_{\mathbf{o}}}) \tag{3.7}$$

Differing from the Ward model, the Ashikhmin-Shirley model has an energy-conserving and view-dependent diffuse term:

$$f^{\mathrm{D}}_{\mathrm{A-S}}(\boldsymbol{\omega_{\mathbf{i}}}, \boldsymbol{\omega_{\mathbf{o}}}) = \frac{28 k_{\mathrm{d}}}{23\pi}(1 - k_{\mathrm{s}})(1 - (1 - \frac{\boldsymbol{N} \cdot \boldsymbol{\omega_{\mathbf{i}}}}{2})^5)(1 - (1 - \frac{\boldsymbol{N} \cdot \boldsymbol{\omega_{\mathbf{o}}}}{2})^5) \tag{3.8}$$

In addition to obeying basic physical laws, the Ashikhmin-Shirley model also considers both the Fresnel effect and microfacets. The specular term is defined in Equation 3.9:

$$f^{\mathrm{S}}_{\mathrm{A-S}}(\boldsymbol{\omega_{\mathbf{i}}}, \boldsymbol{\omega_{\mathbf{o}}}) = \frac{\alpha + 1}{8\pi} \frac{(\boldsymbol{N} \cdot \boldsymbol{H})^{\alpha}}{(\boldsymbol{\omega_{\mathbf{o}}} \cdot \boldsymbol{H}) \max((\boldsymbol{N} \cdot \boldsymbol{\omega_{\mathbf{i}}}), (\boldsymbol{N} \cdot \boldsymbol{\omega_{\mathbf{o}}}))} F(\boldsymbol{\omega_{\mathbf{o}}} \cdot \boldsymbol{H}) \tag{3.9}$$

where $F(\boldsymbol{\omega_{\mathbf{o}}} \cdot \boldsymbol{H})$ is the Fresnel term, which is Schlick's approximation [Schlick, 1994] in Equation 3.10:

$$F(\boldsymbol{\omega_{\mathbf{o}}} \cdot \boldsymbol{H}) = k_{\mathrm{s}} + (1 - k_{\mathrm{s}})(1 - (\boldsymbol{\omega_{\mathbf{o}}} \cdot \boldsymbol{H}))^5 \tag{3.10}$$

Despite the differences in mathematical formulae, the above gloss models share common characteristics that the reflected light is assumed to be a sum of two parts which are parameterised by the component of diffuse reflection (k_{d}), the component of specular reflection (k_{s}), and the exponent parameter (α). k_{d} and k_{s} control the strength of diffuse and specular reflections. The exponent parameter α controls

the spread of specular lobes (Figure 2.1c). From the perspective of appearance, α characterises the sharpness of reflection. All of the above models can be encompassed by microfacet models, in which α plays an important role. This is described in the next subsection.

3.2.2 Microfacet and Microscale Roughness

The fact that the specular reflection on surfaces is not a perfect mirror reflection but is blurred can be explained by the existence of microfacets [Torrance and Sparrow, 1967] and the microfacet model proposed by Blinn [1977]. The microfacet model assumes that the surfaces are not perfectly smooth but are composed of many very tiny facets (microfacets). A simplification assumes that each microfacet is a perfect mirror reflector. Microfacets can be occluded by other microfacets, lie in the shadow of neighboring microfacets, and reflect more light than predicted due to inter-reflection. These microfacets have normals that are distributed about the normal of the approximating local surface patch. The degree to which microfacet normals differ from the surface local normal is determined by the roughness of the surface in the microscale. An illustration of the microfacet surface and its imaging process is shown in Figure 3.5.

The blurred specular highlights can then be explained by the microfacets. At surface points where the surface local normal is close to the half-angle direction, many of the microfacets point in the half-angle direction and so the specular highlight is bright. As one moves away from the centre of the highlight, the surface local normal and the half-angle direction become farther apart; the number of microfacets oriented in the half-angle direction falls, and so the intensity of the highlight falls off. Thus, a surface which is smooth at the microscale can reflect more "specular" light, and a surface which is rough in microscale will lose specular appearance. Both specular reflection and diffuse reflection can be explained using microfacet theory, and an improved diffuse model that uses microfacet theory was proposed by Oren and Nayar [1994]. This model provides improved simulation of real-world matte surfaces compared with Lambert's law.

The specular terms of the BRDF models discussed in the previous subsection can be encompassed by the microfacet model using different microfacet distribution func-

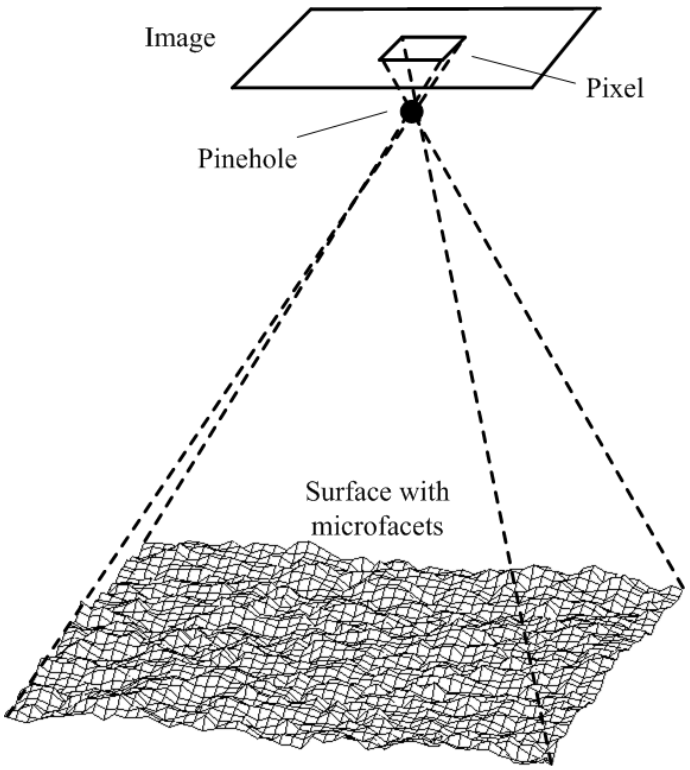

Figure 3.5: Graphical demonstration of microfacet in the imaging process.

tions. The specular terms of Phong and Blinn-Phong models can be generalized to the distribution of microfacets without integral constant. A slightly better model results from the use of a Gaussian distribution. The Ashikhmin-Shirley Model employs the Blinn-Phong distribution. All of these models utilise a parameter "α" to characterise the distribution of microfacets, in other words, the roughness of the microscale structure.

Because the imaging and rasterization process are always band limited, this kind of roughness occurs at the sub-pixel or microscale level. It cannot be directly observed from the surface shape but only estimated from the optical appearance. We therefore name it "microscale roughness" in contrast to the mesoscale roughness of the surface geometry model.

3.2.3 Summary

In this section, we introduced four analytical BRDF models. Table 3.1 shows how well they meet the criteria described in the beginning of this section:

Table 3.1: The tabulated criteria met by the introduced BRDF models.

	Lambertian	Phong & Blinn	Ward	Ashikhmin-Shirley
Widely used	Yes	Yes	Yes	Yes
Computationally attractive	Yes	Yes	Yes	Yes
Realism	Empirical, and proposed only for matte surfaces	Empirical, can generate glossy appearance, but not realistic	Empirical, can generate realistic appearance, constant diffuse term	Physically-based and can generate a more realistic appearance
Major parameters	k_{d}	k_{s}, α	k_{d}, k_{s}, α	k_{d}, k_{s}, α
Cited within literature	Apparent gloss was observed by Wijntjes and Pont [2010]	[Nishida and Shinya, 1998]	Perceptual space proposed by Pellacini et al. [2000]	Popular in the computer graphics field

The models described in Table 3.1 are all widely used and computationally attractive. They all have advantages and disadvantages, and thus will be used in different chapters.

The Lambertian model has often been used in investigations of characteristics such as roughness and directionality. It was designed to model matte surfaces and yet Wijntjes and Pont [2010] reported apparent gloss on high RMS height surfaces rendered using Lambert's law. Hence the Lambertian model was employed in Chapter 4 to investigate the findings of Wijntjes and Pont [2010].

Nishida and Shinya [1998] and Wendt et al. [2008] used the Phong/Blinn-Phong model to render glossy surfaces but produced implausible and cartoon level stimuli. Additionally, these two models do not obey the basic physical rules of light reflection. Therefore, they were not chosen as the reflectance models for use in the research reported here.

Although the Ward model is capable of describing most significant reflection phenomena and is a good candidate for generating visual stimuli in vision studies, it is an empirical model and not physically based. It also lacks the capability of describing other important reflection phenomena, such as illumination-dependent diffuse reflection and the Fresnel effect. For these reasons, we will only use the Ward model in Chapter 5 to measure the effect of variations in microscale parameters on perceived gloss.

More complex models are used in computer graphics, for example, the Torrance-Sparrow model [Torrance and Sparrow, 1967] and the height correlation model (HTSG model) [He et al., 1991]. The latter can simulate most physical phenomena such as wave optics effects. However, these models are too computationally intensive for use in this study. A relatively complete model which obeys basic physical laws and is able to render surfaces of realistic and glossy appearance is sufficient for the study of gloss perception with simulated rough surfaces. The Ward model and the Ashikhmin-Shirley model are both eligible. The Ashikhmin-Shirley model is chosen as the reflectance model for generating more realistic stimuli in later chapters because of its balance of complexity and capability. Furthermore, it is the native reflection model of the rendering software used in this study. Detailed reasons for why the Ward model has not chosen for rendering more realistic stimuli will be

discussed in Chapter 6.

3.3 Investigation Strategy

We have introduced the models and model parameters that will be investigated by experiments described in later chapters. This section will describe the investigation strategy to be used.

According to the thesis scope, the experiments will focus on surface geometry and reflection properties. From the previous sections we know that there are two parameters in our surface geometry model: surface RMS height (σ) and magnitude roll-off factor (β); and there are three parameters in the surface reflection models: the diffuse component coefficient (k_d), the specular component coefficient (k_s) and the microscale roughness coefficient (α). Thus there are a total of five parameters to be investigated. In addition, other factors, although not involved in the primary focus of this thesis, will inevitably be involved in the experimentation, such as inter-reflection, illumination and viewing conditions. Therefore, the measurement of perceived gloss will be conducted incrementally.

Thus the experiments are divided into two stages according to the sophistication of the rendering system used for generating the stimuli.

3.3.1 Stage 1

In this stage, the rendering technique, reflection model, illumination and viewing conditions are all constrained to simple cases. This system in some ways simulates the situation and environment used for measuring physical gloss.

Chapter 4 examines the effect of variations in one surface mesoscale parameter (RMS height σ) on gloss perception. The reflection model was chosen to be Lambertian. Perceived gloss of high RMS height but "matte" surfaces was first reported by Wijntjes and Pont [2010] and we will repeat the experiment using a wider RMS height range.

Under the same conditions with Chapter 4, the effect of variations in surface microscale (BRDF) parameters on perceived gloss is first presented in Chapter 5. Then

we examine whether adjusting the gloss BRDF parameters can produce a similar gloss level to the apparent gloss of high RMS height Lambertian surfaces.

3.3.2 Stage 2

The simple rendering system used in stage 1 has limitations in terms of accuracy. As the perception of gloss is affected by multiple factors [Adelson, 2001] [Hanson, 2006], we will model more realistic stimuli paticularly in terms of rendering technique, illumination and viewing conditions. The impact of these improvements in rendering will be examined on removing the apparent gloss of high RMS height Lambertian surfaces.

The effect of the other mesoscale roughness parameter (β) on gloss perception will be investigated in Chapter 7, while in Chapter 8, we will describe the effect of simultaneously varying both mesoscale roughness (β) and microscale roughness (α) on perceived gloss.

3.4 Summary

In this chapter, the surface geometry model and BRDF reflection models were described in detail.

The $1/f^{\beta}$ noise surface model can be controlled in terms of surface RMS height (σ) and roll-off factor (β). Both affect "surface mesoscale roughness" [Padilla, 2008] and will be investigated separately.

Four analytical BRDF models were described. The parameters of analytical BRDF models (k_{d}, k_{s}, α) form the parametric space for sampling microscale characteristics. These models were discussed with reference to the microfacet model. The exponent parameter α in the specular term in particular controls the microfacet distribution and we refer to this as the "microscale roughness" parameter. The Lambertian model, the Ward model and the Ashikhmin-Shirley model were selected for further investigation.

The investigation strategy was developed with reference to the parameters of the mesoscale and microscale models and the rendering methods. We will first mea-

sure the apparent gloss of high RMS height Lambertian surfaces and then examine whether using a gloss BRDF model with a low RMS height surface can produce similar perceptions. After describing methods for generating more realistic stimuli, we will incrementally investigate the effect of variations in surface mesoscale roughness and microscale roughness on perceived gloss.

However, first we will investigate the apparent gloss of Lambertian surfaces as reported by Wijntjes and Pont [2010] in Chapter 4.

Chapter 4

PERCEIVED GLOSS OF LAMBERTIAN SURFACES

In Chapters 2 and 3, we discussed models of surface geometry and reflection. In this chapter we will investigate how people perceive gloss on rough surfaces.

More specifically, the aim of the work reported in this chapter was to investigate the effect of the mesoscale parameter, RMS height (σ), on perceived gloss of Lambertian $1/f^{\beta}$ noise surfaces.

Sections 4.2 and 4.3 describe the experiment, and the results are reported in Section 4.4. The chapter is concluded and discussed in Section 4.5. However, we will first describe the work of Wijntjes and Pont [2010] whose study of the apparent gloss of Lambertian (matte) surfaces motivated the investigation presented in this chapter.

4.1 The Work of Wijntjes and Pont [2010]

Wijntjes and Pont [2010] reported that observers perceived increasing gloss from high RMS height Lambertian surfaces within the σ range $[16, 128]$. They simulated a collimated light source and a viewing direction, both orientated perpendicular to the surface, and used simple single-bounce rendering with a local Lambertian reflectance model.

Their goal was to examine the image histogram hypothesis proposed by Motoyoshi

et al. [2007]. They formally derived a general relationship between surface RMS height, illumination direction and image intensity transformation [Wijntjes and Pont, 2010]. However, their results did not match those of Motoyoshi et al. [2007] and they reinterpreted them using the bas-relief ambiguity [Belhumeur et al., 1999].

We will repeat their experiment in this chapter with two modifications. The reasons are as follows: first, Wijntjes and Pont [2010] only used four levels of surface RMS roughness which were within a narrow range. We will sample a wider range of σ.

Secondly, the surface geometry model used by Wijntjes and Pont [2010] is reported to be that of a Brownian surface: a $1/f^{\beta}$ noise surface with magnitude roll-off factor $\beta = 1$. We found the rendered images of such surfaces were too noisy to present the appearance they reported (see Figure 4.1).

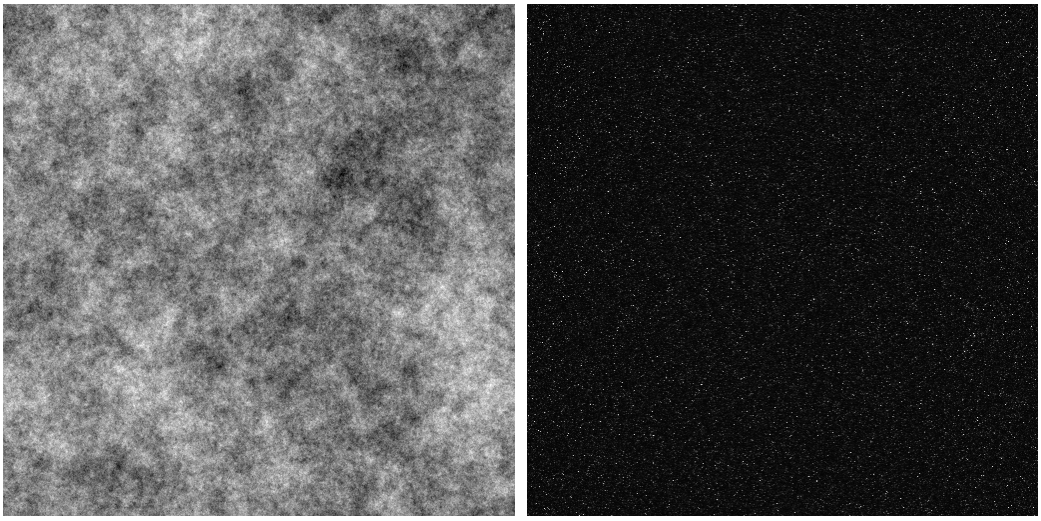

Figure 4.1: Left: the height map of a Brownian surface. Right: the rendered image of the height map with RMS height $\sigma = 32$ pixel width. The parameter values of the surface model and RMS height used are as reported by Wijntjes and Pont [2010].

Based on the above reasons, the surfaces used by Wijntjes and Pont [2010] were not used here. Instead, we varied surface RMS height over a wider range and used a magnitude roll-off factor β=2.3.

4.2 Experiment Setup

The experiment setup described below will be used in later chapters; changes will be noted when relevant.

4.2.1 Surface and Rendering Algorithms

The stimuli in this experiment were produced using surface height maps and the Lambertian reflection model as described in Chapter 3. The rendering technique employed a local model of reflection, i.e. no inter-reflections from either the surface itself or the environment were taken into account. The albedo k_{d} was set to unity, and the illumination strength was set to white (one). The local normal vectors ($\boldsymbol{n}$) were calculated as follows. Given the surface height map, a [1 -1] differential operator was applied on both horizontal (x-direction) and vertical (y-direction) dimensions to generate the gradients p and q respectively. Thus, the local normal vector $\boldsymbol{n}$ was obtained using Equation 4.1.

$$\boldsymbol{n} = (\frac{-p}{\sqrt{p^2+q^2+1}}, \frac{-q}{\sqrt{p^2+q^2+1}}, \frac{1}{\sqrt{p^2+q^2+1}}) \tag{4.1}$$

As shown in Figure 3.4, the illumination vector $\boldsymbol{\omega_{\mathrm{i}}}$ or $\boldsymbol{L}$ can be represented by its zenith angle θ_{i} and azimuth angle ϕ_{i} (Equation 4.2).

$$\boldsymbol{L} = (\cos\phi_{\mathrm{i}} \sin\theta_{\mathrm{i}}, \sin\phi_{\mathrm{i}} \sin\theta_{\mathrm{i}}, \cos\theta_{\mathrm{i}}) \tag{4.2}$$

According to Lambert's law (Equation 3.3), the intensity I was calculated using Equation 4.3.

$$I = \frac{-p\cos\phi_{\mathrm{i}} \sin\theta_{\mathrm{i}} - q\sin\phi_{\mathrm{i}} \sin\theta_{\mathrm{i}} + \cos\theta_{\mathrm{i}}}{\sqrt{p^2+q^2+1}} \tag{4.3}$$

In this experiment, the light source was set to perpendicularly illuminate the surface plane, i.e. $\theta_{\mathrm{i}} = 0$. Thus the image intensity is calculated using Equation 4.4:

$$I = \frac{1}{\sqrt{p^2+q^2+1}} \tag{4.4}$$

The resulting images are double float two dimensional arrays within the range [0,1], which will be linearly displayed on a calibrated monitor with the 0 shown as minimum luminance and the 1 shown as maximum luminance.

4.2.2 Tools

This section introduces the tools used to present the stimuli.

Display

Padilla [2008] discussed display technologies and concluded that high specification LCD monitors are now superior to CRT monitors in terms of the spatial modulation transfer function, gamma correction and luminance uniformity.

A 20-inch TFT LCD monitor (NEC MultiSync LCD2090UXi) was chosen for the experiment. Compared to cheaper LCDs, this monitor has improved viewing angle, colour reproduction, a 10-bit look up table, more natural whites, increased gamut, contrast ratio and support for true 8-bit colour without dithering. The monitor has a pixel pitch of 0.255 millimetre (mm) (100 dots per inch (dpi)) and a resolution 1600×1200 pixels.

Display Calibration

A spectrophotometer (Gretag Macbeth Eye One Pro) was used to calibrate and linearise the gamma response (1.0). The colour temperature was set to 6500K. The maximum and minimum luminance was calibrated to 120 cd/m^2 and 0 cd/m^2. Figure 4.2 shows the resulting profile.

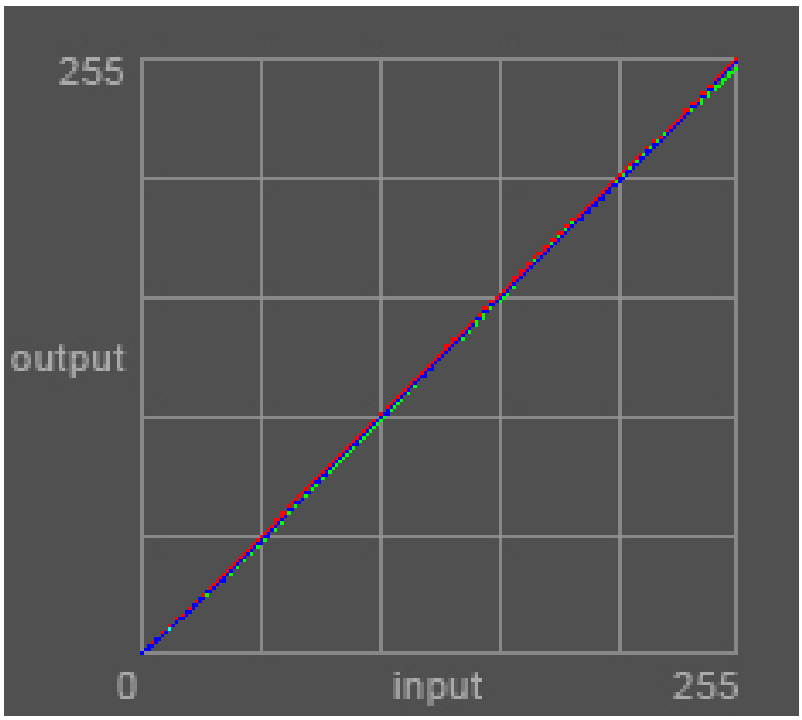

Figure 4.2: Monitor calibration profile.

4.2.3 Environment

The general environment of our visual experiments requires an observer to sit in front of a monitor display, and make responses to the stimuli on the monitor using a computer mouse or keyboard.

The stimuli images have a resolution of 512×512 pixels, thus are square of side 13.056 centimetre (cm). In this study, the monitor was set at a distance of 50 cm from the observer to provide an angular resolution of approximately 17 cycles per degree (cpd). The stimuli subtended an angle of 14.89° in the vertical direction. The eyes of observer were approximately in line with the centre of the screen.

The experiments were all conducted in a dark room with opaque, matte, black curtains in front of the windows and matte walls without obvious specular reflections. The monitor was the only source of light.

4.3 Experiment

Having defined the surface model, reflection model and experiment environment, we will describe the first experiment in this section. The goal of this experiment is to examine how perceived gloss of Lambertian surface varies with RMS height (σ).

4.3.1 Stimuli

Ten surface RMS height (σ) values (in pixel width) were logarithmically sampled in the range [64.5, 322.4]. The resulting surfaces were denoted as $S_{\sigma_i}, i = 1, 2, \cdots, 10$. Note that one unit of height corresponds to one image pixel width. These surfaces were rendered using the algorithm described in the previous section. The ten stimuli are shown in Figure 4.3.

4.3.2 Observers

Ten paid observers with normal or corrected to normal vision participated in the experiment. All were students or University employees working in different fields,

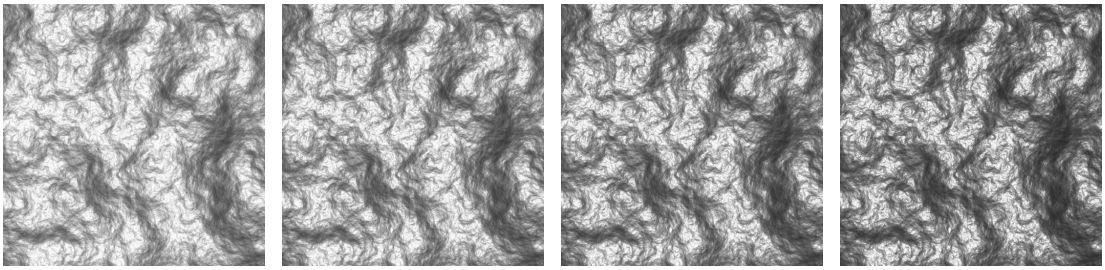

(a) S_{σ_1} (b) S_{σ_2} (c) S_{σ_3} (d) S_{σ_4}

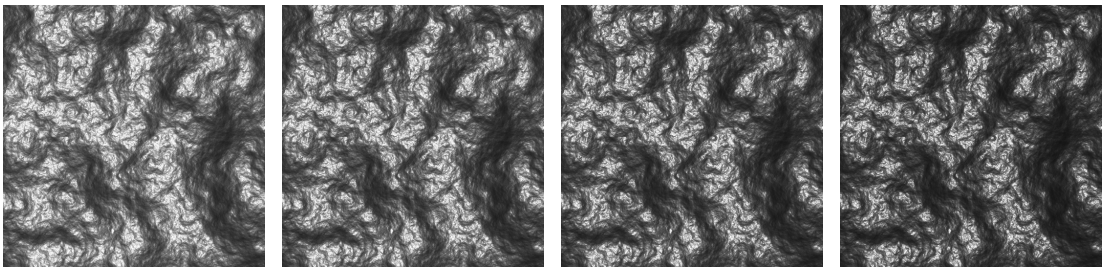

(e) S_{σ_5} (f) S_{σ_6} (g) S_{σ_7} (h) S_{σ_8}

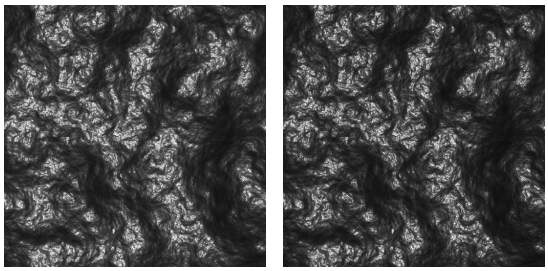

(i) S_{σ_9} (j) $S_{\sigma_{10}}$

Figure 4.3: The ten stimuli images used in the psychophysical experiments.

were less than 35 years of age, mixed gender and nationalities. All were naïve with respect to the purpose and design of the experiment.

4.3.3 Procedure

The magnitude estimation method was used as it is relatively simple. The observer was presented with a series of stimuli in random order. Before the experiment, observers were shown printed instructions:

> You will be shown 10 images of textured surfaces. Your task is to evaluate glossiness of the surfaces on the scale [0-1]. Please enter your value by slider and press button "Submit".

The surface images were shown in the middle of the screen with the background set to dull green (R=56,G=66,B=64) to avoid distracting contrast. The background colour chosen here was not further examined, since the concern that how background affects perceived gloss has only received limited study [Doerschner et al., 2010b]. The observers' task was to evaluate the magnitude of the glossiness on a scale [0,1] by setting the value of a horizontal slider, where 0 corresponds to the extreme matte, on the left, and 1 extreme gloss, on the right. A number next to the slider bar indicated the current value. Observers were instructed to do the task quickly to express their first impressions. Observers clicked a submit button when they were satisfied with the gloss value set for that trial and then the next trial was shown. There was a pause of one second between trials to avoid point-wise comparison of two stimuli. As a verification experiment of that Wijntjes and Pont [2010] conducted, the stimuli were shown only once without a measure of observer repeatability.

4.4 Results and Analysis

The estimated gloss of the ten stimuli were recorded and averaged across all observers. Figure 4.4 shows the mean values of estimated gloss for each stimulus with error bars representing ± the standard errors.

A one-way repeated measurement ANalysis Of VAriance (ANOVA) was conducted. Mauchly's test indicated that the assumption of sphericity had been violated for the

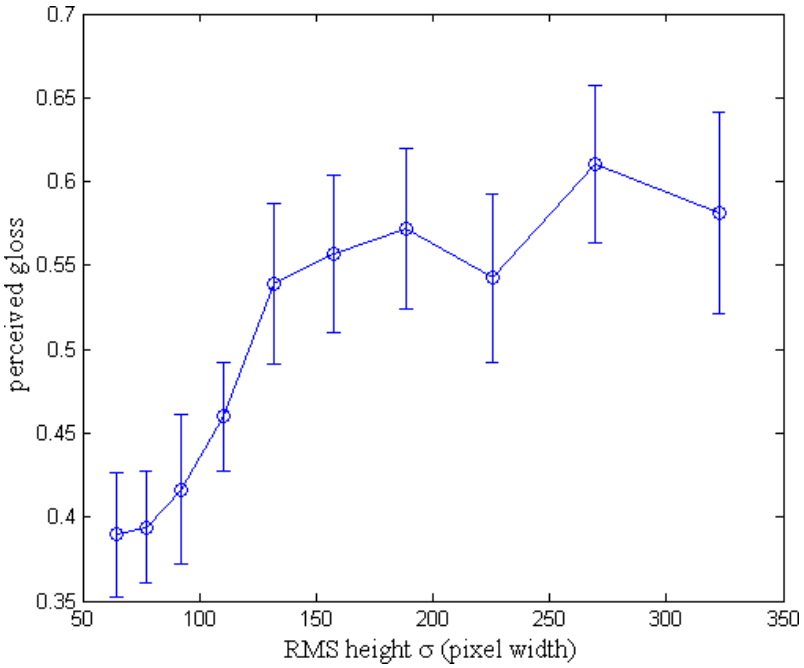

Figure 4.4: Experiment result averaged across all observers for the estimated gloss of surfaces with different surface RMS height (σ). These are relative glossiness representing difference scales. The error bars denote $\pm$ standard errors.

main effect of σ: $\chi^2(44) = 76.62, p < 0.01$. Therefore the degree of freedom was corrected using Greenhouse-Geisser estimates of sphericity ($\varepsilon_{\mathrm{g}} = 0.341$ for the main effect of σ). The test shows that perceived gloss is significantly affected by surface RMS height ($F(3.07, 27.66) = 8.25$, $p < 0.01$). The large standard errors and the fluctuation from surface S_{σ_8} are possibly because of the absence of a measure of observer repeatability.

4.5 Conclusion and Discussion

From the results of the experiment reported in this chapter, we can conclude that increased gloss was observed on Lambertian surfaces when surface RMS roughness was increased. The results are consistent with the findings of Wijntjes and Pont [2010]. However, the surfaces used in our experiment have a value of $\beta = 2.3$ and cover a wider RMS height range. Increases in gloss are not obviously observed for surfaces with $\sigma > 150$.

Surfaces used in this chapter are of very high RMS height (see the cross sections and absolute slope angles shown in Figure 4.5). The absolute slope angle is the angle

between surface normals and the z-axis (the surface lies in the x-y plane). The mean absolute slope angle is above 60° for $\sigma > 131.9$, indicating high roughness.

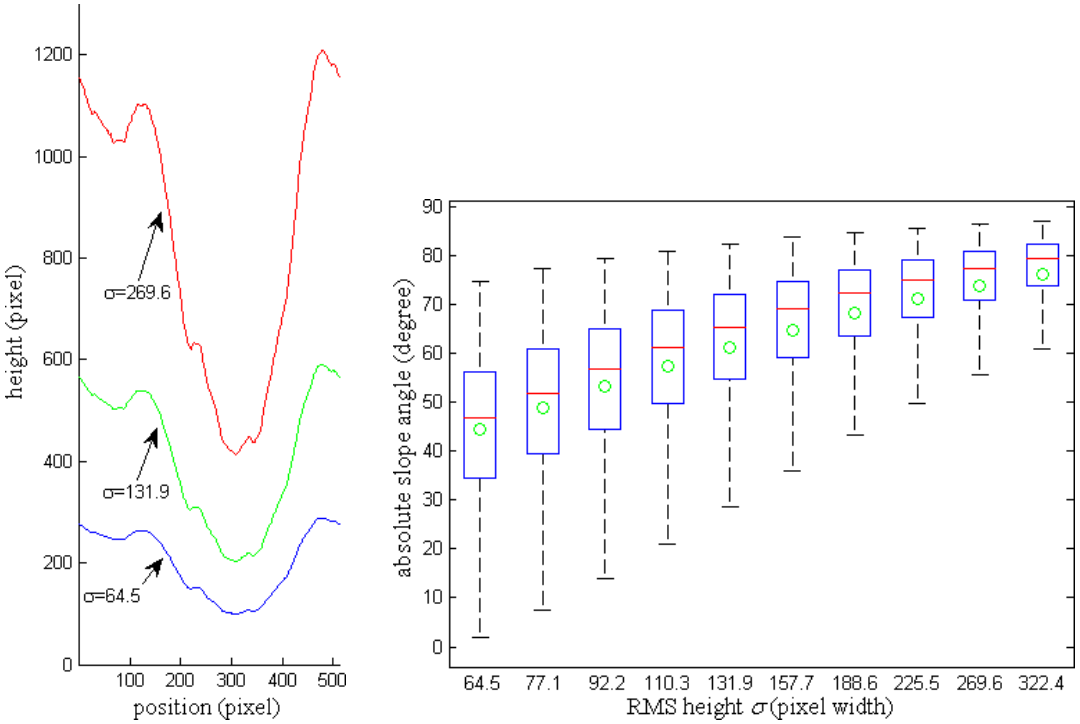

(a) (b)

Figure 4.5: (a): Cross sections of three surfaces used in this chapter of differing RMS height σ (surface S_{σ_1}, S_{σ_5}, S_{σ_9} in Figure 4.3). (b): Box plot of the absolute slope angles of the surfaces used in the experiment. For each surface, the green circle indicates the mean, the central red line indicates the median, the edges of the box are the 25th and 75th percentiles, the whiskers extend to the most extreme data points (within 1.5 times distance between 25th and 75th percentiles).

Although surfaces are of high RMS height, every surface facet was illuminated by the perpendicular collimated light and can be viewed by observers due to the orthogonal projection used. In addition, the rendering algorithm did not consider inter-reflections. Thus the gloss perceived by observers may be an artifact of these particular viewing and rendering conditions. Some of these conditions will be relaxed in Chapter 6.

However, in the next chapter we will examine the effect of variation in microscale (gloss BRDF) parameters on perceived gloss, and investigate whether adjusting the gloss BRDF of a moderate RMS height surface can produce similar gloss levels to those of the high RMS height Lambertian surfaces used in this chapter.

Chapter 5

THE EFFECT OF MICROSCALE BRDF PARAMETERS ON PERCEIVED GLOSS

In Chapter 4, we investigated the effect of variations in the mesoscale parameter, surface RMS height (σ), on the perceived gloss of Lambertian surfaces.

The aim of the work reported in this chapter was to investigate the effect of variations in surface microscale (gloss BRDF) parameters on perceived gloss. We also investigate whether adjusting BRDF parameters on a moderate RMS height surface can generate similar perceived gloss levels to those of the high RMS height Lambertian surfaces as reported in Chapter 4.

We will use a constant $1/f^{\beta}$ noise surface and replace the Lambertian model with the Ward BRDF model. The Ward model parameters will be varied to generate stimuli, and their influence on perceived gloss will be investigated (Exp 1) in Section 5.2. In the next section we investigate whether or not the apparent gloss observed in Chapter 4 can be matched to the perceived gloss of the low RMS height, Ward surfaces (Exp 2). However, first we will describe the experimental setup which is common to both of these investigations.

5.1 Common Experimental Setup

The experiments described in this chapter were conducted under a common environment which was the same as that used in Chapter 4 with the same observers in a different session. However, the surface geometry was held constant and the Lambertian reflection model was replaced with the Ward model.

The surface has roll-off factor $\beta = 2.3$, RMS height $\sigma = 6.4$ pixel width, and random phase $\Theta = 0$.

The surface normals were calculated in the same way as described in Section 4.2. The collimated illumination and viewing direction were set to be perpendicular to the surface plane and the illumination strength was set to one to maintain consistency with Chapter 4.

In contrast with the Lambertian model which has only one parameter k_{d}, there are three parameters in the Ward model. In this experiment, all three parameters were varied in order to investigate their influence on perceived gloss. The rendering used a local model of reflection, i.e. inter-reflections were not considered (as described in Section 4.2).

5.2 Measuring Perceived Gloss in the Ward Model Parametric Space (Exp 1)

5.2.1 Stimuli

All three Ward model parameters (k_{d}, k_{s}, α) were uniformly sampled to provide $4 \times 5 \times 5$ (100) stimuli. The values of the parameters were: $k_{\mathrm{d}} = 0.285, 0.576, 0.867, 1.157$; $k_{\mathrm{s}} = 0.0186, 0.051, 0.083, 0.116, 0.148$; $\alpha = 0.0498, 0.0718, 0.0938, 0.116, 0.138$. The ranges of values were obtained from a pilot experiment. All 100 stimuli are shown rendered in Appendix A.

In the pilot experiment, observers produced results without clear trend using our stimuli which span a wide gloss range. This may have been due to the task overtaxing the observers [Ehrenstein and Ehrenstein, 1999]. To avoid this problem, a pair of

two reference images (modulus) were shown side-by-side with the test stimuli to help observers make their judgements. The two reference images comprise one extreme matte surface and one extreme glossy surface placed to the left and right of the central stimuli respectively (see Figure 5.1). The parameters for these images were taken from [Pellacini et al., 2000] (k_{d}=0.760, k_{s}=0.033, α=0.100) for matte and (k_{d}=0.030, k_{s}=0.099, α=0.040) for gloss. While the glossy reference corresponded to the most extreme gloss obtainable from the model, the parameters of the matte reference had to be modified to (k_{d}=1.157, k_{s}=0.019, α=0.138) so as to account for the most matte stimuli obtainable from the model. The 300×300 pixels reference images were obtained by cropping from 512×512 pixels parent images (the position of the crops being randomised for each stimulus).

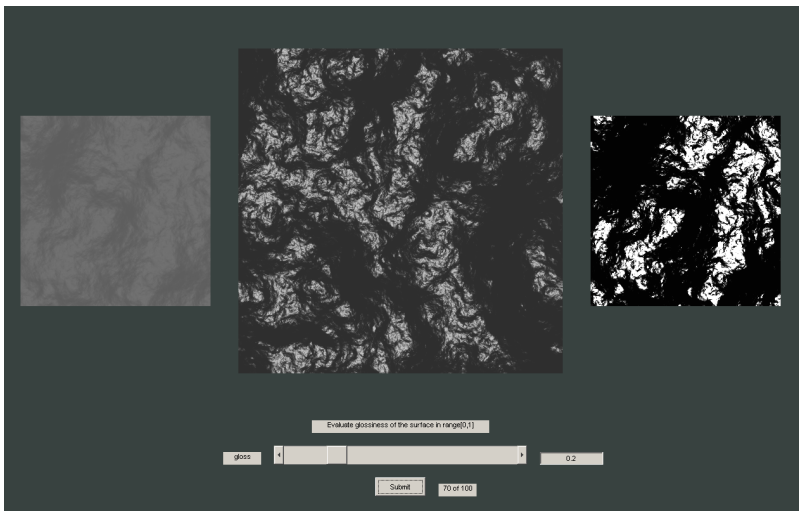

Figure 5.1: The experiment application interface: the stimulus image is shown in the middle, full size. Smaller reference images are shown on either side (extreme matte and extreme gloss).

5.2.2 Observers

The same ten observers used in the experiment described in Chapter 4 participated in the experiment.

5.2.3 Procedure

Prior to the experiment, observers were shown printed instructions below and a set of 15 training stimuli which were randomly chosen from the stimuli pool.

> You will be shown 100 images of textured surfaces. Your task is to evaluate the glossiness of these surfaces on the scale [0-1]. Please enter your value by slider and press button "Submit". As a guidance you will be shown extreme cases of matte and glossiness for such a surface side-by-side with the query image.

Observers were then shown the 100 stimuli images in a random order. The same magnitude estimation method as used in Chapter 4 was used again. The observers' task was to evaluate the magnitude of glossiness on the scale [0,1] by means of setting a value on a horizontal slider (see Figure 5.1), where 0 corresponds to the extreme matte on the left and 1 corresponds to the extreme gloss on the right. A number next to the slider bar indicated the current value. A submit button was clicked when the observer was satisfied with the gloss value and then the next trial was shown. There was a pause of one second between the trials to avoid point-wise comparison of two stimuli. All subjects finished the experiment in 30 minutes.

5.2.4 Results and Analysis

Experiment Results

The mean values of glossiness across all subjects from the experiment were plotted against k_d, k_s, and α (Figure 5.2). From this figure, we can observe that high glossiness is perceived for high values of k_s and low values of k_d and α.

We also computed the standard errors and observed a slight tendency to higher error (i.e., less consistent results across subjects) for combinations of both lower and higher values of k_d and k_s.

A three-way repeated-measures ANOVA was conducted on the results. Mauchly's test indicated that the assumption of sphericity had been violated for the main effects of k_d ($\chi^2(5) = 17.05$, $p < 0.01$), k_s ($\chi^2(9) = 32.18$, $p < 0.001$) and α ($\chi^2(9) = 31.5$, $p < 0.001$). Therefore the degrees of freedom were corrected using Greenhouse-Geisser estimates of sphericity ($\varepsilon_\mathrm{g} = 0.499$ for the main effect of k_d, 0.343 for the main effect of k_s and 0.394 for the main effect of α).

All effects were reported as significant ($p < 0.001$). The F-ratios for the three independent variables are k_d: $F(1.496, 13.467) = 32.919$, k_s: $F(1.373, 12.357) =$

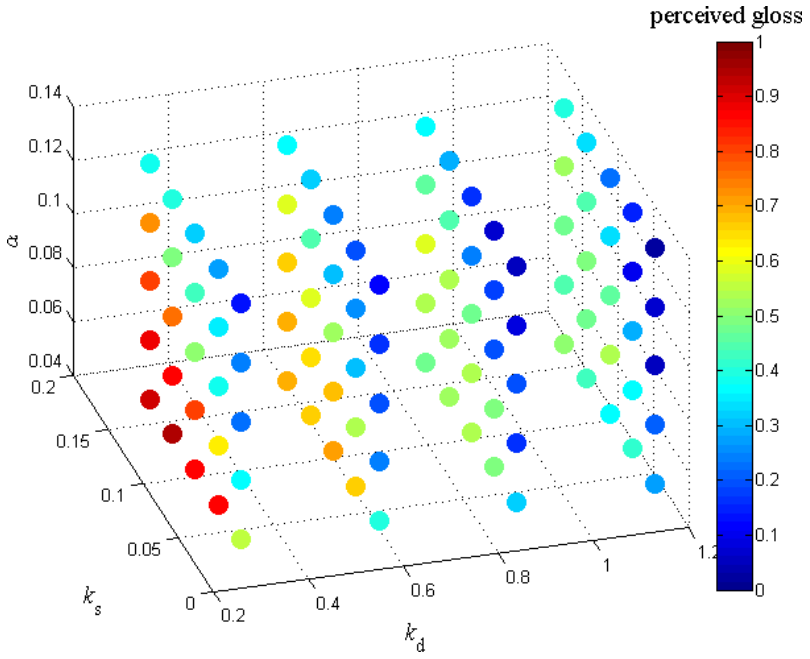

Figure 5.2: Result of the experiment. Mean values of estimated gloss averaged across all observers are plotted against the three Ward model parameters (k_s, k_s and α) by the colour of the dots. These are relative glossiness representing difference scales.

37.936, and α: $F(1.574, 14.166) = 62.427$.

There is significant interaction between k_d and α ($F(12, 108) = 10.106$, $p < 0.01$) and between k_s and α ($F(16, 144) = 7.499$, $p < 0.01$). The interaction between k_d and k_s was not significant ($F(12, 108) = 1.609$, $p = 0.1$). The interaction among k_d, k_s and α was significant ($F(48, 432) = 1.799$, $p < 0.01$). However, the small F-ratio values indicate that the interaction effects are low compared with the effects of the independent variables.

In summary, the statistical test shows that the perceived gloss is significantly affected by the three parameters k_d, k_s and α.

Trend analysis was performed by conducting polynomial contrasts to examine whether or not the group means increase proportionately with the variables. The tests of within-subjects polynomial contrasts show that k_d, k_s and α all have significant linear contrasts at $p < 0.001$. k_d: $F(1, 9) = 38.25$; k_s: $F(1, 9) = 45.09$; α: $F(1, 9) = 91.66$. This suggests that the perceived gloss measured in this experiment has a strong linear relationship with the Ward model parameters. Hence, it is appropriate to use multiple linear regression to analyse the results.

5.2.5 Multiple Linear Regression Model

Before applying multiple linear regression the Pearson correlation analysis was conducted for each variable (k_d, k_s, α and mean perceived gloss). The correlation coefficients between perceived gloss and each variable of k_d, k_s and α are $\rho = -0.398, 0.593, -0.566$ respectively. All have one-tailed significance at $p < 0.001$. The correlation coefficients between each pair of k_d, k_s and α are all below 0.001 at $p = 0.5$, indicating that there is no multicollinearity.

Multiple linear regression was conducted for the mean values of perceived gloss averaged across all observers. The prediction model is expressed in Equation 5.1.

$$G = (b_0 + b_1 k_\mathrm{d} + b_2 k_\mathrm{s} + b_3 \alpha) + \epsilon \tag{5.1}$$

where G is the outcome variable (perceived gloss); b_0 is the constant term; b_1, b_2 and b_3 are coefficients for the variable k_d, k_s and α respectively; and ϵ is the residual term.

The model coefficients b_0, b_1, b_2 and b_3 were obtained by the method of least squares. The resulting coefficients are: $b_0 = 0.757$, $b_1 = -0.267$, $b_2 = 2.814$, and $b_3 = -3.961$. Thus the linear model for the perceived gloss as a function of the Ward model parameters is shown in Equation 5.2.

$$G = (0.757 - 0.267 k_\mathrm{d} + 2.814 k_\mathrm{s} - 3.961 \alpha) + \epsilon \tag{5.2}$$

This model accounts for 83% of the variance ($R^2 = 0.83$, $F(3, 96) = 156.68$, $p < 0.01$). The adjusted $R^2 = 0.825$ shows a small difference for the final model (0.83-0.825=0.005, about 0.5%), indicating that the prediction model generalizes well. A value of 1.362 for Durbin-Waston statistic means the assumption of independent errors is tenable.

Additionally, diagnostics were conducted on the model. The t-statistic for each coefficient indicates that they are all significantly different from zero:

- k_d: $t(96) = -9.48$, $p < 0.01$;
- k_s: $t(96) = 14.11$, $p < 0.01$;
- α: $t(96) = -13.46$, $p < 0.01$.

The standardized model coefficients for k_d, k_s and α are $-0.398, 0.593, -0.566$ respectively, which indicate how much standard deviation the dependent variable increases when the independent variable increases one standard deviation.

Finally the behaviour of the residuals was investigated. A scatter plot is shown in Figure 5.3 for the regression standardized predicted values against regression standardized residuals. The random and even dispersion of the points indicates that the assumptions of linearity and homoscedasticity are met.

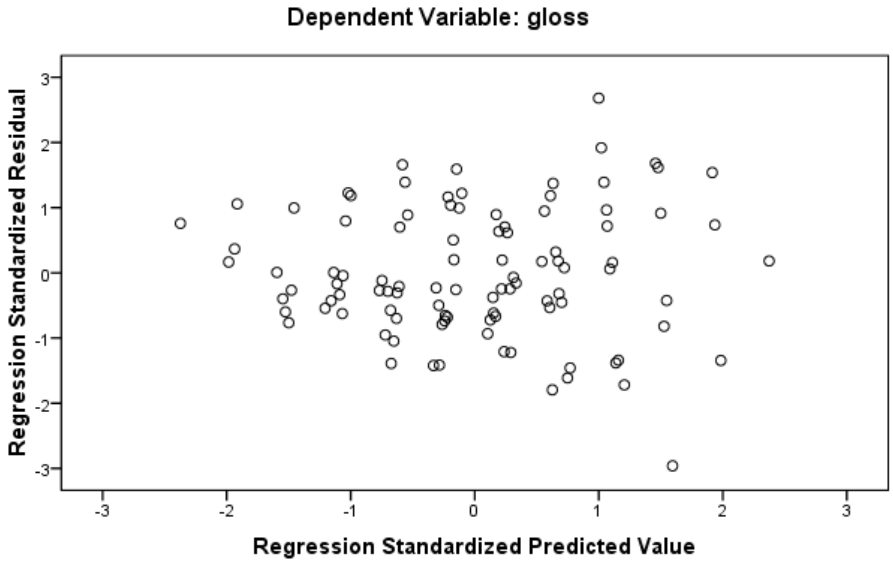

Figure 5.3: Scatter plot of regression standardized predicted value and residual.

The normality of residuals was also tested. The histogram of the standardized residuals is shown at the top of Figure 5.4, and the normal probability plot is shown at the bottom of Figure 5.4. The Kolmogorov-Smirnov test for normality shows a statistic $D(100) = 0.074$, $p = 0.197$, indicating that the normality of standardized residual is met.

The partial regression plots are shown in Figure 5.5, which are scatter plots of the residuals of the outcome variable (perceived gloss) against each of the predictors (k_d, k_s, α) when both variables are regressed on the remaining predictors. k_d and α show a negative relationship with perceived gloss and k_s shows a positive relationship.

In summary, the linear model relating perceived gloss and the Ward parameters appears to be accurate for the sample and generalizable to the population.

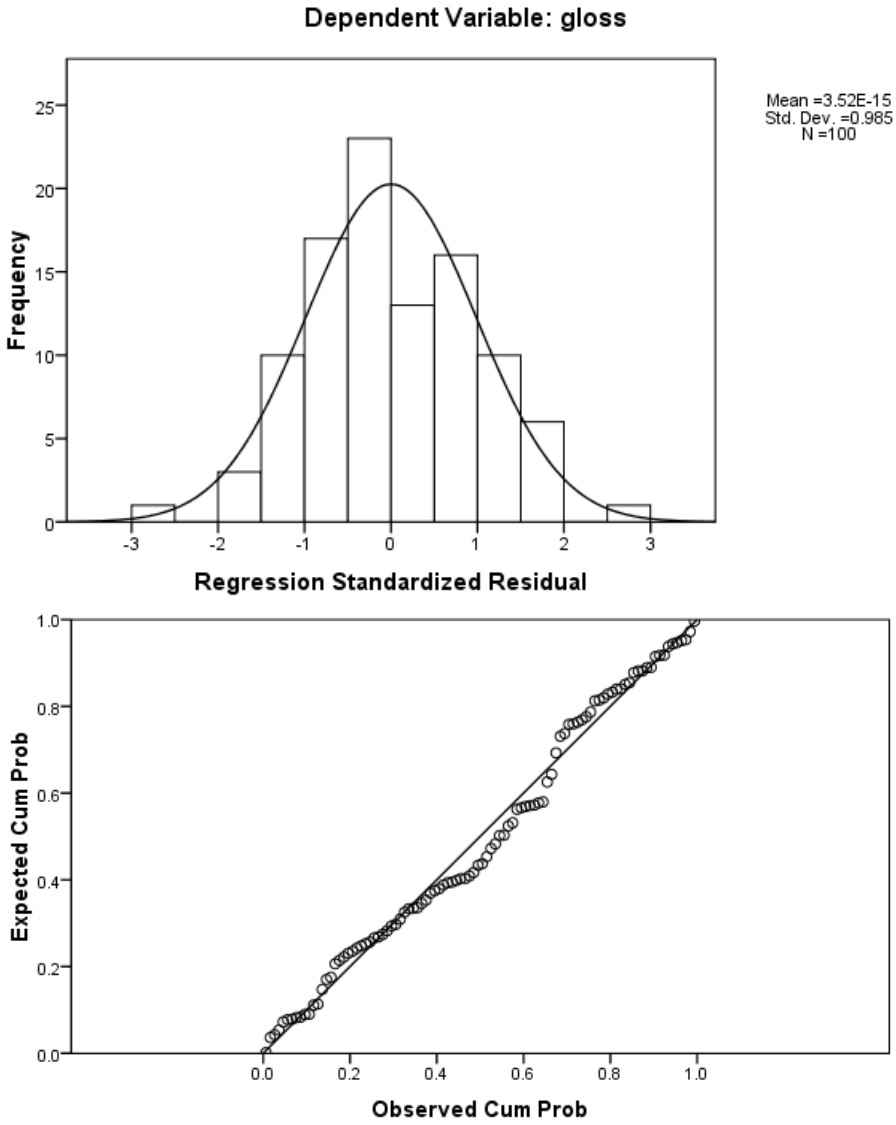

Figure 5.4: Histogram of regression standardized residual (top) and the normal P-P plot of normal probability (bottom).

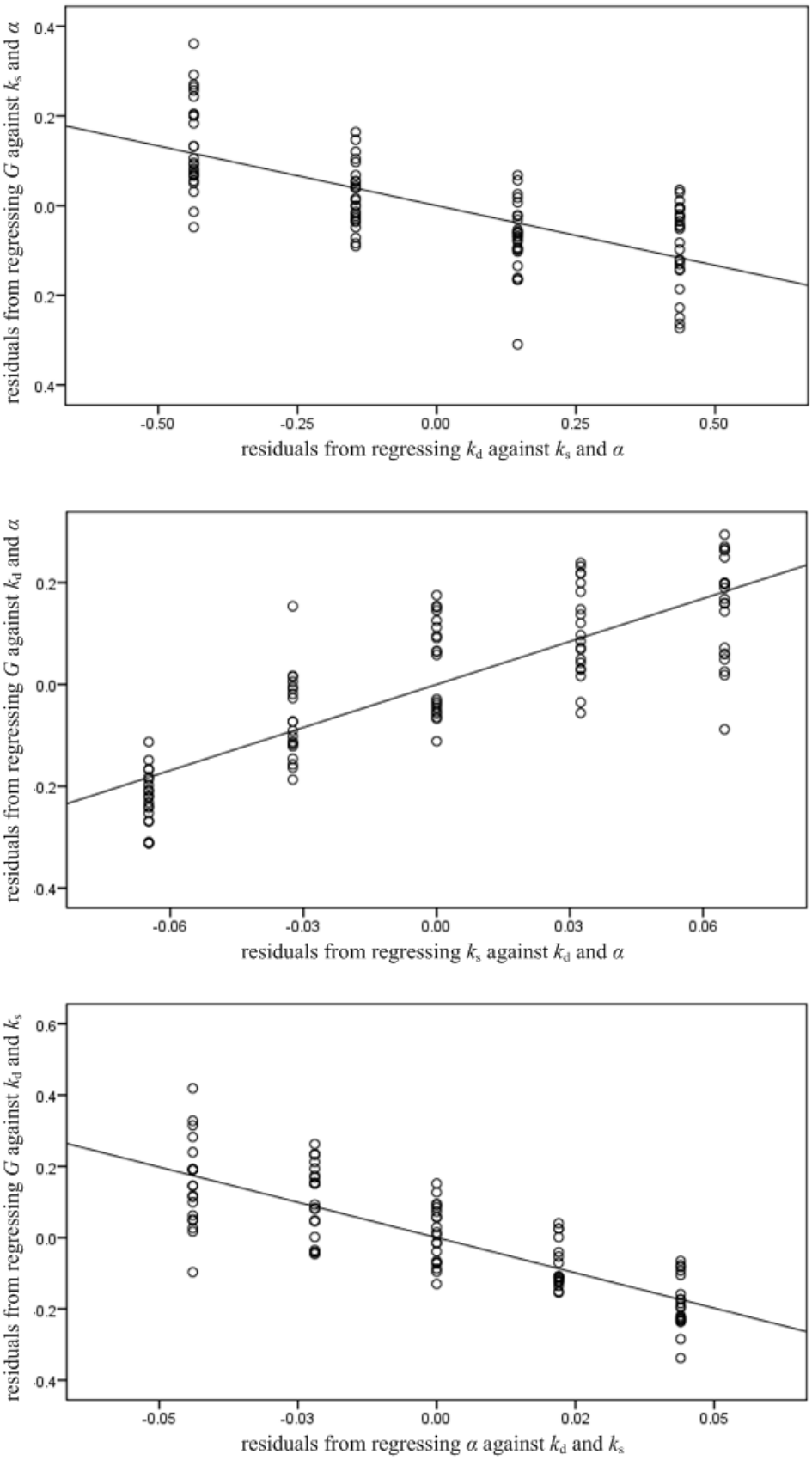

Figure 5.5: The partial regression plots of perceived gloss G against k_d, k_s and α respectively.

5.2.6 Summary

From this experiment, we found that perceived gloss is significantly affected by the three Ward model parameters and can be represented using a linear model (Equation 5.2).

5.3 Equivalence between Apparent Gloss of Lambertian Surfaces and Gloss of Ward Surfaces (Exp 2)

Having shown that the perceived gloss of a Ward model rendered $1/f^{\beta}$ surface can be represented as a linear function, we now investigate whether or not a Ward model used to render a moderate RMS roughness surface can be made to appear as glossy as the high RMS height Lambertian surfaces investigated in Chapter 4.

This investigation used the same rendering technique as described for the previous two experiments: collimated illumination and viewing direction were set perpendicular to the surface plane; the rendering algorithm was a local model of reflection without considering inter-reflections; $1/f^{\beta}$ noise surface with identical roll-off factor ($\beta = 2.3$).

The equivalence of perceived gloss between the two types of surface was investigated using an adjustment experiment. The observers were allowed to adjust the Ward parameters in order to adjust the perceived gloss such that it matched that of the high RMS height Lambertian surfaces. Details of this experiment are described below.

5.3.1 Stimuli

The ten Lambertian surfaces with different RMS roughness used as stimuli in the experiment of Chapter 4 were reused here as the reference surfaces (see Figure 4.3). The adjustable surfaces were rendered using the Ward model as described in Section 5.1, except the model parameters were initially randomised.

5.3.2 Observers

The same ten observers from Exp 1 participated in this experiment.

5.3.3 Procedure

In this experiment, observers adjusted the three Ward model parameters to produce a similar level of perceived gloss with the Lambertian surfaces (method of adjustment). Before the experiment, observers were shown printed instructions:

> Your task will be to match glossiness of image on left by changing three parameters modifying image on the right. You can change the parameters using three sliders below the image on the right. When you are satisfied with your settings please press button "Submit". Note, that the exact match might not be possible so please concentrate mainly on good match of glossiness.

Observers were randomly shown the ten surface images rendered by the Lambertian model with different RMS height (σ). These images were shown on the left side of the screen and observers were asked to match the glossiness of each of them by modifying the image on the right. The adjustment image was generated from the three Ward parameters, as set by observers using three sliders located below the image. To avoid point-wise comparison, a random rotation of 90°, 180°, 270° was applied to the right image. An example of an experimental screen is shown in Figure 5.6.

Observers had opportunity to become accustomed to the impact of the sliders on the surface appearance during their training session. Observers were instructed to take their time and try to match the glossiness of the surfaces as much as possible. All observers finished the experiment in 30 minutes.

5.3.4 Results and Discussion

The adjusted Ward model parameters are plotted for each Lambertian surface in Figure 5.7.

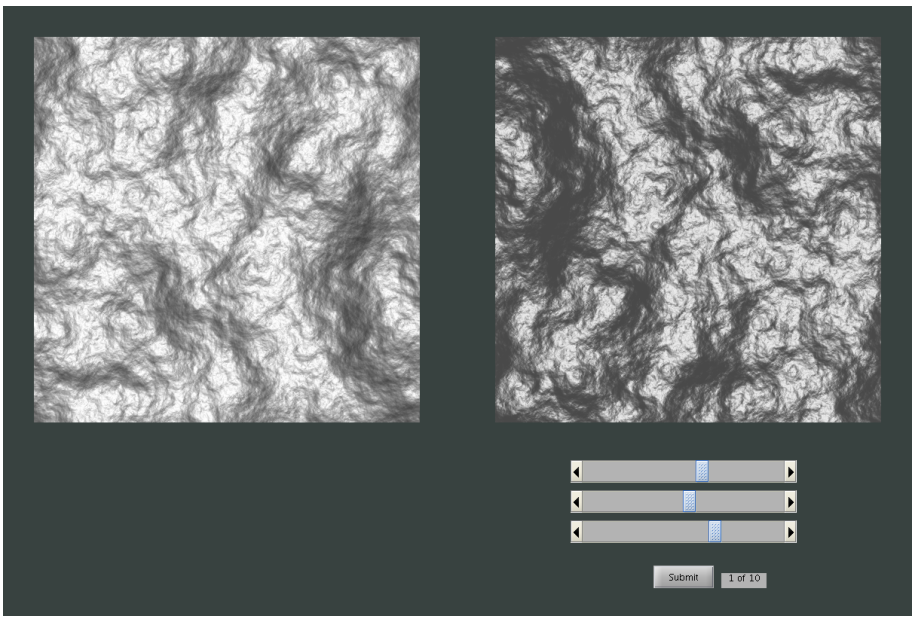

Figure 5.6: Example of the screen in the adjustment experiment.

A one-way repeated-measures ANOVA was conducted for each Ward model parameter against the Lambertian surfaces under Greenhouse-Geisser corrected degree of freedom. They showed that all three parameters are significantly varied when matching the gloss of high RMS height Lambertian surfaces and Ward surfaces.

- k_{d}: $F(3.88, 34.91) = 242.71$, $p < 0.001$
- k_{s}: $F(2.41, 21.70) = 93.12$, $p < 0.001$
- α: $F(2.34, 21.14) = 125.05$, $p < 0.001$

The experiment results were then averaged across all observers. The adjustment results from this experiment provided each Lambertian surface with a triplet of Ward model parameters. Figure 5.8 shows the locations of the ten Lambertian surfaces in the parametric space of the Ward model.

Using the linear model (Equation 5.2) developed in subsection 5.2.4, we estimated the perceived gloss of the adjustment surfaces from their Ward parameters. The estimated gloss is indicated by the colour of the dots plotted in the three-dimensional Ward parametric space (Figure 5.8) and plotted against the RMS height (σ) of the ten Lambertian surfaces in Figure 5.9. The latter implies that the perceived gloss of the adjustment surfaces increases monotonically with increasing RMS roughness of the Lambertian reference. This is consistent with the findings of Chapter 4. The estimated gloss and the perceived gloss of the high RMS height Lambertian surfaces

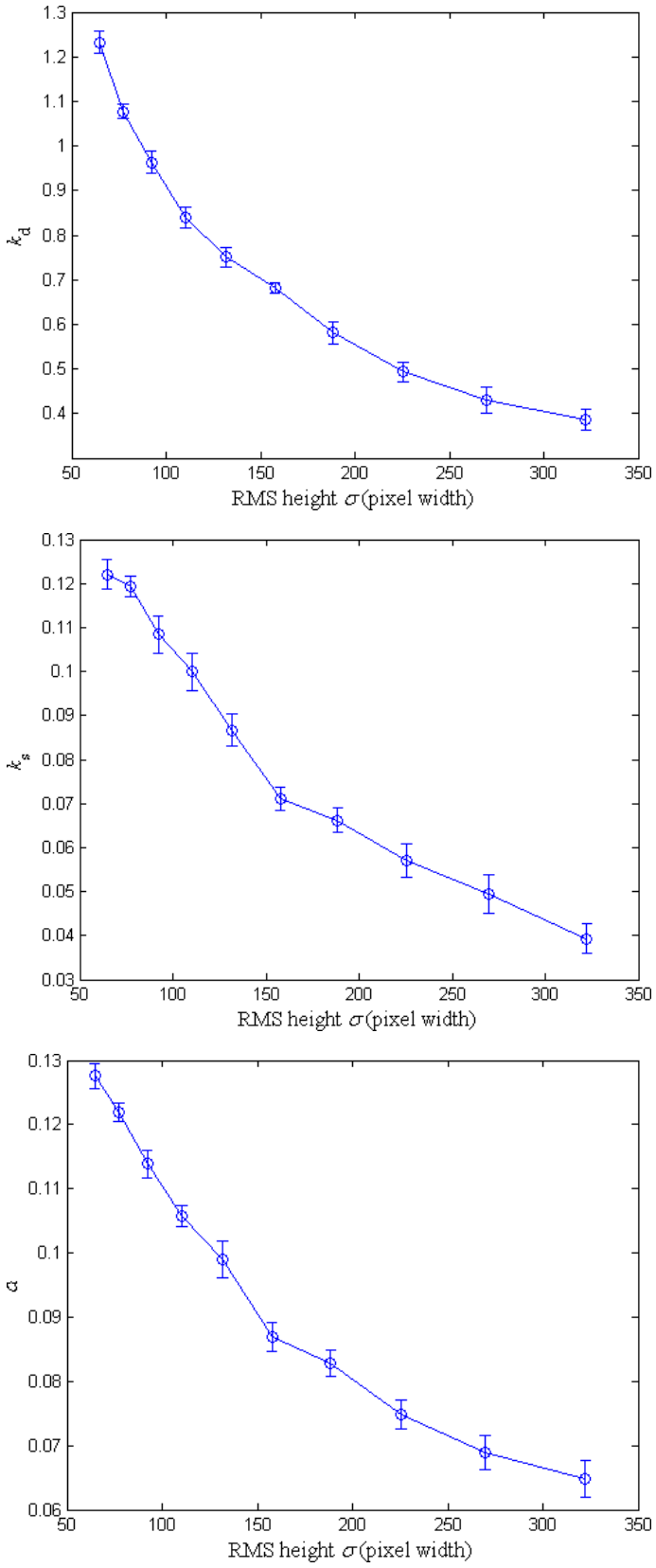

Figure 5.7: Result of the adjustment experiment. The means and ± standard errors across all observers are plotted for each of the three parameters of the Ward model against the RMS height (σ) of the Lambertian surfaces.

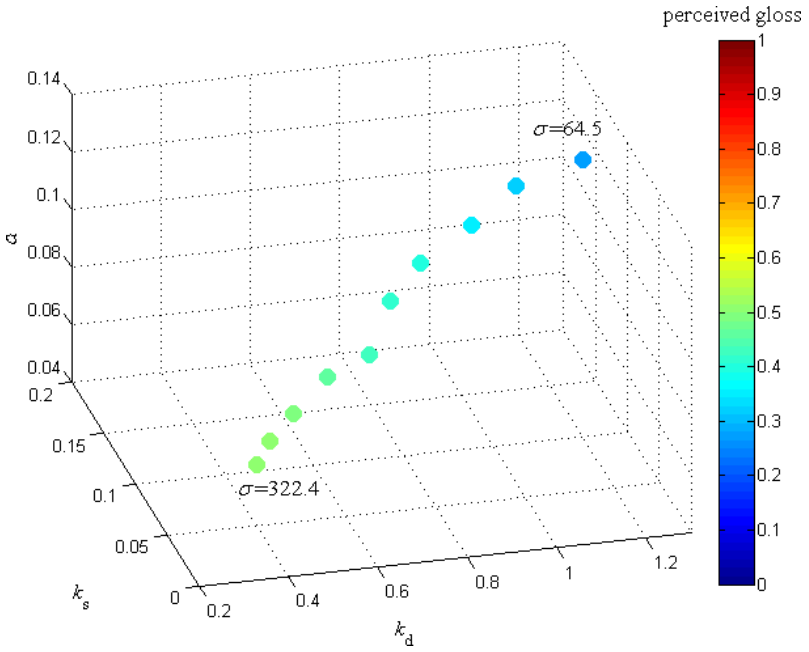

Figure 5.8: Scatter plot of adjustment results in the Ward parametric space. The derived Ward model parameters averaged across all observers are plotted as scattered dots in the Ward model parametric space. The estimated gloss of the adjustment surfaces from the linear model (Equation 5.2) are represented by the colour of the dots.

were plotted in Figure 5.10. Analysis of these data showed significant correlation with the Pearson coefficient $\rho = 0.93$, $p < 0.01$ (1-tailed).

5.4 Summary

In this chapter we measured the effect of variation of microscale (BRDF) parameters on perceived gloss of rough surfaces. Surface geometry was held constant. A $1/f^{\beta}$ noise surface with a low RMS roughness, and the same roll-off factor and random phase as those defined in Chapter 4 was used. The Ward BRDF model was sampled over a range of its three parameters (k_{d}, k_{s}, α).

The psychophysical experiment revealed that perceived gloss of $1/f^{\beta}$ surfaces is significantly affected by all three Ward model parameters. A linear model as a function of the three Ward parameters accounted for 83% of the variance.

The second half of this chapter has shown that moderate RMS roughness Ward surfaces may be adjusted by observers to have a similar level of perceived gloss

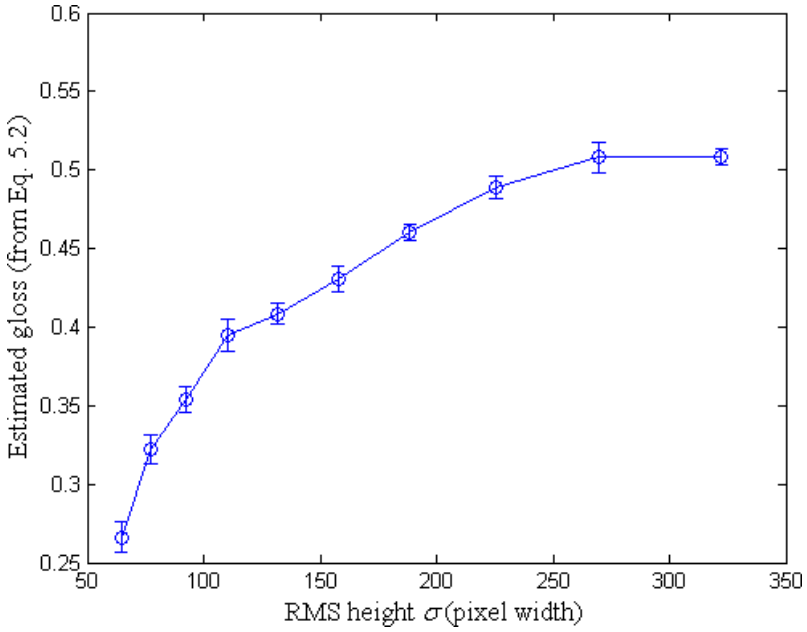

Figure 5.9: The estimated gloss of adjustment surfaces using the linear model (Equation 5.2) are plotted against corresponding RMS height (σ). The error bars denote the $\pm$ standard error across all observers.

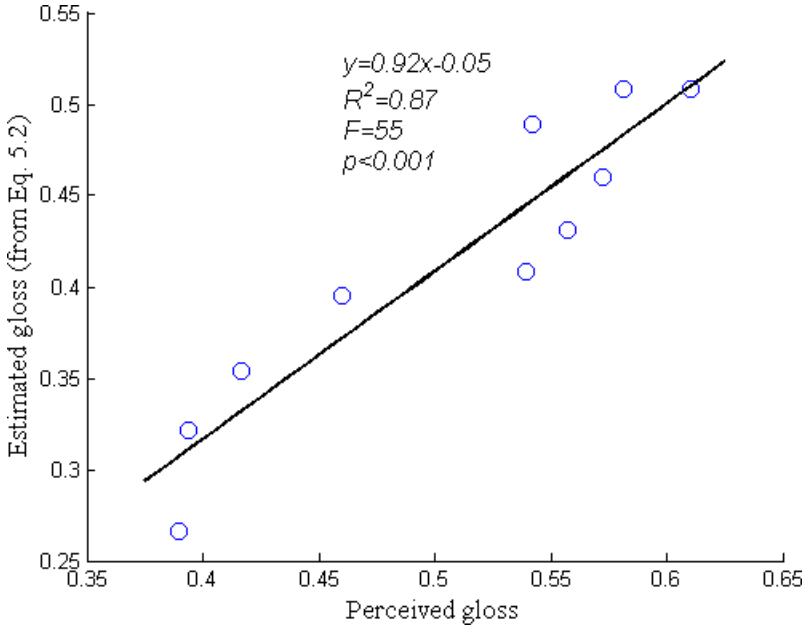

Figure 5.10: Perceived gloss of the Lambertian surfaces as investigated in Chapter 4 is plotted against the estimated gloss from the linear model (Equation 5.2). A regressed line is shown with statistics.

to high RMS height Lambertian surfaces, and this was confirmed using the linear model (Equation 5.2).

In the previous chapter we raised the hypothesis that the apparent gloss of the high RMS height Lambertian surfaces may be due to the rendering environment. In the next chapter therefore, we will model more realistic stimuli by improving the simple rendering system used in Chapters 4 and 5.

Chapter 6

MODELLING MORE REALISTIC STIMULI

The experiments reported so far have been used to investigate the effect of changing both mesoscale and microscale surface parameters on perceived gloss and were carried out under highly constrained conditions using simple rendering techniques. However, it is known that the perception of gloss is affected by several intrinsic and extrinsic factors. Previous studies reviewed in Chapter 2 have shown that more realistic stimuli can be obtained by making improvements in rendering techniques, reflection models, and illumination and viewing conditions.

The purpose of the work reported in this chapter therefore, was to specify a more realistic rendering system for later experiments, and to use this to investigate the apparent gloss of the high RMS height Lambertian $1/f^{\beta}$ surfaces used in Chapter 4.

The constraints imposed on the stimuli described in previous chapters are discussed in Section 6.1. Each will be discussed and relaxed in the following sections. The improved rendering technique is described in Section 6.2. The illumination is discussed and tested experimentally in Section 6.3. The animation stimuli are described in Section 6.4. All of these improvements are aggregated in Section 6.5. Section 6.6 summarizes the chapter as a whole.

6.1 Constraints in Previous Experiments

The aim of this section is to discuss the constraints in stimuli modelling imposed in previous chapters. This includes rendering technique, BRDF model, illumination and viewing conditions.

The rendering algorithm used in previous experiments employed a local model of reflection. Although the rendering is efficient, the stimuli are not of high fidelity. In the real world, incident light interacts with surfaces in a more complex manner (e.g. inter-reflections), resulting in effects such as indirect lighting, self-shadow, and soft-shadow. None of these effects were considered in previous experiments. In addition, the reflection models used in previous chapters were not physically based, especially the Lambertian reflection model which violates basic physical laws.

The white collimated perpendicular lighting used in previous experiments is not representative of natural lighting conditions. Illumination conditions have been found to be important when people infer surface properties [Dror et al., 2001a] [Dror et al., 2001b] [Dror et al., 2004] [Fleming et al., 2001] [Fleming et al., 2003]. People can infer familiar illumination conditions from the reflection on surfaces, and they can estimate surface properties more accurately under real-world illuminations than simple artificial illuminations [Fleming et al., 2003].

The use of still images is also a limitation. People cannot accurately or reliably estimate surface shape (geometry) from a single surface image under certain illumination conditions [Belhumeur et al., 1999] and accuracy of depth perception of surfaces affects perceived gloss [Kim et al., 2011] [Marlow et al., 2011].

Several approaches have been used by researchers to improve stimuli fidelity, including: rendering technique, illumination, object motion, binocular stereo viewing and head motion. These will be discussed in following sections.

6.2 Physically Based Rendering

As discussed in Chapter 2, the experiment stimuli used in this study are synthetic images simulated by computer algorithms. The fidelity of synthetic surfaces should approach the appearance of real-world surfaces. However, the simple rendering sys-

tem used in previous chapters does not meet this requirement well. To generate more realistic stimuli, we will describe a more advanced rendering technique: physically based rendering. The term "physically based" indicates that the rendering uses physical models and supports physical simulations of light and shading. The discussion will be split into two parts: path tracing and the BRDF model.

6.2.1 Path Tracing

It is technically impractical to trace every particle of light in a scene. Therefore, researchers have proposed many efficient rendering algorithms, which are employed by rendering packages. The techniques that are widely used in computer graphics fall into four loose categories: rasterization, ray casting, ray/path tracing and radiosity. The first two techniques are relatively fast but do not model advanced optical effects such as soft-shadows and inter-reflections, while radiosity is not usually employed as a rendering technique. Therefore, the path tracing method becomes the most suitable rendering technique for this study.

Path tracing simulates the physical behaviour of the light rays and provides better image quality than conventional rendering methods at the cost of expensive computations. Path tracing naturally simulates many effects that other methods do not, such as soft shadows and indirect lighting. To obtain high quality images from path tracing, a large number of rays must be traced to avoid visible artifacts.

In path tracing, rays are traced from the camera through the image plane to the scene, bounce off or pass through objects until they reach a light source or reach the preset maximum number of bounces. The resulting ray intensity is then written to the image. Path tracing technology has been used for rendering stimuli in many vision studies [Ho et al., 2008] [Pellacini et al., 2000] [Ferwerda et al., 2001] [Fleming et al., 2003], and it will also be used in this thesis.

The path tracer chosen in this study is LuxRender [LuxRender, 2009], which is a cross-platform and open source rendering package. It uses scene description files which can be exported from free, open source modelling software. The other main renderer, Radiance, was not chosen as it runs on and requires commercial software, which was unavailable during this study. LuxRender has its root in the Physically Based Rendering Toolkit (PBRT) [Pharr and Humphreys, 2004] and has advantages

in rendering efficiency. These two renderers (Radiance and PBRT) have been examined by David Brainard for simple scenes and found to be in good agreement [Brainard and Broussar, 2007].

The following will describe how we developed 3D geometry models of the surfaces and set parameters for the path tracing. More details about the path tracing rendering technique were described by Pharr and Humphreys [2004] and Ward [1994].

Surface Representation

The stimuli rendered by path tracing were created under the scene configuration as described in previous chapters. The $1/f^{\beta}$ noise surfaces were sampled at 512×512 pixels to generate height maps using Equation 3.1. Surfaces were represented by perturbing a mesh grid (512×512) with the magnitude determined by the height maps, a technique called 'displacement mapping'. This technology builds realistic surface geometry [Padilla, 2008]. The viewing direction was set perpendicular to the surface plane. Perspective projection was used instead of the orthogonal projection used previously. The 3D scene specification is completed by adding a light source and the path tracer can then render the image.

Tone Mapping

The images rendered by LuxRender are of High Dynamic Range (HDR) [Ward, 1994], which exceeds the dynamic range of the display used in the experiment. A linear tone mapping method was used to scale the images down to low dynamic range to suit the display monitor [LuxRender, 2009]. This method utilizes a camera model with three parameters: sensitivity, exposure and f-stop. HDR images were linearly translated to low dynamic range by multiplying a factor:

$$\frac{exposure * sensitivity}{10 * f\text{-}stop^2} * \left(\frac{118}{255}\right)^{gamma} \tag{6.1}$$

gamma was set to 1.0 to keep linearity. We manually tuned the parameters of the tone mapping method to keep most pixels ($> 95\%$) in the clamped range by cutting-off the out-of-range pixels to maximum intensity. The linear tone mapping parameters were kept constant throughout all succeeding experiments: $sensitivity = 50$, $exposure = 0.01$, $f\text{-}stop = 64$. Note that the parameter values chosen here are

not a normal setting for a real camera in practice, but they are possible in computer simulations and different combinations of parameter values can lead to an identical factor.

Number of Bounces

The number of bounces, which is the maximum number of times that a ray can bounce before it reaches the light source, is an important parameter in a path tracer. Multiple bounces cause indirect lighting, inter-reflections and soft shadows, which are important phenomena for a complex 3D scene or object. We tested this on the high RMS height Lambertian surface investigated in Chapter 4. A distant area light was used to approximate the collimated light source used previously. The Lambertian surface with RMS height $\sigma = 157.7$ (S_{σ_6}) was rendered by the path tracer with maxima of one bounce and three bounces. The rendered images are shown in Figure 6.1.

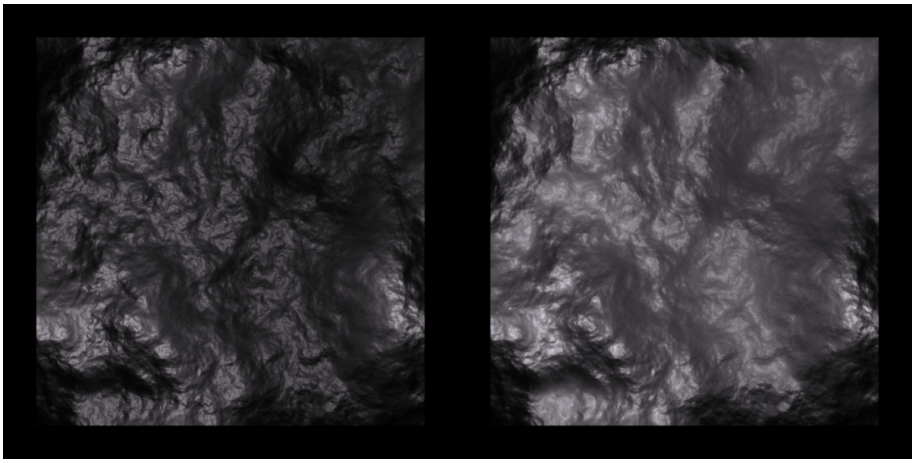

(a) maximum bounce=1 (b) maximum bounce=3

Figure 6.1: The Lambertian surface used in Chapter 4 (RMS height $\sigma = 157.7$) was rendered by path tracing with maximum bounce set to 1 (a) and 3 (b). A distant area light was used to simulate the collimated light. The path tracing rendered surface slope areas brighter in (b) because of inter-reflections. The apparent gloss was not observed by the author in (b).

Compared with the stimulus image labeled S_{σ_6} in Figure 4.3, the apparent gloss was eliminated for maximum bounce=3. More surface areas were illuminated by the simulated inter-reflections. This observation suggests that path tracing generates

more realistic stimuli. In all subsequent stimuli, the maximum number of bounces was set to 10.

6.2.2 BRDF Models

More realistic stimuli can be created by using BRDF models which obey physical laws, including:

1. positivity: $f_r(\boldsymbol{\omega_i}, \boldsymbol{\omega_o}) \geqslant 0$,
2. obeying Helmholtz reciprocity: $f_r(\boldsymbol{\omega_i}, \boldsymbol{\omega_o}) = f_r(\boldsymbol{\omega_o}, \boldsymbol{\omega_i})$,
3. conserving energy: $\forall \boldsymbol{\omega_i},\ \int_\Omega f_r(\boldsymbol{\omega_i}, \boldsymbol{\omega_o}) \cos\theta_o \, d\boldsymbol{\omega_o} \leqslant 1$.

However, the BRDF models used in previous chapters have limitations.

The BRDF model used in Chapter 4 is the Lambertian model, which is an empirical model. The Lambertian model does not obey rules of reciprocity or energy conservation and was only intended to be used as a model of diffuse reflection.

The Ward model used in Chapter 5 is also an empirical model but obeys the three physical laws identified above [Ward, 1992]. It was chosen in Chapter 5 due of its popularity in literature. However, we do not use it as the BRDF model for generating stimuli in subsequent experiments. Instead, we chose the Ashikhmin-Shirley model, based on the reasons described below:

- The Ward model is an empirical model which is loosely based on microfacet theory; while the Ashikhmin-Shirley model is physically-based but balances complexity and efficiency. The Ashikhmin-Shirley model achieves similar quality to strictly physical models such as the Cook-Torrance model [Cook and Torrance, 1982] but has simpler parametrization and computation [Kurt and Edwards, 2009].
- The Ward model has a uniform diffuse term that obeys the energy conservation law; while the Ashikhmin-Shirley model has a view-dependent diffuse term. Additionally, the Ashikhmin-Shirley model considers the Fresnel effect while the Ward model does not. These characteristics allow the Ashikhmin-Shirley model to produce more realistic rendering results [Ngan et al., 2005] [Kurt and Edwards, 2009].

- The Ward model is convenient for researchers using Radiance, as it is the built-in BRDF model [Ward, 1994]. However, in this study, the 'physically-based' path tracer LuxRender [LuxRender, 2009] was used, which employs the Ashikhmin-Shirley model. It is therefore easier to use the latter model for this study.

Based on the above discussion, the Ashikhmin-Shirley model was chosen as the BRDF model for all succeeding experiments.

6.2.3 Summary

In this section, we relaxed constraints and improved stimuli fidelity in terms of rendering technique and BRDF model. From the comparisons with previous rendering results, the physically based rendering (path tracing and Ashikhmin-Shirley model) appears to show considerable improvements over the simpler technique used previously and will be used in all subsequent experiments. The surface representation and parameter settings were also described and discussed. These settings were kept constant throughout the experiments described in the following chapters.

6.3 More Complex Illumination

The literature concerning gloss perception often uses simple lighting conditions [Ho et al., 2008] [Nishida and Shinya, 1998] [Wendt et al., 2008] [Wijntjes and Pont, 2010] [Pellacini et al., 2000] [Ferwerda et al., 2001]. This simplifies the stimuli modelling and reduces computational complexity. However, real-world illumination is complicated and its characteristics play an essential role in the perception of material properties [Dror et al., 2001a] [Dror et al., 2001b] [Dror et al., 2004]. Observers often perform more accurately and reliably when stimuli are viewed under real-world patterns of illumination [Fleming et al., 2001] [Fleming et al., 2003]. Fleming et al. [2004b] found that mirror reflections of the environment can provide reliable and accurate cues (constraints) on 3D shape. Recent research has shown that gloss perception is not constant under changing environments [Doerschner et al., 2010a] [Olkkonen and Brainard, 2010] [Olkkonen and Brainard, 2011] or illumination geometric changes [Ramanarayanan et al., 2007]. However, these studies were

performed using spheres or smooth objects, they did not use rough surfaces. Leloup et al. [2011] found that illumination conditions need to be considered for deriving perceived gloss metrics using real material samples.

The aim of this section, therefore, is to introduce a more realistic illumination condition into stimuli modelling. The simple collimated light used in Chapters 4 and 5 will be replaced by more complex illumination derived from real scenes. We will firstly show the advantage of using real-world illumination in producing more realistic stimuli by examining the apparent gloss of high RMS height Lambertian surfaces as reported in Chapter 4. The influence of variations in the complex illumination on the perceived gloss of rough surfaces will be discussed. At the end of this section, an illumination map will be chosen for subsequent experiments.

6.3.1 High Dynamic Range Real-World Environment Maps

Advanced capturing techniques and computer graphics make it possible to record real-world high dynamic range illumination maps [Debevec and Malik, 1997]. Such illumination maps can be used for the realistic rendering of synthetic objects and 3D scenes [Debevec, 1998]. The illumination map is an omnidirectional, high dynamic range image or spherical function that records the incident light at a particular point in 3D space.

It has been found that perceived gloss depends on the spatial distribution and strength of the light sources in the environment [Fleming et al., 2003]. Simple illumination models are inferior not only in the amount and strength of light sources but also in the familiarity of observers [Fleming et al., 2003]. High dynamic range environment maps from Debevec's Light Probe Image Gallery were chosen to provide the illumination in this study since they are widely used in computer graphics and vision research fields. Figure 6.2 shows three such environment maps (denoted as 'LF1', 'LF2', 'LF3'). The environment maps are in the format of angular maps, which cover the full 360×360 degrees, or 4π steradian range.

Fleming et al. [2001] and Fleming et al. [2003] found that the use of real-world illumination improves stimuli fidelity in gloss perception. We rendered the Lambertian surface S_{σ_6} (RMS height $\sigma = 157.7$) used in Chapter 4 using the path tracer described in the previous section under the illumination map 'LF3' (Figure 6.2(c)).

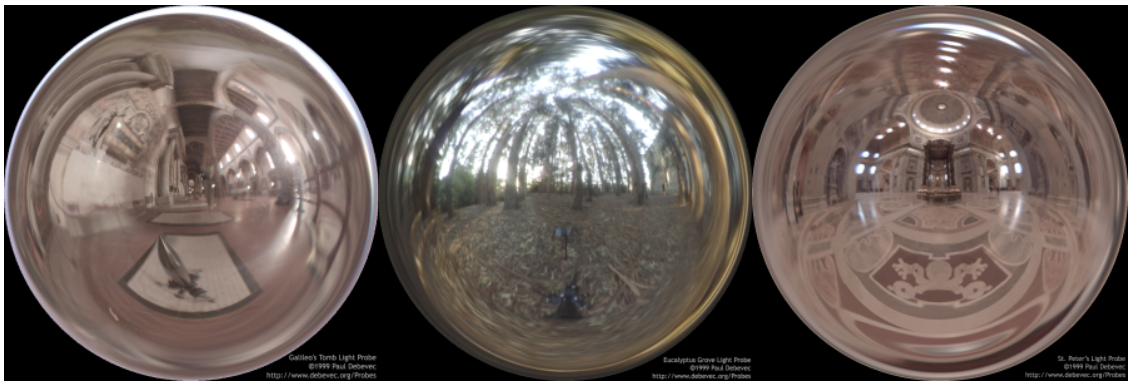

(a) LF1 'galileo' (b) LF2 'rnl' (c) LF3 'stpeters'

Figure 6.2: Angular maps of three real-world illuminations, all of which are from Debevec's Light Probe Image Gallery (http://ict.debevec.org/ debevec/Probes/). They are denoted by LF1, LF2, LF3 respectively. The abbreviation names from Debevec are also shown. Two of them are indoor environment (a) (c), and the other one is an outdoor environment (b). They are all tone mapped from high dynamic range for display.

The resulting image is shown in Figure 6.3. The apparent gloss of Lambertian surface S_{σ_6} was not observed by the author under environment map 'LF3'.

Therefore, the HDR real-world illumination map will be used as an improvement in modelling more realistic stimuli.

6.3.2 Variations within Environment Maps

Ramanarayanan et al. [2007] found visual equivalences by manipulating the illumination map, surface geometry and BRDF model. The manipulations of the illumination map used were blurring and warping.

Dror et al. [2004] used spherical harmonics to characterise real-world illumination maps. They found that they were well approximated by $k/L^{2+\eta}$ with η small, where L is the spherical harmonic order and k is a constant. They reported that spatial maps of natural illumination show statistical regularities similar to those found in natural images [Simoncelli and Olshausen, 2001], where natural images have a linear log-log roll-off power spectra of $1/f^{2+\eta}$ [Mandelbrot, 1983] [Voss, 1988].

As spherical harmonics can be thought of as the equivalence of a Fourier series

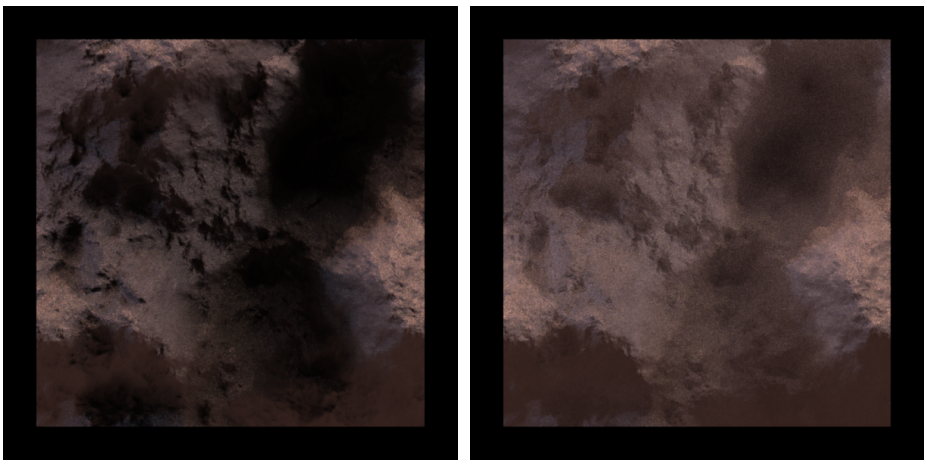

(a) maximum bounce=1 (b) maximum bounce=10

Figure 6.3: The Lambertian surface with $\sigma = 157.7$ used in Chapter 4 was illuminated by the environment map shown in Figure 6.2(c). It was rendered using path tracing with maximum bounce 1 (a) and 10 (b). The surface image with maximum bounce 10 shows brighter slope areas because of inter-reflections. The apparent gloss was not observed under the environment map in either images.

decomposition but performed in the spherical domain, we decided to use them as a tool to manipulate our environment. Figure 6.4 shows the result in applying such filtering to our environment maps. They were decomposed and then reconstructed using the first nine spherical harmonics as it has been found that these harmonics correspond to ambient light and are sufficient for diffuse rendering [Ramamoorthi and Hanrahan, 2001]. A glossy $1/f^{\beta}$ noise surface was rendered under the original and filtered environment maps. The results are shown in Figure 6.5. It can be seen that the surface does not appear glossy when rendered under the filtered environment maps. Even though the surface in Figure 6.5(d) looks very bright, it does not look glossy compared with the top row.

Therefore, the illumination environment chosen for generating glossy appearance should contain concentrated light sources as characterised by higher frequency harmonics as well as ambient light [Fleming et al., 2003] [Dror et al., 2004].

6.3.3 Changing Environment Maps

Due to resource limitations, we chose to use only one environment map for the subsequent experiments. The influence of changing illumination maps on gloss perception

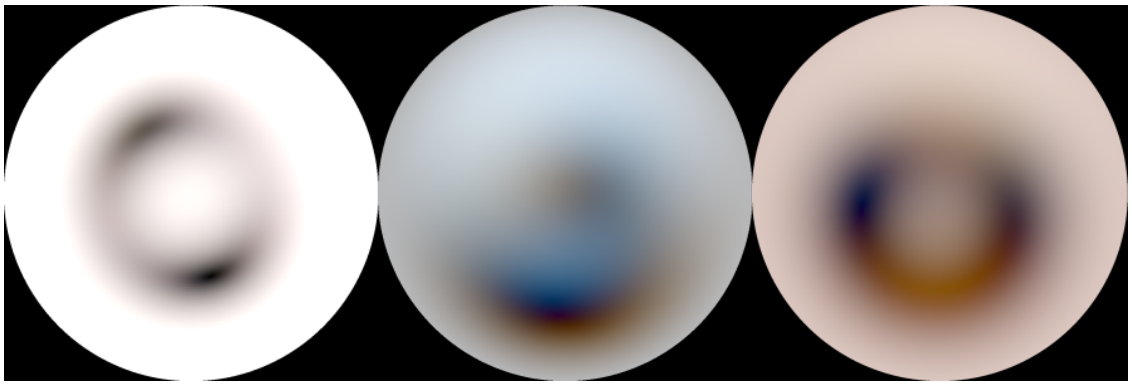

(a) LF1 'galileo' (b) LF2 'rnl' (c) LF3 'stpeters'

Figure 6.4: Reconstructed environment maps of those shown in Figure 6.2. They were decomposed into spherical harmonics and reconstructed using the first nine harmonics. The high frequencies which correspond to strong concentrated light sources have been removed and only the ambient component is left.

is discussed in this subsection using $1/f^{\beta}$ noise surfaces.

This was carried out in a repetition experiment of Doerschner et al. [2010a], who investigated the effect of illumination variation on gloss transfer functions. They investigated the perception of gloss on synthetic spheres as a function of three real-world illumination maps. They found linear gloss transfer functions between any two illumination maps. These transfer functions also exhibited a linear transitivity pattern.

We repeated Doerschner et al. [2010a]'s experiment to examine whether the perceived gloss transfer functions across illumination maps are also linear and transitive, however, we replaced the spheres that they had used with $1/f^{\beta}$ rough surfaces. The experiment is described in Appendix B.

The experimental results showed that the linear gloss transfer function between illumination maps does not exist across all observers and the linear transitivity of the transfer functions was not observed. For rough surfaces, the variation of perceived gloss between different illumination maps cannot simply be modelled or predicted using linear functions.

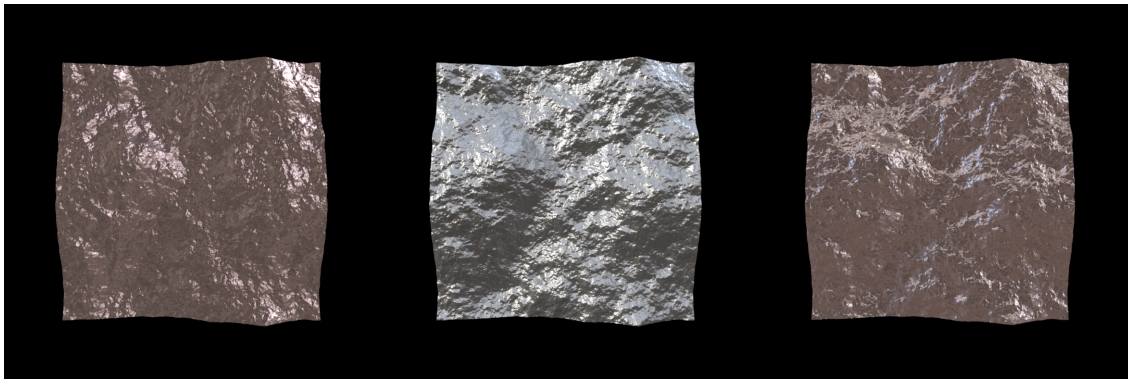

(a) LF1 original (b) LF2 original (c) LF3 original

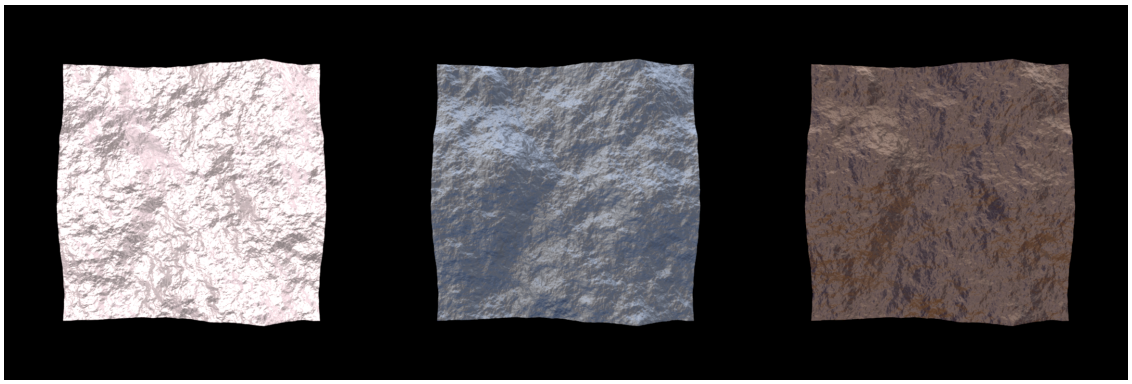

(d) LF1 filtered (e) LF2 filtered (f) LF3 filtered

Figure 6.5: A surface with gloss microscale parameters was rendered using the original (top row) and filtered (bottom row) environment maps (Figure 6.2 and Figure 6.4 respectively). The surface is a $1/f^{\beta}$ noise surface with roll-off factor $\beta = 2$, the Ashikhmin-Shirley BRDF model parameters are $k_{\mathrm{d}} = 0.4$, $k_{\mathrm{s}} = 0.6$, $\alpha = 0.01$. The surface does not look glossy under the filtered environment maps, although (d) is very bright.

6.3.4 Summary

Although the effect of illumination on perceived gloss is not part of the primary focus of this thesis, tests and experiments were conducted using HDR environment maps. We found that: 1) real-world illumination contributes to more accurate and reliable gloss perception of rough surfaces than simple illumination; 2) "glossy" $1/f^{\beta}$ surfaces viewed under an illumination environment that only contains the first nine spherical harmonics do not appear glossy (as predicted by Dror et al. [2004] and Fleming et al. [2003]); 3) the perceived gloss of rough surfaces is not linearly predictable under changing illumination maps.

Due to the problem complexity, only one environment map was used to provide illumination in succeeding experiments. We chose the "St. Peters" environment map from Debevec's Light Probe Image Gallery (LF3 in Figure 6.2). This map has the largest resolution (1500×1500) and dynamic range ($200,000 : 1$) among those in the gallery, and is popular in the literature [Doerschner et al., 2010a] [Fleming et al., 2003] [Dror et al., 2004].

6.4 Animated Stimuli

Viewing surfaces from different directions helps people perceive not only surface 3D geometry but also surface gloss [Obein et al., 2004b] [Wendt et al., 2007] [Wendt et al., 2008] [Sakano and Ando, 2008a] [Sakano and Ando, 2010] [Sakano and Ando, 2008b]. Images differing in relative viewpoint may be produced using three methods: binocular viewing, head motion and surface motion.

In binocular viewing, three-dimensional surface geometry viewed by two eyes in different positions produces two slightly different images. Human vision systems are good at fusing these two images to provide information on depth and 3D shape. Furthermore, specular reflection is also viewpoint dependent [Wendt et al., 2007] [Wendt et al., 2008]. The highlight disparity has been found to enhance the authenticity and strength of perceived gloss [Wendt et al., 2007] [Wendt et al., 2008] [Sakano and Ando, 2008a] [Sakano and Ando, 2010]. The correct perception of surface geometry (depth perception) from binocular viewing can help observers perceive other surface properties, such as removing the illusory gloss of high RMS height Lambertian sur-

faces. Figure 6.6 shows the binocular cross-view image pair of one of the Lambertian surfaces used in Chapter 4. The illusory gloss was not observed in binocular viewing since the abnormal depth of the surface is more clearly interpreted.

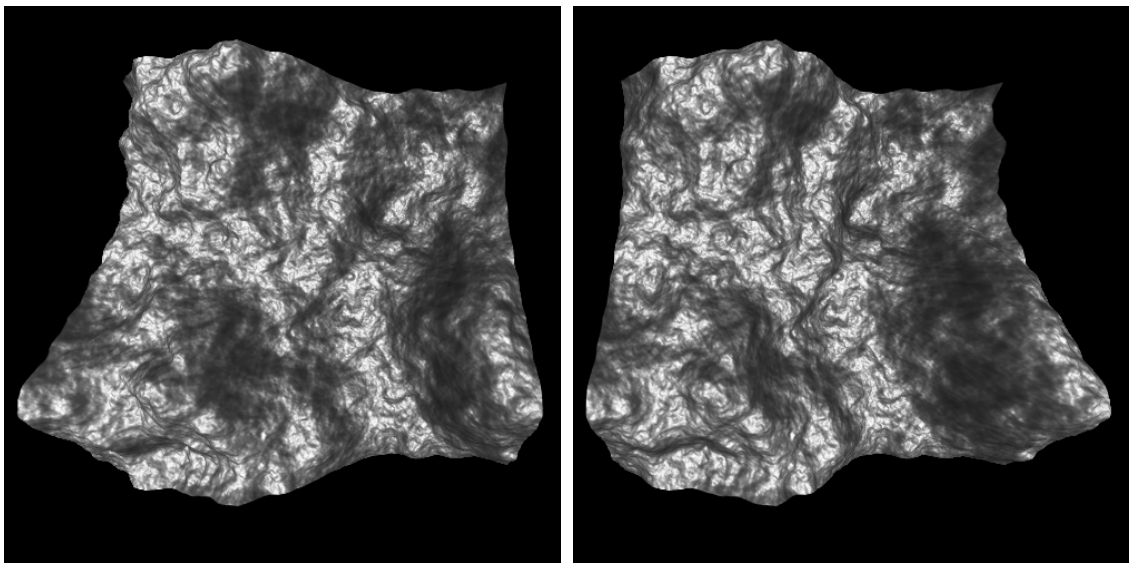

(a) S_{σ_6}, R (b) S_{σ_6}, L

Figure 6.6: The Lambertian surface with RMS height $\sigma = 157.7$ used in Chapter 4 is rendered with perspective projection and binocularly (cross-viewing). The apparent gloss was not observed.

Motion parallax [Gibson et al., 1959] or kinetic depth effect [Wallach, 1953] [Koenderink, 1986] (the relative change in position between surface and observer) can improve the perception of surface shape (geometry) and highlight depth. Anderson and Kim [2009], Kim et al. [2011] and Marlow et al. [2011] have shown that people can perceive gloss more accurately when the surface shape is correctly interpreted. Ji et al. [2006] asked observers to hold and freely tilt real samples in their experiment. These researchers believe that surface motion can help observers inspect surface property and infer surface gloss. Furthermore, the dynamic change of specular reflections on moving surfaces provides additional information for surface reflection property estimation.

After considering the three methods of providing images from different viewpoints to observers, we decided to use motion of the surfaces with fixed observers viewing monocular stimuli. Furthermore, we decided to pre-render the stimuli animations because of computational reasons.

Dijkstra et al. [1995] have shown that it is possible to detect shape from small field

stimuli ($< 8°$) when using object rotation. A range of $[-12°, 12°]$ was therefore used. The surfaces were rotated about their vertical axes 25° in 1° steps at 24 frames per second, producing animations of the surfaces rotating backwards and forwards.

The limitations of this simplified animation are:

- the surface rotation is a subset of that used by Padilla [2008];
- the chosen rotation angles were not derived by experiment, as in Padilla [2008], but preset by the author, since observer preference cannot be easily obtained under the non real-time rendering used in this research.

Despite the limitations described above, the animation stimuli are far more informative than the still images used in previous chapters.

6.5 Towards More Realistic Stimuli

A rendering system has been specified for generating more realistic stimuli. It comprises of a physically based path tracer (LuxRender), a physical BRDF model (the Ashikhmin-Shirley model), an HDR real-world environment map ("St. Peters" environment map from Debevec's Light Probe Image Gallery), and rotating surface animations.

This method of modelling more realistic stimuli will be used in subsequent experiments.

6.6 Summary

In this chapter, certain constraints of the simple rendering system described in Chapters 4 and 5 were cautiously relaxed and tested.

Path tracing was used to replace the simple single-bounce pixel-wise calculations and we showed that it provides more realistic stimuli that incorporate self-shadows and inter-reflections. BRDF models were discussed and the Ashikhmin-Shirley model was chosen for subsequent experiments because of its balance of complexity, efficiency and convenience. The illumination was tested experimentally and an HDR environment map was chosen to provide more realistic lighting. Finally, to improve

the perception of observers on surface geometry and specular reflection, animations of rotating surfaces were used instead of still images.

The gloss of high RMS height Lambertian surfaces reported in Chapter 4 was not apparent when these rendering improvements were used, suggesting that the gloss perceived is likely to be an artifact of the simple rendering system employed in Chapter 4 and by Wijntjes and Pont [2010].

With the more realistic stimuli, the effect of mesoscale and microscale roughness on perceived gloss will be investigated in the following chapters.

Chapter 7

THE EFFECT OF MESOSCALE ROUGHNESS ON PERCEIVED GLOSS

Chapter 4 showed that under certain conditions, variation of the surface mesoscale parameter σ can significantly affect gloss perception even when a 'matte' microscale reflection model is employed [Wijntjes and Pont, 2010]. Ho et al. [2008] also found that increasing mesoscale surface 'bumpiness' increases perceived gloss. In Chapter 4 we reported that the increasing trend of perceived gloss is not obvious for surfaces with $\sigma > 150$; Ho et al. [2008] reported "the trend was less clearly monotonic" for their highest bump level surface. This observation inspired us to further investigate the perceived gloss of rougher surfaces.

The previous chapter introduced a more sophisticated rendering environment. In this chapter we use this environment to investigate the effect of changing mesoscale roughness on gloss while holding the microscale surface parameters constant.

Padilla [2008] showed that varying the mesoscale roughness parameter, RMS height (σ) has the limitation that surfaces with high σ appear unrealistic, whereas variation of the roll-off factor β could produce realistic surfaces over a higher perceived roughness. Hence, we decided to investigate the effect of this mesoscale roughness parameter (β) on perceived gloss.

7.1 Experiment

This experiment used the method of magnitude estimation to investigate the relationship between perceived gloss and the mesoscale roughness parameter (β).

7.1.1 Stimuli

$1/f^{\beta}$ noise surfaces were synthesized for 14 levels of roughness with β=1.5 to 2.8 in steps of 0.1. The RMS height was held constant at $\sigma = 17$ pixel width. The surfaces used in previous experiments were generated using a fixed random phase spectrum with seed $\Theta = 0$. This constraint was removed in this chapter. Surfaces were generated using varied seeds with Θ sampled from 1 to 14 in steps of 1. It has been found by Padilla [2008] that variation of random phase does not affect perceived roughness. We also found that it does not affect perceived gloss (see pilot experiments described in Appendix C).

The rendering of surfaces used the method described in Chapter 6. The parameters of the Ashikhmin-Shirley model were set to a medium gloss level ($k_{\mathrm{d}} = 0.4$, $k_{\mathrm{s}} = 0.6$, $\alpha = 0.01$). Note that the gloss level (α) used in producing stimuli was chosen to be lower than that required to exhibit DOI gloss [Pellacini et al., 2000] [Ferwerda et al., 2001]. Figure 7.1 shows the central frame images ($slant = 0°$) of each animation stimulus, and the last two images show the surface with $\beta = 2.8$ under *slant* angles $12°$ and $-12°$ respectively.

7.1.2 Observers

Nine naïve observers with normal or corrected to normal vision were paid to participate in the experiment. All were students or University employees working in different fields, were less than 35 years of age, mixed gender and nationalities.

7.1.3 Procedure

Example images of glossy spheres and surface textures were shown to observers before the experiment to enable observers to be aware of the property we were

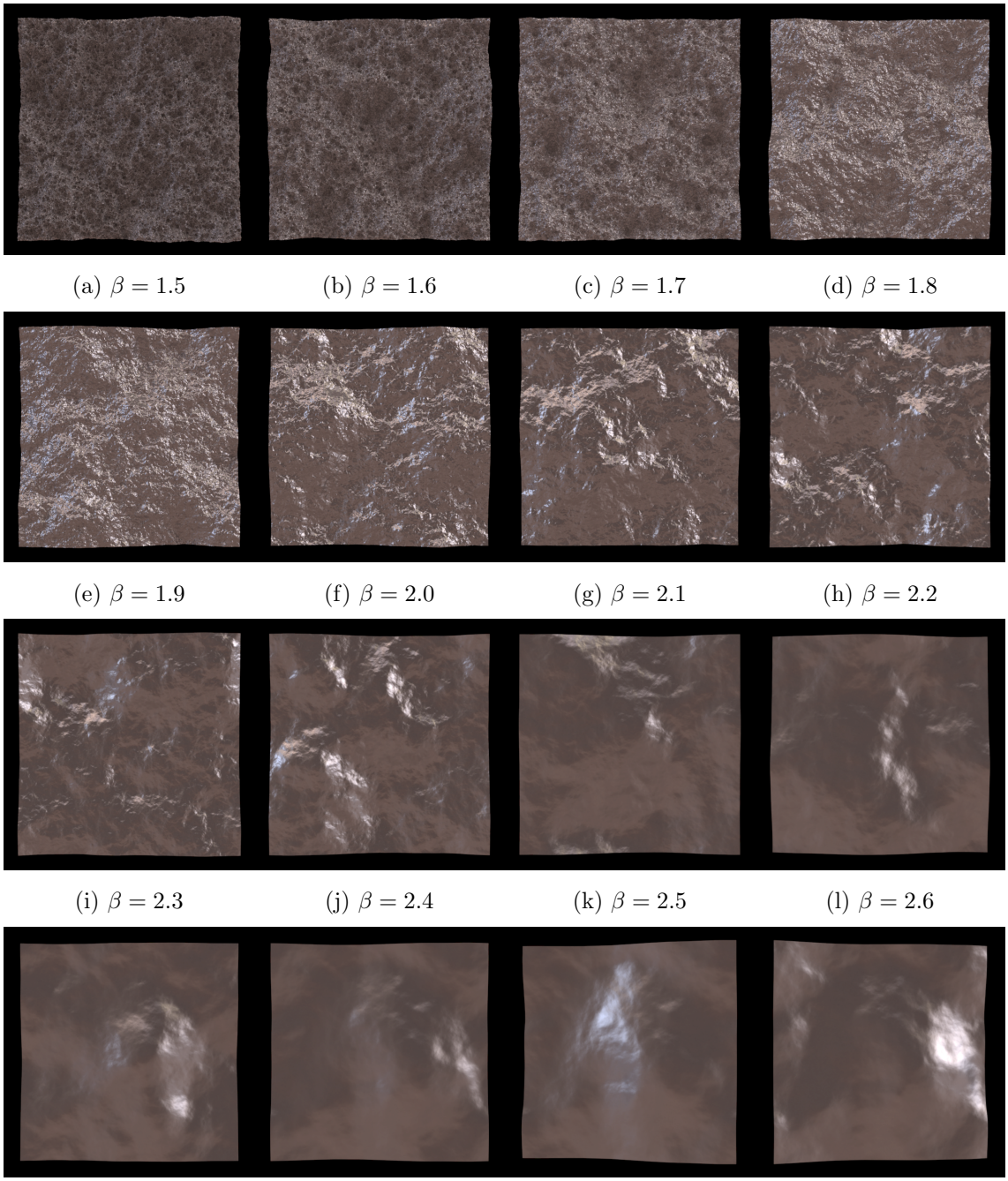

(a) $\beta = 1.5$ (b) $\beta = 1.6$ (c) $\beta = 1.7$ (d) $\beta = 1.8$

(e) $\beta = 1.9$ (f) $\beta = 2.0$ (g) $\beta = 2.1$ (h) $\beta = 2.2$

(i) $\beta = 2.3$ (j) $\beta = 2.4$ (k) $\beta = 2.5$ (l) $\beta = 2.6$

(m) $\beta = 2.7$ (n) $\beta = 2.8$ (o) $\beta = 2.8, s = 12°$ (p) $\beta = 2.8, s = -12°$

Figure 7.1: (a)-(n): The central image (slant angle 0°) of rendered surface textures with β varying from 1.5 to 2.8. (o)(p): surface $\beta = 2.8$ under slant angle 12° and $-12°$. These images have been adjusted by a nonlinear gamma for display purpose. Linear scaling was used for the stimuli shown to observers.

focusing on. In the experiment, observers were shown thumbnail images (239*239 pixels) of all 14 surfaces which were randomly positioned on the screen in a 4×4 matrix (the last 2 are blanks) on a secondary monitor. This monitor is of the same model as the one described in Chapter 4, and it was calibrated to the same settings (see Section 4.2). The thumbnail images were not animated having a surface slant of $0°$. Clicking any thumbnail provided the full resolution animation of the surface on the main monitor. Observers were able to view the full size animations in any order and for any duration.

In the pilot experiment, observers reported that stimuli not only exhibit different levels of glossiness but also seem to be made of different materials. Therefore we designed two tasks. First, observers were asked to provide a number that represented the 'gloss' strength of each surface (magnitude estimation). Both the range and precision of the number were unconstrained ('free modulus method' [Han et al., 1999]). Secondly, observers grouped these surfaces by assigning a group number to each surface according to the materials they thought they were made of. In other words, surfaces in the same group were thought by observers to be made of the same material. No time restrictions were imposed. All of the observers finished the experiment in between 30 and 45 minutes. The following instructions were shown to observers on a printed paper before the experiment:

> You will be presented with several surface thumbnails in a window. Clicking any thumbnail will show the full resolution rotating surface animation in the other window. You will finish two tasks:
>
> 1. Tell me how glossy each surface is by assigning a number to its glossiness. Call the first surface any number that seems appropriate to you. Then assign numbers to other surfaces in such a way that they reflect your impression of how glossy they are. You can modify your decision at will. There is no limit to the range of numbers that you may use. You may use whole numbers, fractions, or decimals. But try to make each number match the glossiness that you see.
> 2. Group these surfaces by assigning a group number to each surface so that the surfaces in the same group are made of the same materials.

7.2 Results and Analysis

7.2.1 Gloss Estimation Results

Magnitude estimation results for all 9 observers are shown in Figure 7.2.

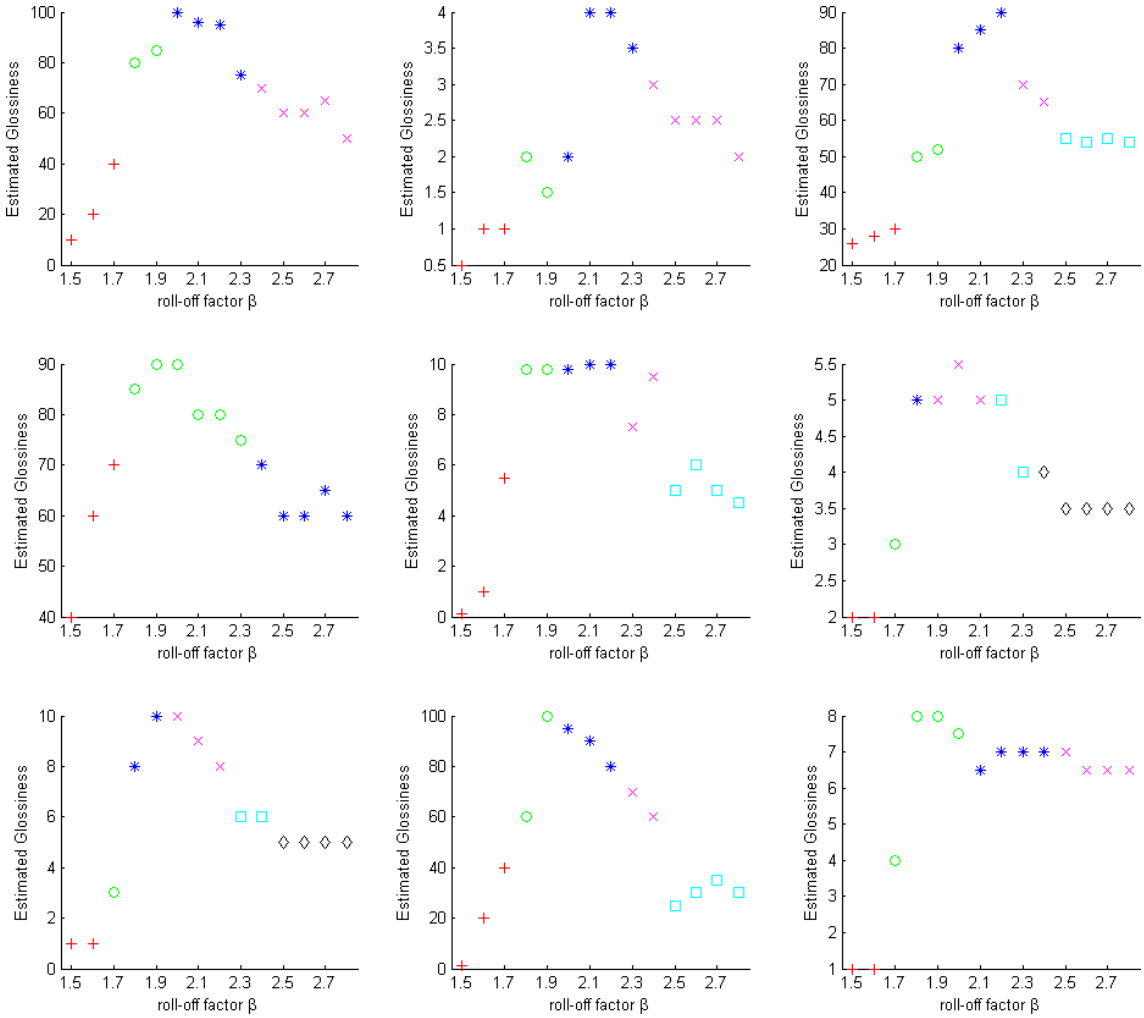

Figure 7.2: Gloss estimation and free grouping results of all 9 observers. The x-axis denotes the roll-off factor β and the y-axis denotes the raw estimated gloss. The free grouping results are shown by the markers of different shapes and colours. Note that the numbers of groups are different across observers (between 3 and 6), thus we used up to 6 markers to denote the grouping results ('red plus sign', 'green circle', 'blue asterisk', 'magenta cross', 'cyan square' and 'black diamond'). The same markers used in different plots do not indicate any between-subject relationship.

In the gloss magnitude estimation experiment, observers picked their own numbers. Hence, both the numeric range and precision differed across observers. To analyze the results, we normalized the raw data of each observer by its minimum and max-

imum values. The arithmetic means of normalized results averaged across all nine observers are shown in Figure 7.3. As the geometric means are also useful for showing trends of un-normalised data [Ehrenstein and Ehrenstein, 1999] [Gescheider, 1997] [Stevens et al., 1986], we also plotted these data in Figure 7.3.

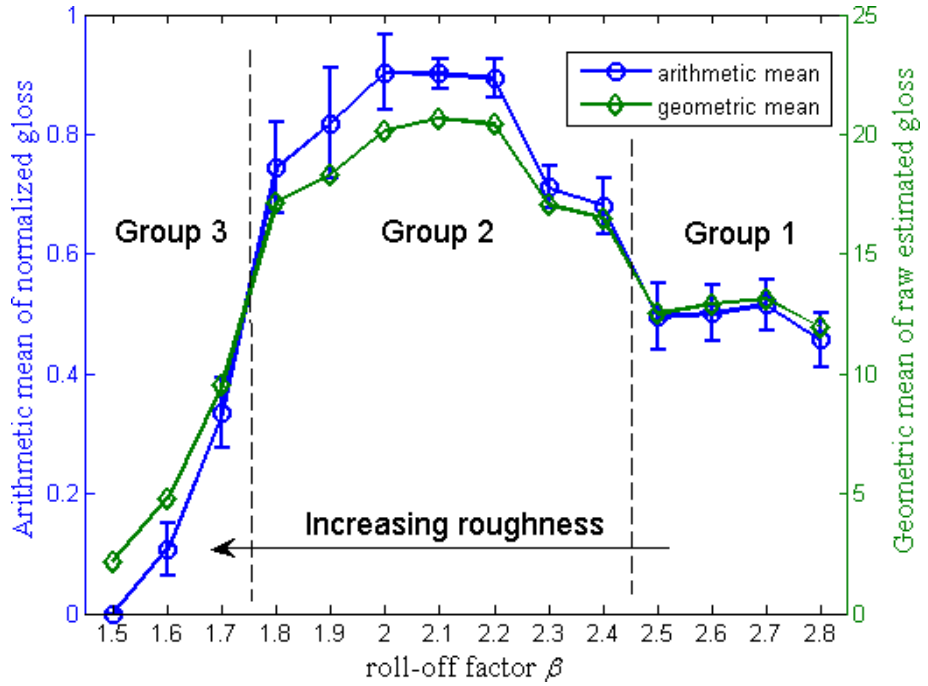

Figure 7.3: Arithmetic means of normalized results from nine observers are plotted with blue dot markers and a blue curve against the left Y-axis. The error bars show ± standard errors. The geometric means of the raw data are plotted with green diamond markers and a green curve against the right Y-axis. The boundaries between the three groups used in the discussion are denoted by dashed lines.

A one-way repeated-measures ANOVA was conducted on the normalized data. The result revealed that perceived gloss is significantly affected by roll-off factor β with $F(13, 104) = 37.375$, $p < 0.001$.

From Figure 7.3 we can see that the perceived gloss follows an asymmetric bell-type curve against roll-off factor β. As the surface roughness increases (from $\beta = 2.8$ to $\beta = 2.0$) the perceived gloss increases in agreement with the findings of Ho et al. [2008]. However, increasing the roughness further results in a sharply decreasing perceived gloss.

7.2.2 Grouping Results

At the end of each experiment session, observers were asked to perform a free grouping task. They grouped the 14 stimuli into between 3 and 6 groups. The grouping results of each observer are shown in Figure 7.2 in different colours and markers. As a way of summarising these results, the grouping data were used to generate a similarity matrix, from which a dendrogram was derived (Figure 7.4). The average group number (five) was used to determine branches which are shown in different colours in Figure 7.4.

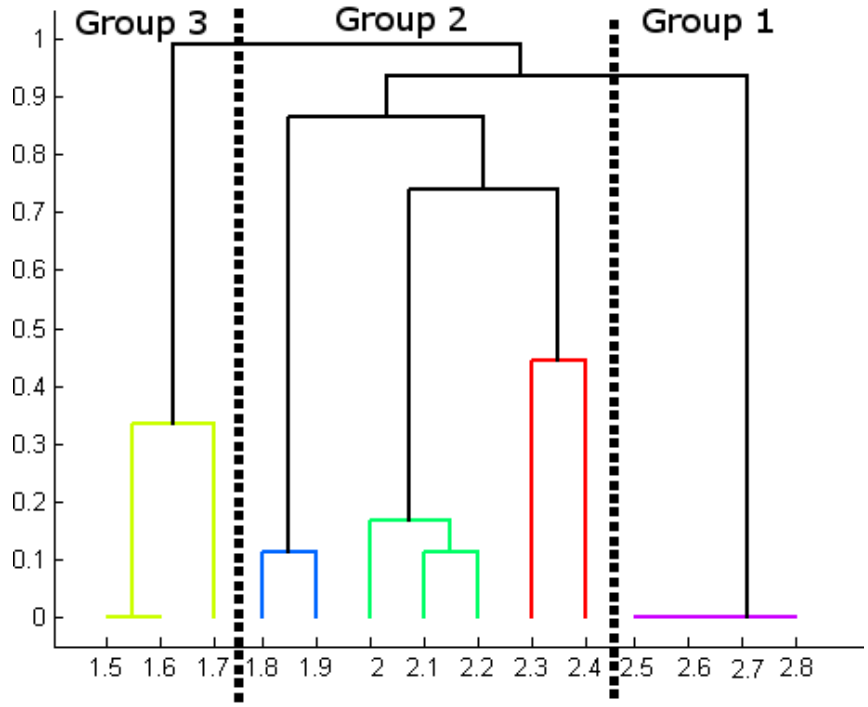

Figure 7.4: Dendrogram from the grouping experiment. Each leaf represents a surface with specific β denoted on x-axis. The y-axis denotes the distance between the two objects being connected. Clusters denoted by different colours were generated by setting a cutoff threshold.

From the dendrogram we can see that 1) surfaces with $\beta = 1.5$ and $\beta = 1.6$ were assigned to the same group by all observers, this also happened to surfaces with $\beta = 2.5$, $\beta = 2.6$, $\beta = 2.7$ and $\beta = 2.8$. These two groups lie at the two ends of the β range we sampled. This means that the surfaces at the two ends have the least variation in perceived appearance. 2) All the surfaces in the same group have successive β values. This means that perceived appearance of $1/f^{\beta}$ noise

surface changes gradually with the variation of sampled β, even though they were all rendered using identical microscale reflection settings.

The dendrogram was used to identify three clustering groups that can be seen to correspond to three types of behaviour in Figure 7.3. While the grouping experiment shows that observers do perceive different groups of stimuli to comprise different types of material, there does not seem to be a consistent agreement as to what these groups are. However, we will use these three groups to simplify discussion in the next section.

7.3 Discussion

The literature has suggested cues people may use to infer surface gloss. Most previous work concentrated on specular highlights and "Distinctive Of Image gloss" (DOI gloss) [Beck and Prazdny, 1981] [Blake and Bülthoff, 1990] [Kim et al., 2011] [Marlow et al., 2011] [Pellacini et al., 2000] [Ferwerda et al., 2001] [Leloup et al., 2011]. The microscale parameters were chosen so that DOI gloss was not obvious in our stimuli. Therefore the specular highlights are likely to be the most important cue. The specular highlights are affected by both surface geometry and reflection properties [Kim et al., 2011] [Marlow et al., 2011]. We will now examine how surface geometry affects our stimuli.

7.3.1 Analysis of Surface Geometry Statistics

To illustrate how roll-off factor β changes surface geometry, we plot a cross section of the height maps of three surfaces with $\beta = 1.6, 1.9, 2.5$ (representing the three groups). Since the surfaces used in the main experiment have different random phase spectra, changes in the cross section due to β are not easily perceived. Instead, for illustrative purposes we used three surfaces with an identical random phase spectrum (Θ=0). Figure 7.5a shows the cross sections, from which we can have a general impression of the changes of mesoscale roughness induced by changes in roll-off factor β. The histograms of the height maps and x-direction partial derivatives are shown in Figure 7.5b and 7.5c (since the surfaces used in this thesis are isotropic, only

the x-direction partial derivatives are shown). The histograms show that rougher surfaces (with smaller β) have a wider spread of distributions.

An alternative descriptor of surface geometry is the mean absolute slope angle [Chantler, 1994]. The absolute slope angle is the angle, ignoring sign, between local normal at each surface location and the z-axis (when we put the surface in the x-y plane). The surface normals are obtained from the partial derivatives of the surface height maps, as $\boldsymbol{n} = (-p, -q, 1)$, where p and q are the partial derivatives of the surface height maps in x-direction and y-direction (as used in Section 4.2). The mean absolute slope angles of the stimuli surfaces are shown as box plots against roll-off factor β in Figure 7.6.

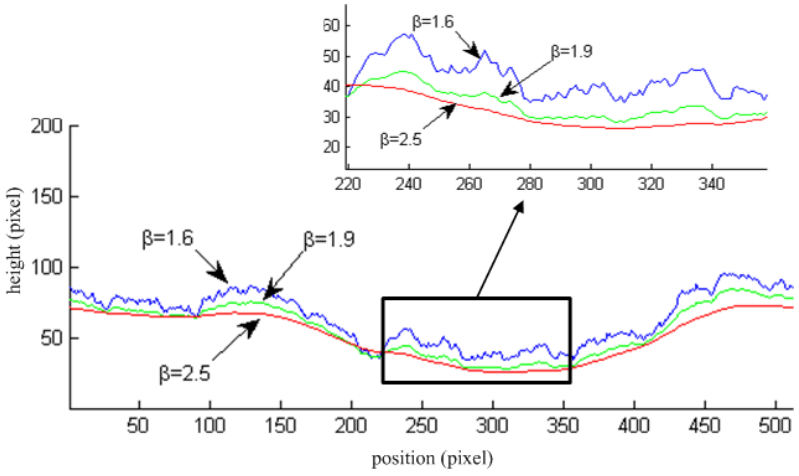

(a)

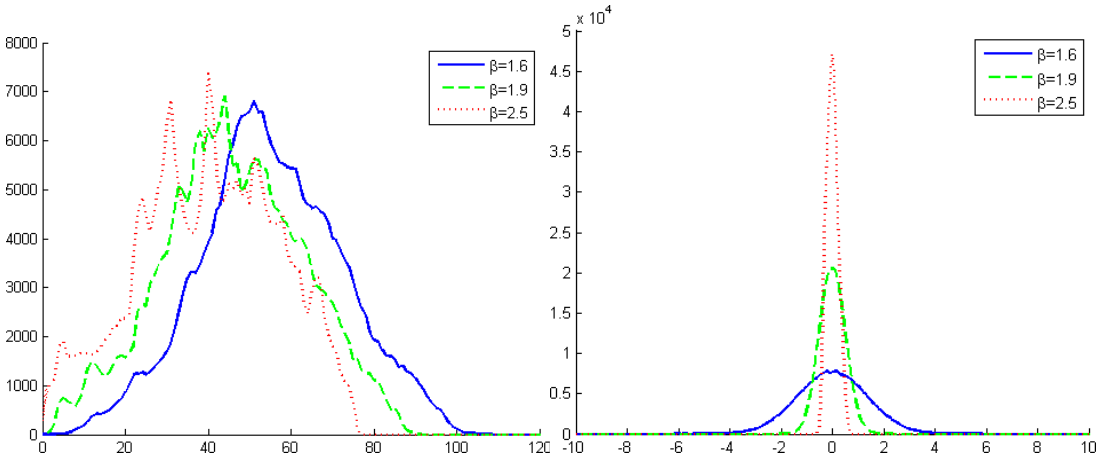

(b) (c)

Figure 7.5: (a): The cross sections of surfaces with $\beta = 1.6, 1.9, 2.5$. The surfaces were generated using an identical random phase spectrum $\Theta = 0$. (b): The histogram of height maps for surfaces in (a). (c): The histogram of partial derivatives in x-direction for surfaces in (a).

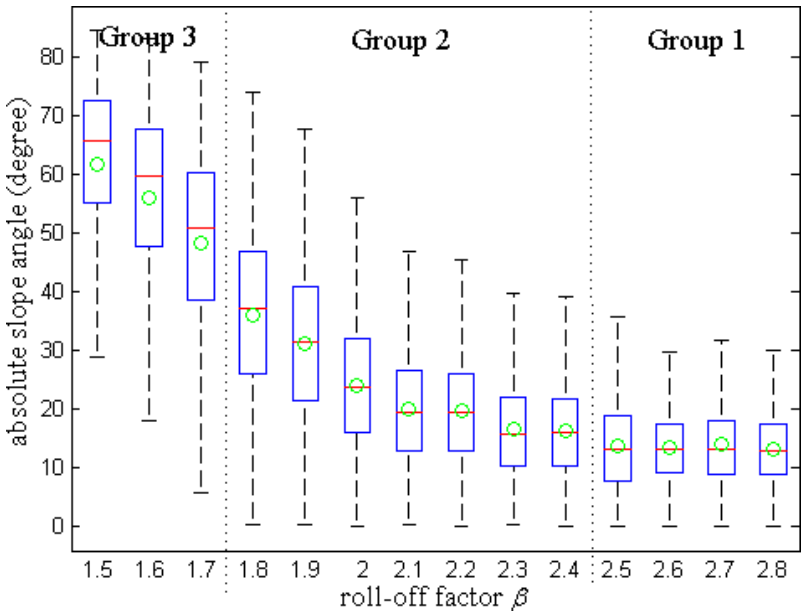

Figure 7.6: Box plot of the absolute slope angle statistics of the stimuli surfaces used in the experiment. Each box is from the statistics of the surface with its roll-off factor β denoted in x-axis. The green circle is the mean absolute slope angle, the central red line is the median, the edges of the box are the 25th and 75th percentiles, the whiskers extend to the most extreme data points (within 1.5 times distance between 25th and 75th percentiles).

We can see that when roll-off factor β decreases from 2.8 down to 2.5 (group 1), the mean absolute slope angle is nearly constant. Then it increases slowly within a small range $[10°, 35°]$ (group 2). After $\beta = 1.8$ it increases rapidly up to 65° (group 3). The dispersion and negative skew of the slope angles also increase with the decreasing of β. Comparing with the perceived gloss, we find that the mean absolute slope angle does not correlate well. Group 3 is particularly at odds with the changing direction of perceived gloss. We therefore decided to investigate the behaviour of other characteristics of the stimuli.

7.3.2 Analysis of Specular Highlights Statistics

Beck and Prazdny [1981], Berzhanskaya et al. [2002], Berzhanskaya et al. [2005], Olkkonen and Brainard [2011], Phillips et al. [2010], Anderson and Kim [2009], Kim et al. [2011], Marlow et al. [2011] have shown that specular highlights are important cues in gloss perception.

The exact properties of specular highlights that people use to infer surface gloss have not been fully discovered. Beck and Prazdny [1981], Berzhanskaya et al. [2005] have provided some heuristics and found that the size, brightness/strength, orientation and placement(spread) of specular highlights affect the rating of people on surface glossiness. However, there is no agreed algorithm for automatically extracting specular highlights from an arbitrary image and most previous investigations have manipulated specular highlights manually [Beck and Prazdny, 1981] [Berzhanskaya et al., 2002] [Berzhanskaya et al., 2005] [Kim et al., 2011] [Marlow et al., 2011]. Manual manipulation is impractical for our stimuli, instead we utilized simple image processing techniques.

Since the entire stimuli set was rendered with an identical reflection setting, a simple global threshold was imposed on the luminance of all stimuli images. Thus we used a very crude definition of specular highlights, in that all pixels whose luminance value is above 50% of the global luminance range were assumed to be "specular highlight pixels". The mean percentage of these pixels for each surface (denoted as P_{hp}) is plotted against roll-off factor β in Figure 7.7. The correlation coefficient between perceived gloss and this estimated percentage of highlight pixels is $\rho = 0.90$, $p < 0.001$.

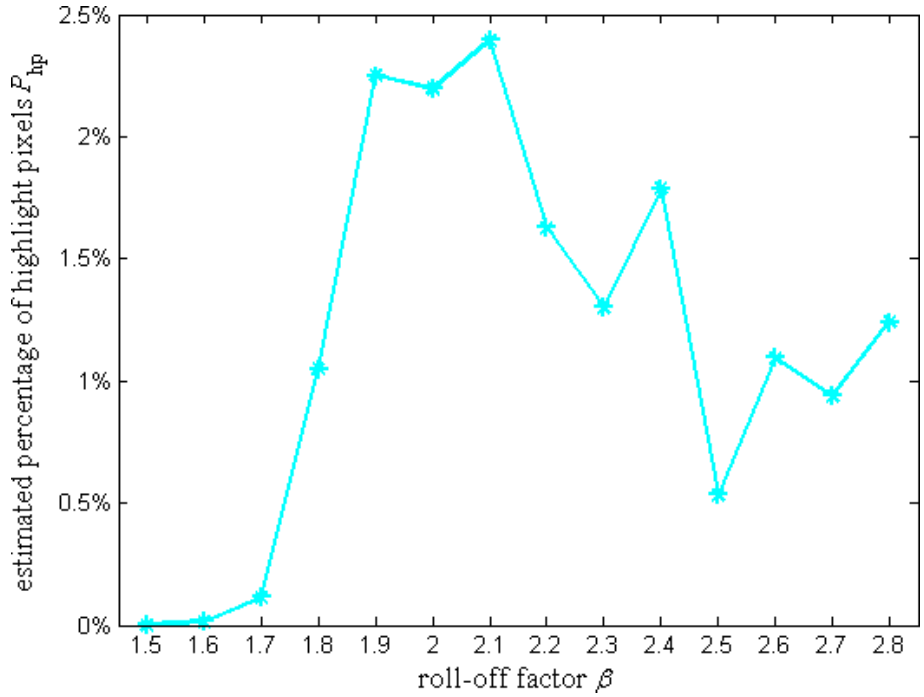

Figure 7.7: The percentage of highlight pixels (P_{hp}) that are estimated using a global threshold of 50% luminance.

Each connected component in the thresholded binary image was assumed to be a specular highlight. The following properties were extracted. The mean luminance of these connected components was used to represent the "strength" of specular highlights. The number of pixels contained within each connected component was used to represent the "size" of specular highlight. The number of connected components was used as the "number" of specular highlights. The two-dimensional centroid of the connected component was used to represent the location of a specular highlight. The average absolute deviation of these centroids (Euclidean distance) within each image was used as a measure of the "spread" of specular highlights. Therefore, the properties of specular highlights were quantified by these four image-based measurements: "strength", "size", "number" and "spread". Their mean values (averaged across the 25 frames of each animation stimulus) are plotted against the roll-off factor β in Figures 7.8, 7.9, 7.10, and 7.11 respectively.

The correlation coefficients were calculated between the perceived gloss and each of these measurements and are shown as follows:

- strength: $\rho = 0.77$, $p < 0.01$;
- size: $\rho = -0.13$, $p = 0.65$;

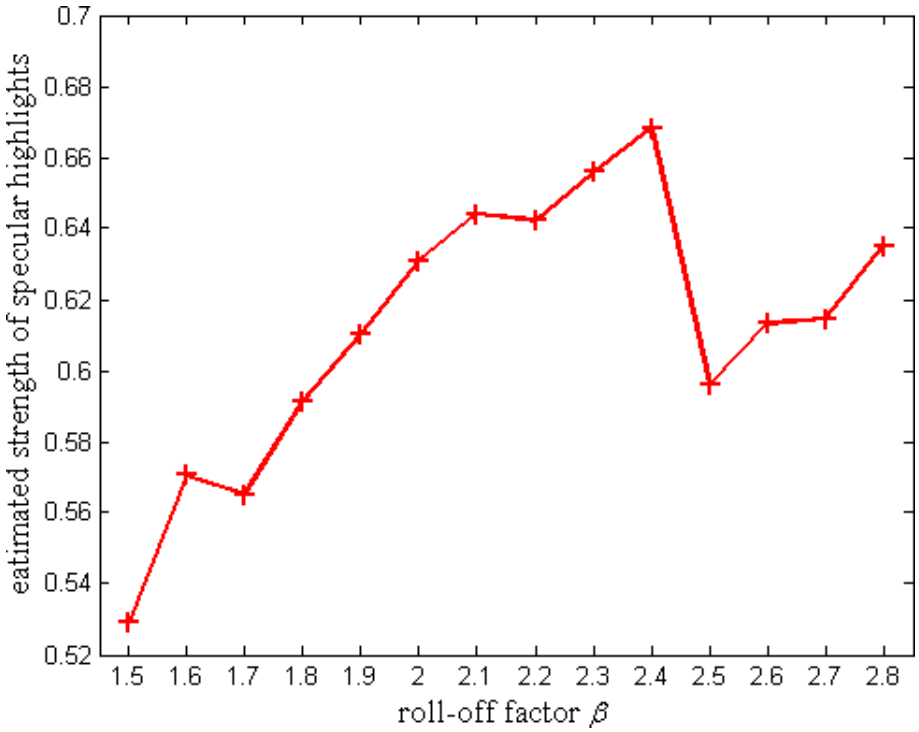

Figure 7.8: Estimated strength of specular highlights against the roll-off factor β.

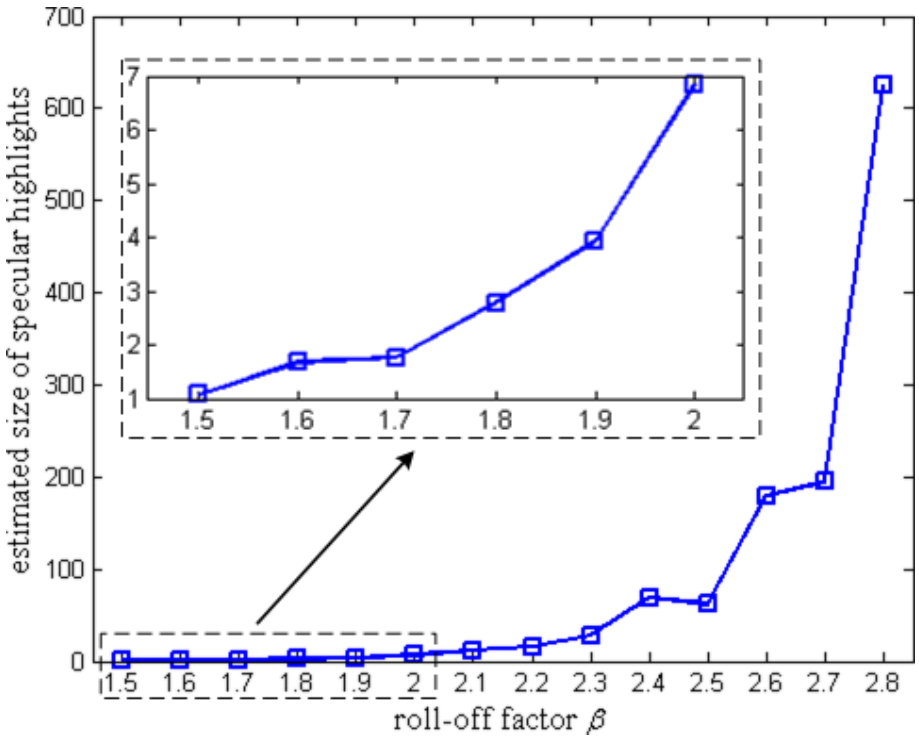

Figure 7.9: Estimated size of specular highlights against the roll-off factor β.

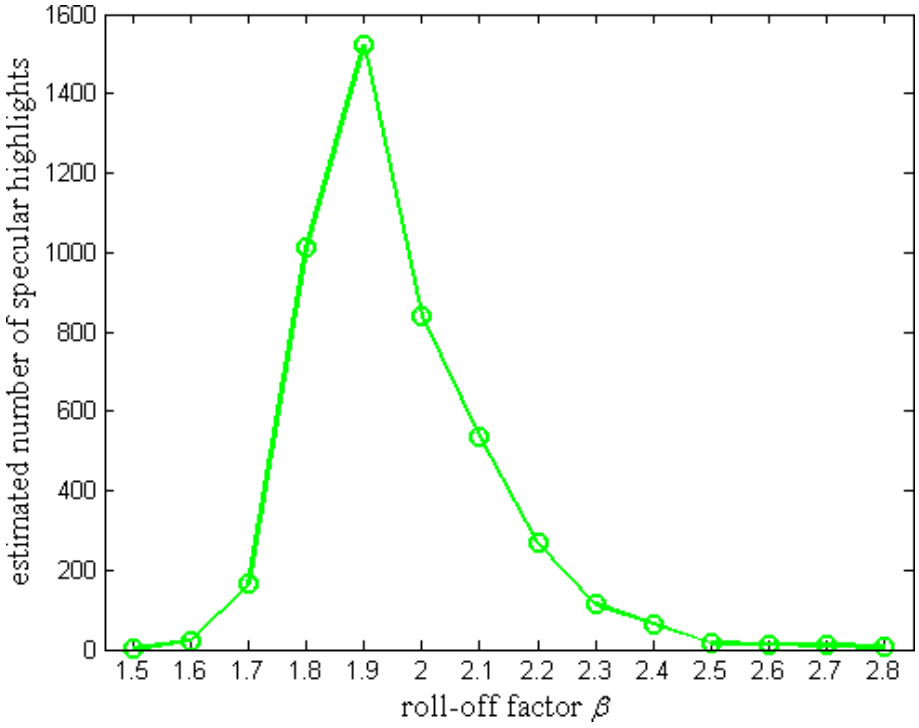

Figure 7.10: Estimated number of specular highlights against the roll-off factor β.

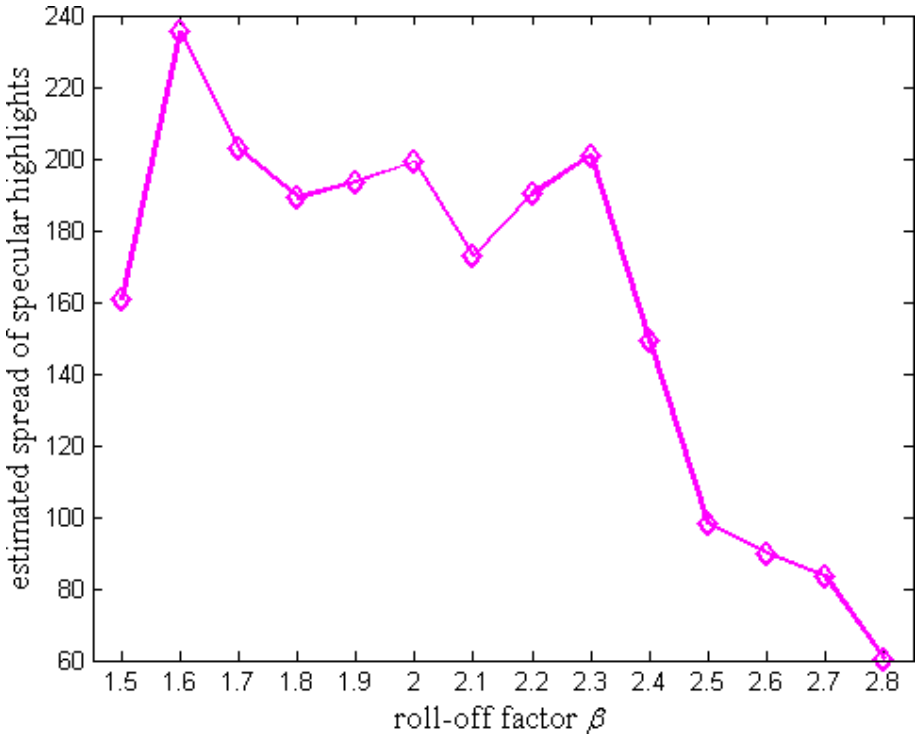

Figure 7.11: Estimated spread of specular highlights against the roll-off factor β.

- number: $\rho = 0.59$, $p < 0.05$;
- spread: $\rho = 0.12$, $p = 0.68$.

It can be seen that the strength and the number of specular highlights both show significant ($p < 0.05$) correlations but account for less than 80% of the variance. This means that none of these properties are as well correlated with perceived gloss as the estimated percentage of highlight pixels (P_{hp} shown in Figure 7.7). We will further discuss the possible reasons for the behaviour of P_{hp}.

7.3.3 Discussion of the Behaviour of P_{hp} (Percentage of Highlight Pixels)

In this subsection we investigate possible reasons for the non-monotonic behaviour of P_{hp}. In particular, we investigated the influence of environment and surface absolute slope angle distributions on this parameter.

The non-monotonic shape of the percentage of highlight pixels (P_{hp}) is affected by surface absolute slope angle distribution and illumination environment map. Figure 7.12 illustrates relationship between the absolute slope angle of a facet and the zenith angle at which the environment map is sampled. For the sake of simplicity, the facet was assumed to be a mirror reflector. The viewing direction is 0°. Facets whose absolute slope angle is above 45° will have very low probability of direct reflection of the environment map. From Figure 7.6 we know that β affects the distribution of absolute slope angles. Therefore to investigate the effect of β and hence absolute slope angle distribution on P_{hp}, we first estimated the number of highlight pixels in the environment as a function of incident zenith angle and combined this with the absolute slope angle distribution.

We cropped the sub-area of the illumination map (incident zenith angle $\theta_{\text{i}} \leqslant 90°$) and converted it to binary image E_{ls} using a crude global threshold (luminance greater than 1 in its original high dynamic range) to extract pixels that were assumed to be strong light sources. The resulting spatial distribution of highlight pixels is shown in Figure 7.13.

Because the surfaces used in this thesis are isotropic, the effect of incident azimuth angle (ϕ_{i}) can be removed. We calculated the percentage of highlight pixels in

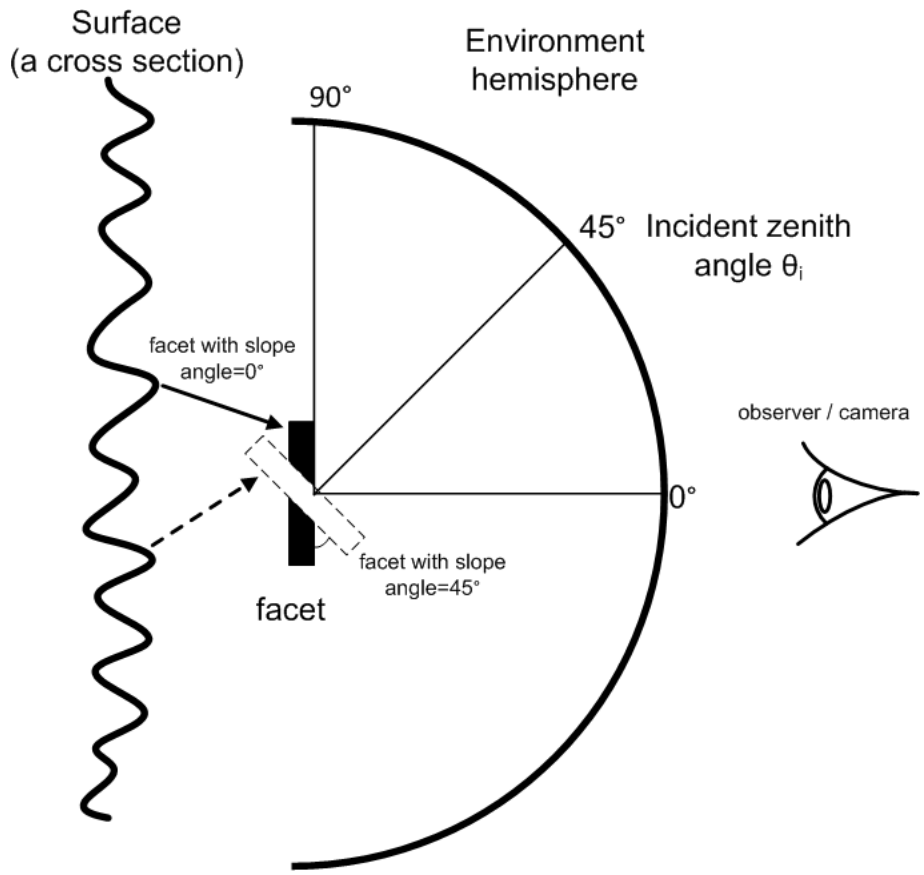

Figure 7.12: The schematic illustration of a facet sampling the environment illumination map. Assumed to be a perfect reflector, the facet can only sample the illumination hemisphere up to 90° with 45° absolute slope angle.

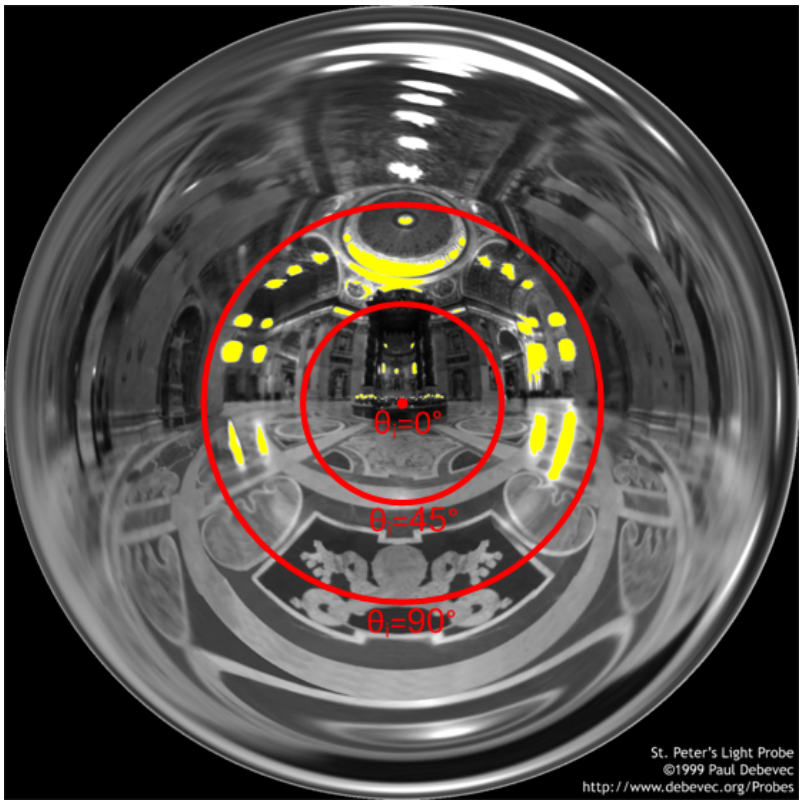

Figure 7.13: The binary image (E_{ls}) is shown as highlighted yellow pixels which are assumed to correspond to strong light sources. The luminance of the the environment map is also shown. The three red circles represent three incident zenith angles respectively ($\theta_{\mathrm{i}} = 0°, 45°, 90°$). Only the sub-area that the front-facing surface can produce direct reflection was considered ($\theta_{\mathrm{i}} \leqslant 90°$).

the environment map for different incident zenith angles θ_{i}, and consider it as the probability of having strong light sources. This is expressed in Equation 7.1, and is shown as bar chart in Figure 7.14a.

$$P_{\mathrm{e}}(\theta_{\mathrm{i}}) = \frac{1}{N(\theta_{\mathrm{i}})} \int_{0^\circ}^{360^\circ} E_{\mathrm{ls}}(\theta_{\mathrm{i}}, \phi_{\mathrm{i}}) \mathrm{d}\phi_{\mathrm{i}} \tag{7.1}$$

$P_{\mathrm{e}}(\theta_{\mathrm{i}})$ is the estimated percentage of strong light sources in the environment map with incident zenith angle θ_{i}; $E_{\mathrm{ls}}(\theta_{\mathrm{i}}, \phi_{\mathrm{i}})$ is the binary environment map after applying the luminance threshold (Figure 7.13); $N(\theta_{\mathrm{i}})$ is the normalization factor which is the total pixel numbers in the environment map with incident zenith angle θ_{i}.

The distribution $P_{\mathrm{e}}(\theta_{\mathrm{i}})$ and the absolute slope angle distribution were used to estimate the percentage of highlight pixels in Equation 7.2.

$$P^*_{\mathrm{hp}}(\beta) = \int_{0^\circ}^{90^\circ} P_{\mathrm{s}}(\theta_{\mathrm{i}}/2; \beta) \cdot P_{\mathrm{e}}(\theta_{\mathrm{i}})) \, \mathrm{d}\theta_{\mathrm{i}} \tag{7.2}$$

where $P^*_{\mathrm{hp}}(\beta)$ is the predicted percentage of highlight pixels for surface with roll-off factor β; $P_{\mathrm{s}}(\theta_{\mathrm{i}}/2; \beta)$ is the distribution of surface absolute slope angle for surface with roll-off factor β.

The predicted percentage of highlight pixels (P^*_{hp}) is shown in Figure 7.14b. The drop-off when β decreases from 1.9 to 1.5 indicates that these surfaces are less likely to have highlight pixels. The prediction of highlight pixels is not a complete explanation to the number of specular highlights, however, the non-monotonic behaviour provides insight as to their behaviour.

The correlation coefficient between the predicted (P^*_{hp}) and the estimated (P_{hp}) percentage of highlight pixels is $\rho = 0.64$, $p < 0.05$. The correlation coefficient between the prediction (P^*_{hp}) and perceived gloss is $\rho = 0.72$, $p < 0.01$. The author would like to state that this is a simple explanation for the variations in highlight pixels, under assumption that facet is mirror reflector, without consideration of more complicated phenomenon such as self-occlusion, self-shadowing and inter-reflection. These may be the reason of the inconsistency between the predicted and estimated values, however, the non-monotonic inverted bell function shown in Figure 7.14b is similar in form to the distribution of "highlights" shown in Figure 7.7 and this suggests that the rapid fall off in the number of highlight pixels for $\beta < 1.8$ is due

to the fact that fewer facets can "see" the bright light sources in the environment (eg. see $\beta = 1.6$ in Figure 7.14a).

7.4 Summary

In this chapter, we used the sophisticated rendering system specified in the last chapter to generate more realistic stimuli. These were used to show that the surface mesoscale roughness parameter (β) significantly affects gloss perception. Although all the surfaces were rendered with identical reflection settings, observers reported that surfaces with different mesoscale roughness (β) have different gloss levels and are made of different materials. In contrast to Ho et al. [2008], the experiment showed that there is a non-monotonic relationship between perceived gloss and mesoscale roughness.

As other researchers have suggested that the characteristics of specular highlights are likely to provide important cues for perceiving surface gloss, four properties of specular highlights and the percentage of highlight pixels (P_{hp}) were estimated quantitatively using simple image processing techniques. We observed that perceived gloss shows weak correlations with the estimated strength and the number of specular highlights, but a stronger correlation with the estimated percentage of highlight pixels (P_{hp}). We developed a simple model of highlights as a function of slope angle and environment distributions and used this to explain the form of the behaviour. Hence we believe that the distribution of intensities in the environment map, together with the absolute slope angle distribution, significantly affects the percentage of highlight pixels (P_{hp}) and the perceived gloss.

This chapter has shown that mesoscale roughness significantly affects perceived gloss, however, it is well known that specular highlights are also affected by the microscale roughness parameter (α). In the next chapter, these two categories of roughness will be varied simultaneously and their joint effect on perceived gloss will be investigated.

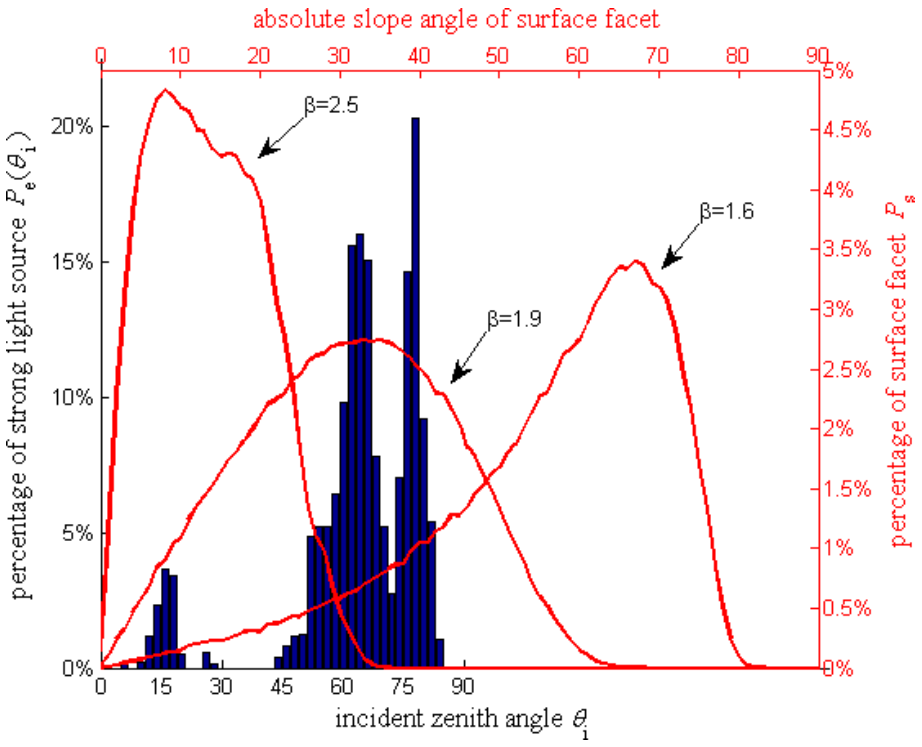

(a)

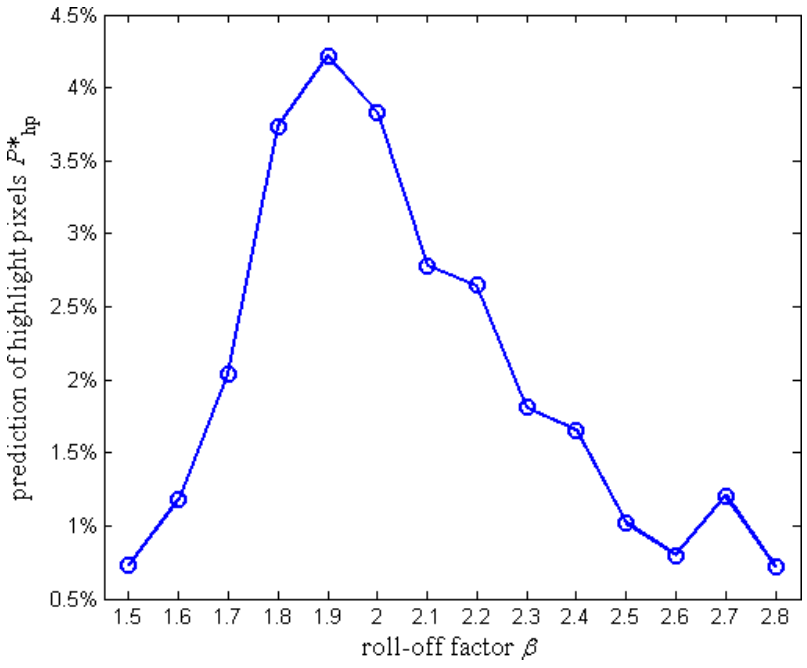

(b) P^*_{hp}

Figure 7.14: (a) The distribution of strong light sources in the illumination map is shown as a bar chart against incident zenith angle θ_i (bottom X-axis) and left Y-axis. Distributions of absolute slope angle (top X-axis) for three surfaces ($\beta = 1.6, 1.9, 2.5$) are also plotted in red curves against right Y-axis. (b) The predicted percentage of highlight pixels (P^*_{hp}) for each surface, which is calculated using Equation 7.2 and the distributions of environment and absolute slope angle.

Chapter 8

THE JOINT EFFECT OF MESOSCALE ROUGHNESS AND MICROSCALE ROUGHNESS ON PERCEIVED GLOSS

This thesis reports the investigation on how perceived gloss is affected by variations in surface mesoscale and microscale parameters. The effect of variation in the microscale roughness parameter (α) on perceived gloss was studied in Chapter 5 using a simple rendering environment. The results were consistent with those reported in the literature in that perceived gloss was shown to increase with decreasing α. In Chapter 7, the experimental results suggested that perceived gloss does not only vary with variation of surface reflection properties, but is also related to mesoscale roughness.

The aim of the work reported in this chapter therefore, was to measure the joint effect of variations in surface mesoscale roughness and microscale roughness on perceived gloss.

The experiment is described in Section 8.2. Section 8.3 introduces the conjoint measurement model used to analyse the experiment results in Section 8.4. The

discussion and conclusion are presented in Section 8.5. However, before describing the experiment, we will examine the work of Ho et al. [2008] in more detail because of its relevance.

8.1 The Work of Ho et al. [2008]

The work in this chapter was related to work carried out by Ho et al. [2008]. They studied how observers judge bumpiness and glossiness of artificial 3D textures and modelled the perceptual interactions of these two factors. Their experimental results showed that increasing "bumpiness" increases perceived gloss, and higher glossiness increases perceived bumpiness.

As discussed in Chapter 2, the surface model used by Ho et al. [2008] is artificial and comprised of specific meso-structures (half ellipsoid). The manipulation of surface geometry was performed by scaling surface height (surface RMS height). However, it has been found that high RMS height surfaces are unrealistic [Padilla, 2008], which naturally limits the range of roughness that can be investigated.

Ho et al. [2008] varied gloss levels by sampling both surface microscale roughness and specular component parameters (α and k_{s}). We will measure how perceived gloss is affected by variations in mesoscale and microscale roughness exclusively, hence k_{s} will be kept constant.

The illumination condition used by Ho et al. [2008] was an area light positioned above and to the left of observer. This simple illumination may limit the accuracy and reliability of the perceptions of observers [Fleming et al., 2001] [Fleming et al., 2003]. Cues from the specific surface model and lighting were discussed by Ho et al. [2008]. They explained their findings by stating that "the bumpiness and glossiness interaction is due to the imperfect cue learning, further visual and haptic training is needed".

Nevertheless, the conjoint measurement models used by Ho et al. [2008] are appropriate tools to study how perceived gloss is simultaneously affected by two or more properties. They will be used in this chapter.

The magnitude roll-off factor (β) will be varied to generate surfaces with different

levels of mesoscale roughness as described in Chapter 7. The microscale roughness will be varied using the BRDF model parameter α. Using the more realistic methods for stimuli generation described in Chapter 6, we conducted the experiment to investigate the joint effect of surface mesoscale roughness (β) and microscale roughness (α) on gloss perception.

8.2 Experiment

8.2.1 Stimuli

Stimuli were generated for 5 levels of mesoscale roughness (β) and 5 levels of microscale roughness (α). The β values were selected based on the results of last chapter. Since surfaces with $\beta > 2.5$ exhibited nearly constant change in perceived gloss, the β values chosen were: $\beta = 1.6, 1.8, 2.0, 2.2, 2.4$. The microscale roughness α was varied logarithmically, the values chosen were: $\alpha = 0.02, 0.01, 0.005, 0.0025, 0.00125$. The diffuse and specular component parameters of the BRDF model were fixed at $k_{\mathrm{d}} = 0.4$, $k_{\mathrm{s}} = 0.6$. The five surfaces with $\alpha = 0.01$ were taken from the stimuli set of last chapter. Another twenty surfaces were generated using the method described in Chapter 6 with different random phase seeds (Table 8.1). All surfaces have the same RMS height ($\sigma = 17$ pixel width).

Table 8.1: The seeds used for generating random phase spectra of the stimuli surfaces.

		α				
		0.02	0.01	0.005	0.0025	0.00125
β	1.6	16	2	30	44	58
	1.8	18	4	32	46	60
	2	20	6	34	48	62
	2.2	22	8	36	50	64
	2.4	24	10	38	52	66

Consistent with previous chapters, the microscale roughness levels used in producing the stimuli were chosen to be lower than that required to exhibit DOI gloss [Pellacini et al., 2000] [Ferwerda et al., 2001].

Since β controls mesoscale roughness and α controls microscale roughness, it will be convenient to denote the levels of these two kinds of roughness, instead of using the real parameter values. Thus the surface S_{11} with parameter values α_1 and β_1 is the roughest stimulus, while the surface S_{55} is the smoothest. Figure 8.1 shows the central frame images ($slant = 0°$) of each stimulus.

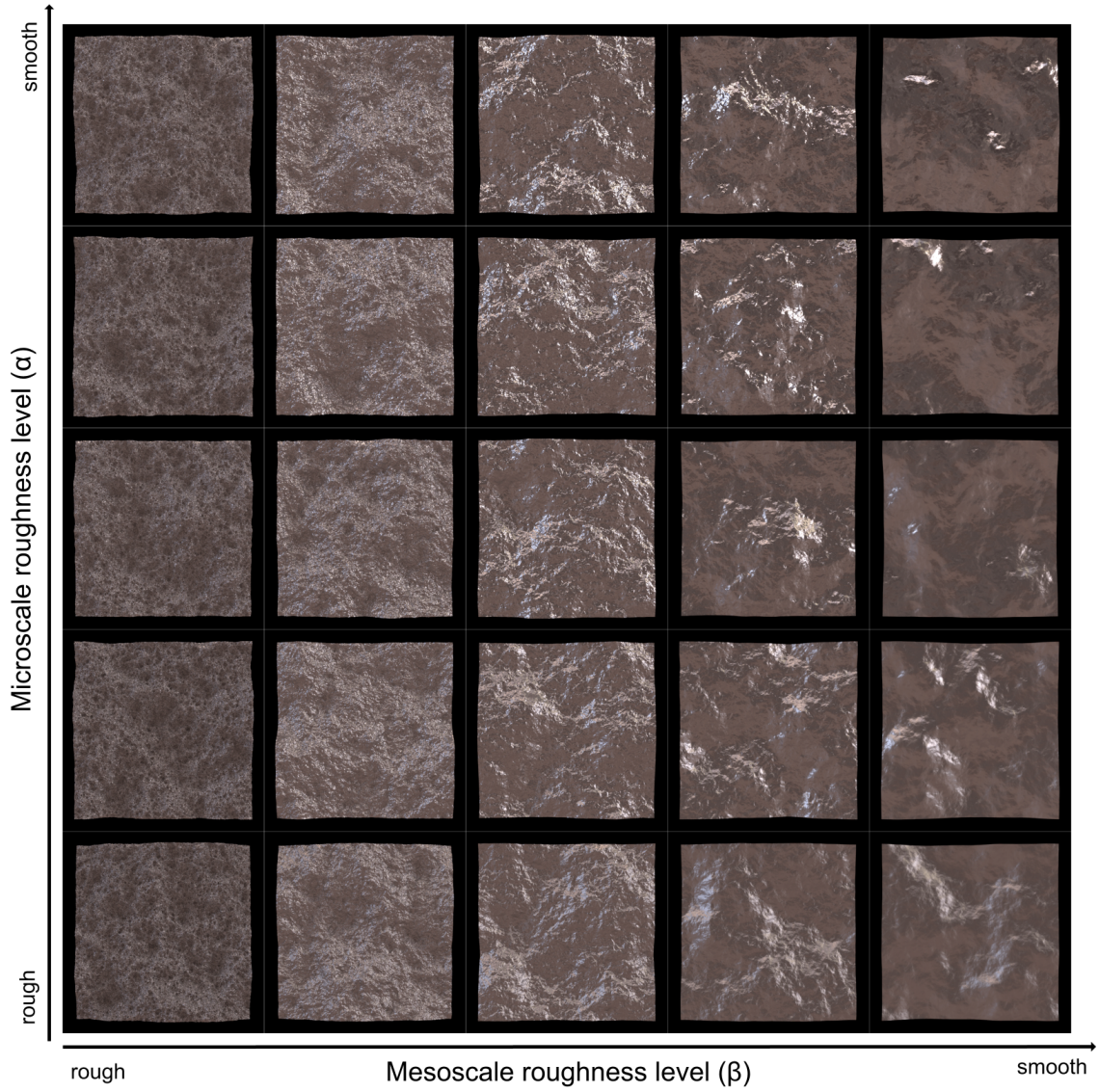

Figure 8.1: Sample images of the stimuli. The central image of each animation stimuli ($slant = 0°$) is shown. The x-axis denotes the mesoscale roughness level and the y-axis denotes the microscale roughness level. These images have been adjusted by a nonlinear gamma for display purpose.

8.2.2 Observers

Eight naïve observers with normal or corrected to normal vision were paid to participate in the experiment. All were students or University employees working in different fields, were less than 35 years of age, mixed gender and nationalities.

8.2.3 Procedure

A magnitude estimation method was first used to measure the perceived gloss of these stimuli in a pilot experiment, but produced noisy results. This may have been due to the task overtaxing the observers [Ehrenstein and Ehrenstein, 1999].

Instead, a 2AFC (2 Alternatives Forced Choice) method was chosen as used by Ho et al. [2008]. In each trial, a pair of stimuli was shown to the observer who was asked to choose the glossier one. This method produces reliable results but is time consuming. The full combination of the 25 stimuli (300 pairs) was randomly shown to observers. Before the experiment, observers were shown printed instructions:

> You will be presented with 300 pairs of rotating surface animations on screen. You will finish one task: indicate which one you think is glossier by pressing the left (the first one) or right (the second one) arrow key on keyboard.

To control the experiment time, the duration of each animation stimulus was fixed. In each trial, we randomly picked one stimulus from the pair and showed the animation once (rotating from 0° to -12°, then to 12°, and finally back to 0°). Following a 0.2 second blank, the other partner in that pair was shown in the same way. The screen was then blanked until the observer made their decision on which one was glossier by pressing the corresponding key. Then the next pair was shown immediately. Each pair was repeated three times. All of the observers finished the experiment in between 60-75 minutes.

8.3 Conjoint Measurement Models

The results were tested against conjoint measurement models as described by Ho et al. [2008]. They found that the additive model was sufficient for explaining their results when compared to the independent model and the full model. In this chapter, we also tested our results against these three models. The independent model was used to examine whether both roughness parameters significantly affect perceived gloss, and the full model was used to test whether the joint effect of these two kinds of roughness is significant.

We will introduce these three models briefly as they are described in [Ho et al., 2008]. Since these models are nested, the independent model which has simplest form will be introduced first, followed by the additive model and finally the full model. Symbol G is used to denote the gloss estimated by these models; superscripts 'I', 'A', 'F' were used to denote the independent model G^{I}, additive model G^{A} and full model G^{F} respectively; subscript 'ij' was used to denote the surface with microscale roughness level 'i' and mesoscale roughness level 'j'.

Independent model: The independent model assumes that the measured property is dependent on only one factor while the contribution from the other factor is assumed to be zero. In the work of Ho et al. [2008], the independent model was only tested against gloss levels, since the 'bumpiness' was assumed not to affect perceived gloss. However, we tested both 'microscale roughness' and 'mesoscale roughness' using the independent model. Thus the two independent models for perceived gloss G^{I}_{ij} of surface S_{ij} are as follows:

$$\text{concerning } \alpha \text{ only:} \quad G^{\mathrm{I}_\alpha}_{ij} = G^{\mathrm{I}_\alpha}(\alpha_i) = G^{\mathrm{I}_\alpha}_i \tag{8.1}$$

$$\text{concerning } \beta \text{ only:} \quad G^{\mathrm{I}_\beta}_{ij} = G^{\mathrm{I}_\beta}(\beta_j) = G^{\mathrm{I}_\beta}_j \tag{8.2}$$

We used similar notions as those used by Ho et al. [2008]. $G^{\mathrm{I}_\alpha}_i$ and $G^{\mathrm{I}_\beta}_j$ are the only parameters of the two models respectively. For example, the model G^{I_α} has a total of five parameters for the stimuli at five α levels: $\{G^{\mathrm{I}_\alpha}_1, G^{\mathrm{I}_\alpha}_2, G^{\mathrm{I}_\alpha}_3, G^{\mathrm{I}_\alpha}_4, G^{\mathrm{I}_\alpha}_5\}$.

Additive model: The additive model assumes that microscale roughness α and mesoscale roughness β affect perceived gloss separately and additively. The perceived gloss in the additive model G^{A}_{ij} is the sum of contributions from microscale

roughness $G^{\mathrm{A}_\alpha}(\alpha_i)$ and mesoscale roughness $G^{\mathrm{A}_\beta}(\beta_j)$ for surface S_{ij}:

$$G_{ij}^{\mathrm{A}} = G^{\mathrm{A}_\alpha}(\alpha_i) + G^{\mathrm{A}_\beta}(\beta_j) = G_i^{\mathrm{A}_\alpha} + G_j^{\mathrm{A}_\beta} \tag{8.3}$$

Full model: The full model uses a parameter for every surface stimulus so that it fits data exactly. In the full model, the perceived gloss G_{ij}^{F} is not constrained to be additive and is instead described as a function of mixed contributions from α and β:

$$G_{ij}^{\mathrm{F}} = G^{\mathrm{F}}(\alpha_i, \beta_j) \tag{8.4}$$

We used the same decision model as Ho et al. [2008] to compare the results. The paired comparison results of observers on perceived gloss of surface S_{ij} and S_{kl} were assumed to be a noise-contaminated decision:

$$\Delta = G_{kl}^{*} - G_{ij}^{*} + \varepsilon, \qquad \varepsilon \sim Gaussian(0, \sigma_{\mathrm{g}}^2) \tag{8.5}$$

where the * represents the model, which can be "I", "A", or "F". $\Delta > 0$ if surface S_{kl} is judged glossier than surface S_{ij}. ε represents the precision of observers in judgement, which we modelled as a Gaussian distribution with 0 mean and variance σ_{g}^2.

We used the same method as Ho et al. [2008] to preprocess the model by setting $G_1^{\mathrm{I}_\alpha} = G_1^{\mathrm{I}_\beta} = G_1^{\mathrm{A}_\alpha} = G_1^{\mathrm{A}_\beta} = G_{11}^{\mathrm{F}} = 0$ as the anchors and scaling model parameters for $\sigma_{\mathrm{g}} = 1$. The left parameters need to be estimated. There are 4 free parameters in each independent model ($G_2^{\mathrm{I}_\alpha}, \ldots, G_5^{\mathrm{I}_\alpha}$; $G_2^{\mathrm{I}_\beta}, \ldots, G_5^{\mathrm{A}_\beta}$), 8 free parameters in the additive model ($G_2^{\mathrm{A}_\alpha}, \ldots, G_5^{\mathrm{A}_\alpha}, G_2^{\mathrm{A}_\beta}, \ldots, G_5^{\mathrm{A}_\beta}$), and 24 free parameters in the full model (G_{ij}^{F}; $i = 1...5$, $j = 1...5$ and $ij \neq 1$). We estimated the remaining free parameters using maximum likelihood estimation with the package from Knoblauch and Maloney [2009].

8.4 Results and Analysis

8.4.1 Raw Results

The results from all observers showed a similar trend and the averaged results across all eight observers are shown in Figure 8.2. This comparison matrix shows the raw

experimental results and is not easy to observe patterns in. We will therefore fit conjoint measurement models using these data.

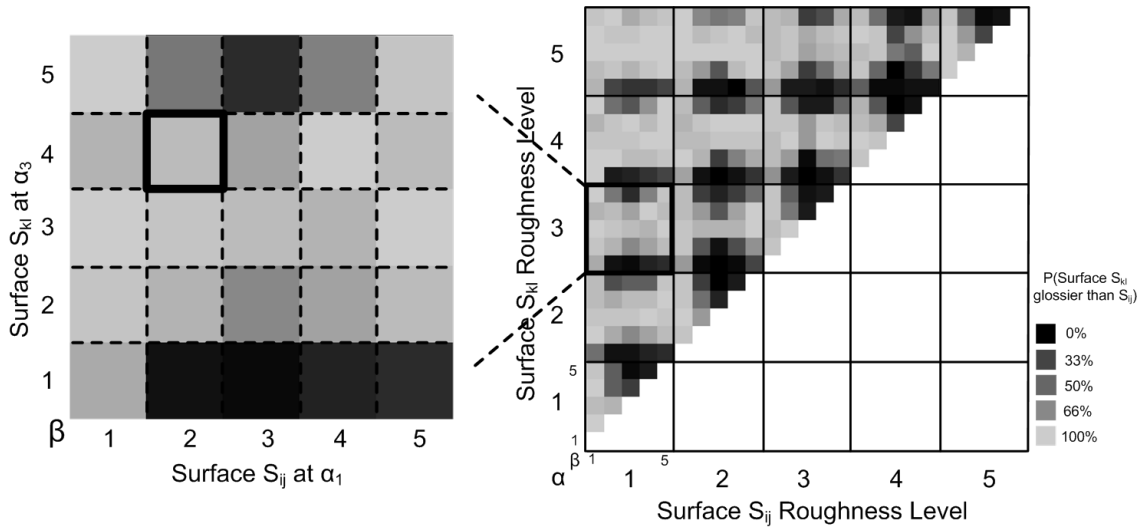

Figure 8.2: Glossiness judgement results averaged across all 8 observers (the right matrix). The grey levels of the squares in the matrix represent the proportion of time that a surface S_{kl} was perceived to be glossier than another surface S_{ij}, for each pair-wise comparison. Microscale roughness (α) level i (or k) is indicated by the large numerical labels (1,2,...,5), and mesoscale roughness (β) level j (or l) is indicated by the small numerical labels (1,2,...5). The blocks in the solid grid represent different α levels, and the bolded block is magnified and shown for example (the left matrix). The grey level of the bolded square in the left matrix represents the proportion of time that surface S_{34} was perceived to be glossier than surface S_{12}.

8.4.2 Fitting Conjoint Measurement Models

The pair-wise comparison results from the experiment were used to fit the conjoint measurement models for each observer. The resulting model parameters were normalized before averaging across observers. Appendix D shows the fitting results of each observer.

The two independent models were estimated first, and the mean values of the estimated parameters are shown in Figure 8.3. As the independent model defines itself, the perceived gloss is assumed to be accounted for by only one property. Using the estimated independent model parameters, we can obtain the predicted perceived gloss from the two independent models for every stimulus. These are shown in

Figure 8.4.

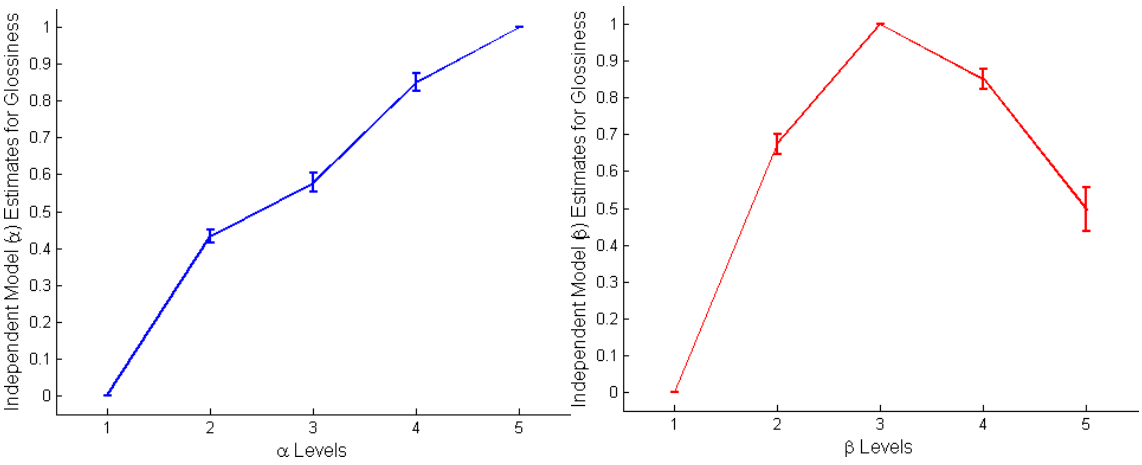

(a) G^{I_α} (b) G^{I_β}

Figure 8.3: Fitted independent model parameters (the mean values averaged across all observers). (a): independent model concerning α only. (b): independent model concerning β only. The error bars denote $\pm$ standard errors.

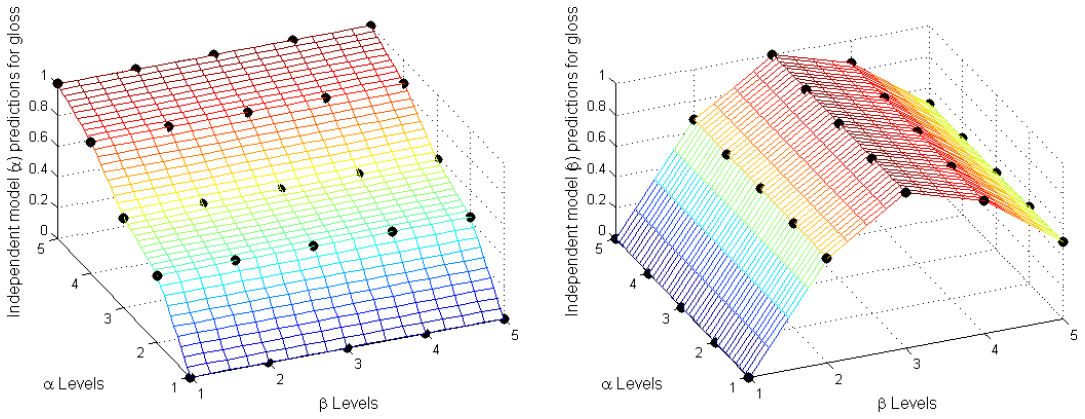

(a) Prediction of $G_{ij}^{\mathrm{I}_\alpha}$ (b) Prediction of $G_{ij}^{\mathrm{I}_\beta}$

Figure 8.4: Perceived gloss predicted by the two independent models. (a) is from the independent model that concerns α only. (b) is from the independent model that concerns β only.

We then fitted the additive model. All eight observers showed very similar responses, and we plotted the means of the model parameters in Figure 8.5 with error bars showing the $\pm$ standard error. This model suggests that observers judged glossiness using additive cues affected by mesoscale roughness and microscale roughness. Since the contribution from α shows a linear shape, we ran a linear regression on $G_i^{\mathrm{A}_\alpha}$ against α level, obtained coefficients: $slope = 0.165$, $intercept = -0.107$ with statistics: $R^2 = 0.966$, $F(1,3) = 85.97$, $p < 0.01$.

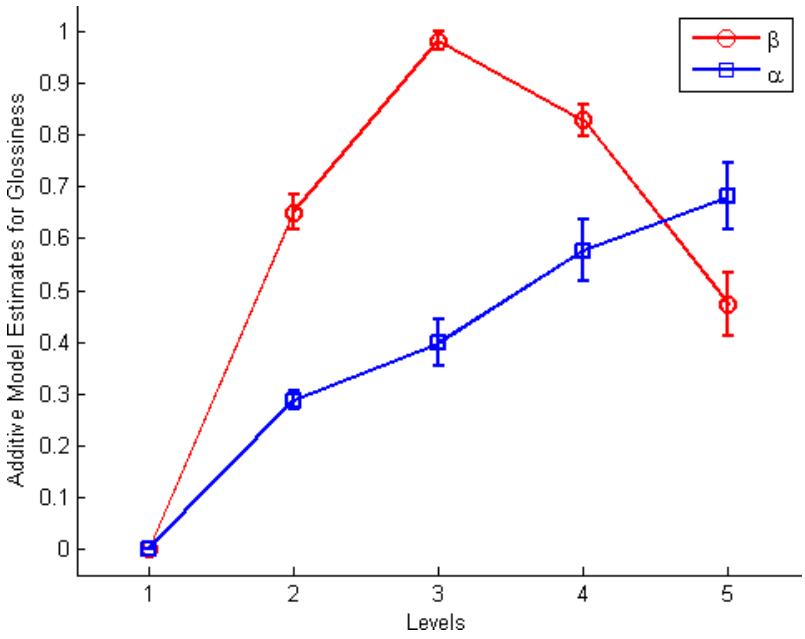

Figure 8.5: Fitted parameters of the additive model. These are mean values averaged across the eight observers with the error bars denoting ± standard errors. The two curves correspond to the parameters $G_i^{\mathrm{A}_\alpha}$ $(i = 1...5)$ and $G_j^{\mathrm{A}_\beta}$ $(j = 1...5)$ respectively. The estimated gloss of a particular surface is the sum of the values from corresponding parameters.

Figure 8.6 shows the predictions of perceived gloss using the additive model, which were scaled using the method suggested by Ho et al. [2008].

The full model parameters were estimated last. The mean results across all observers are shown in Figure 8.7 against β levels and α levels separately with error bars denoting the ± standard errors. These parameters were directly used as the predicted perceived gloss from the full model, shown in Figure 8.8.

8.4.3 Comparing Conjoint Measurement Models

The log likelihood values for fitting the two independent models, the additive model, and the full model are shown in Table 8.2. To statistically test whether both mesoscale roughness (β) and microscale roughness (α) have significant influence on perceived gloss, we compared the additive model with the two independent models using a nested hypothesis test as suggested by Ho et al. [2008]. The likelihood-ratio was calculated and the results of all eight observers revealed that the independent model was rejected at Bonferroni-corrected level with significance $p < 0.001$. The

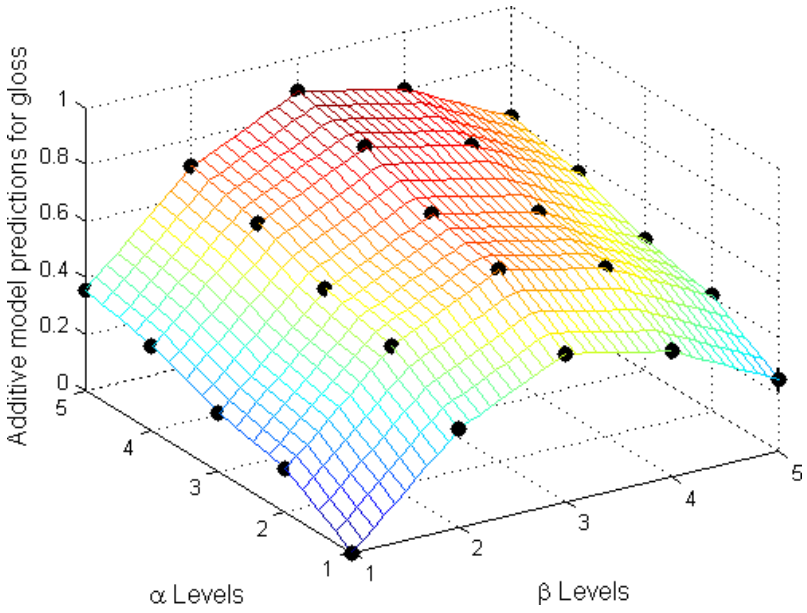

Figure 8.6: Perceived gloss predicted by the additive model.

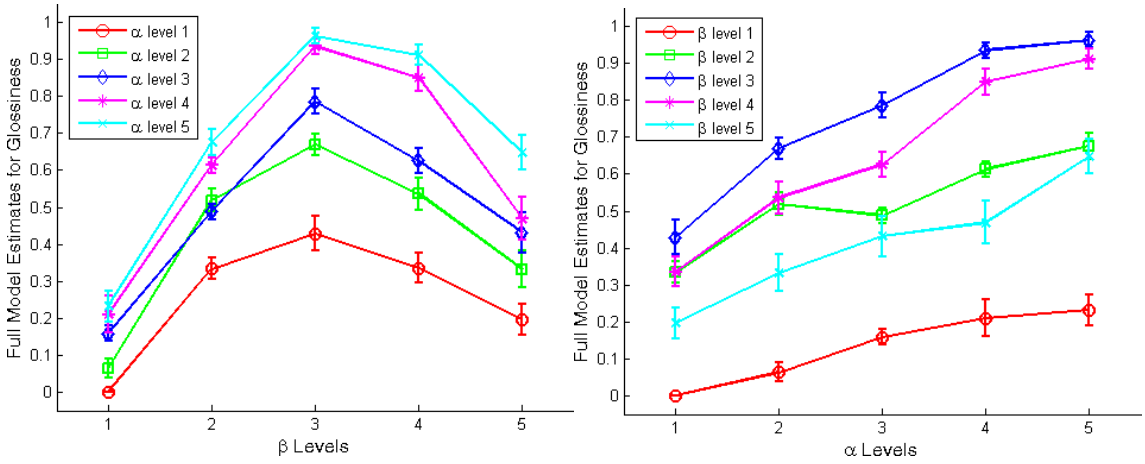

(a) (b)

Figure 8.7: Fitted parameters of the full model. These are mean values averaged across the eight observers with the error bars denoting ± standard errors. The left one is the plot against β levels, where separate lines denote different α levels. The right one is the plot against α levels, where separate lines denote different β levels.

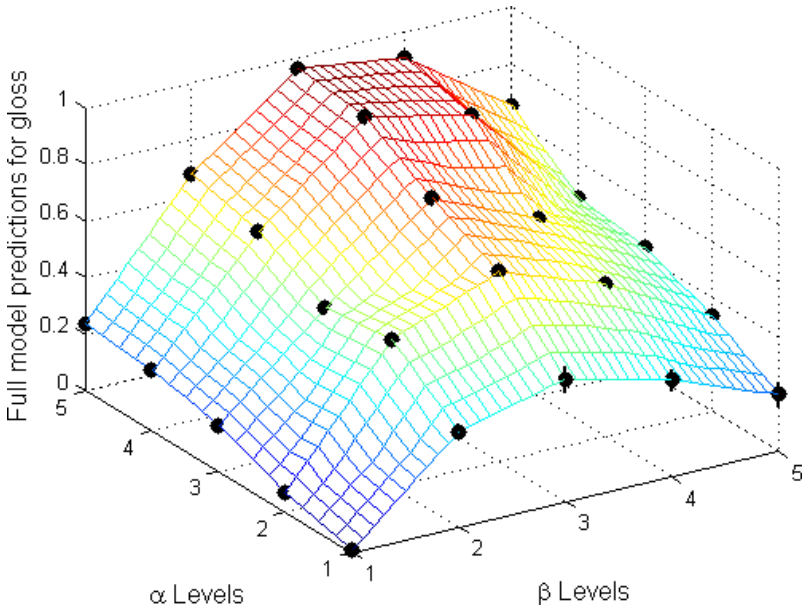

Figure 8.8: Perceived gloss predicted by the full model.

χ^2 values can be found in Table 8.2. This suggests that both kinds of roughness significantly affect perceived gloss. This finding is consistent with that reported by Ho et al. [2008].

When comparing the additive model with the full model, Ho et al. [2008] found that the additive model can adequately account for the interaction between bumpiness and glossiness, based on the results that 3 out of 6 observers showed significant results in a nested hypothesis test. However, this means that half of their results cannot be accounted for by the additive model. They conducted linear regression on the predictions of the additive model against those of the full model, and obtained high R^2 values for all observers. However, there is no dependence between the full model and the additive model, or one-way causal effect from one to the other.

To test whether the additive model accounts for our results, we compared the additive model with the full model in a nested hypothesis test. Table 8.2 shows the χ^2 values for the test. In contrast to Ho et al. [2008], we found that the results of all eight observers were significant at Bonferroni-corrected level ($p < 0.01$). This suggests that the full model is significantly better than the additive model at describing the joint effect of mesoscale and microscale roughness on perceived gloss.

From the models, we can see that perceived gloss shows a monotonic relationship with α. This finding is consistent with literature [Pellacini et al., 2000] [Fleming et al., 2004b] [Ho et al., 2008] and Chapter 5. However, at each α level, the effect

of mesoscale roughness, shows a non-monotonic (asymmetric bell-type curve) relationship with perceived gloss, which is consistent with the finding in Chapter 7, but differs from the findings of Ho et al. [2008] with regard to "bumpiness".

Table 8.2: Log likelihood of fitted models for each observer and χ^2 values for nested hypothesis tests for comparing the models. All tests show significant results with $p < 0.01$.

Model or Test	Observer							
	AC	DB	NC	NJ	NL	TM	WL	XD
I. Independent model (β)	-544.01	-376.20	-367.41	-463.65	-448.89	-345.39	-473.58	-432.14
I. Independent model (α)	-510.23	-560.25	-553.21	-580.44	-529.01	-574.05	-515.96	-557.85
II. Additive model	-406.22	-259.93	-223.08	-404.66	-303.34	-138.15	-313.24	-331.97
III. Full model	-379.44	-139.50	-204.16	-385.43	-273.62	-210.43	-285.09	-291.39
Test: I (β) vs. II, $\chi^2(4) >$	275.59**	232.52**	288.65**	117.97**	291.10**	214.48**	320.68**	200.35**
Test: I (α) vs. II, $\chi^2(4) >$	208.02**	600.64**	660.25**	351.56**	451.33**	671.80**	405.44**	451.77**
Test: II vs III, $\chi^2(16) >$	53.56**	40.86**	37.84*	38.46*	59.46**	55.45**	56.29**	81.16**

*: $p < 0.01$, **: $p < 0.001$

8.4.4 Difference between the Additive and Full Models

In our experiment, the full model was found to be better than the additive model at describing the results. We compared the predictions of these two models for further analysis.

We calculated the differences between the full and additive model predictions, and show these in Figure 8.9.

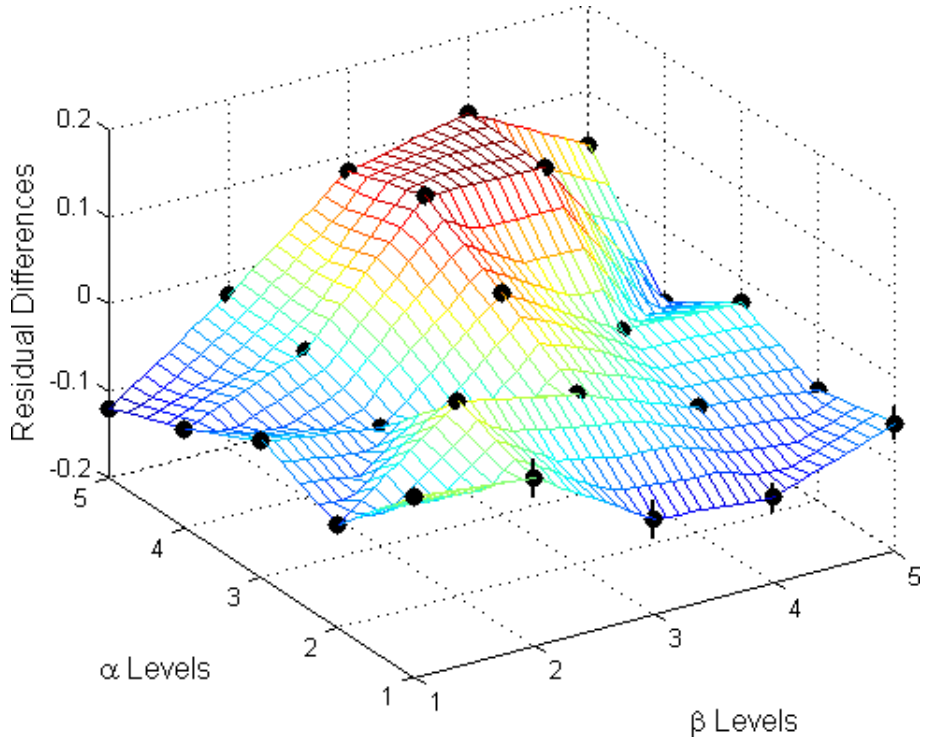

Figure 8.9: 3D scatter plot of the residual differences between the full model and the additive model predictions. The dots are mean values averaged across all observers. The error bars show the ± standard errors.

Figure 8.9 is not informative for inspecting the pattern of differences between the models, we therefore used separate plots. Figure 8.10 shows the predictions of additive model as dashed lines, and shows the full model as solid lines. Note that the full model parameters are the same as those shown in Figure 8.7 but the error bars were removed for clarity.

From Figure 8.10, we can see that the general difference between the full model and the additive model is that the additive model curves are parallel, whereas the full model curves show a clear changing pattern. We will further analyse this in more detail.

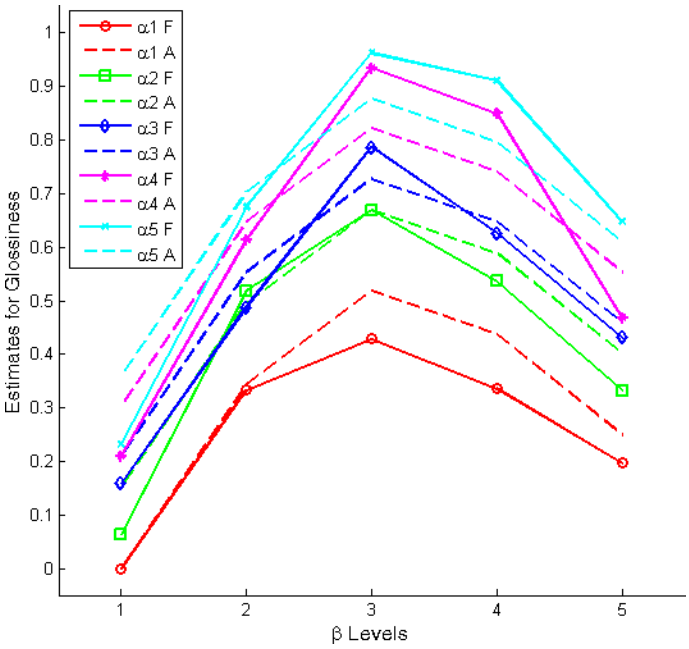

(a)

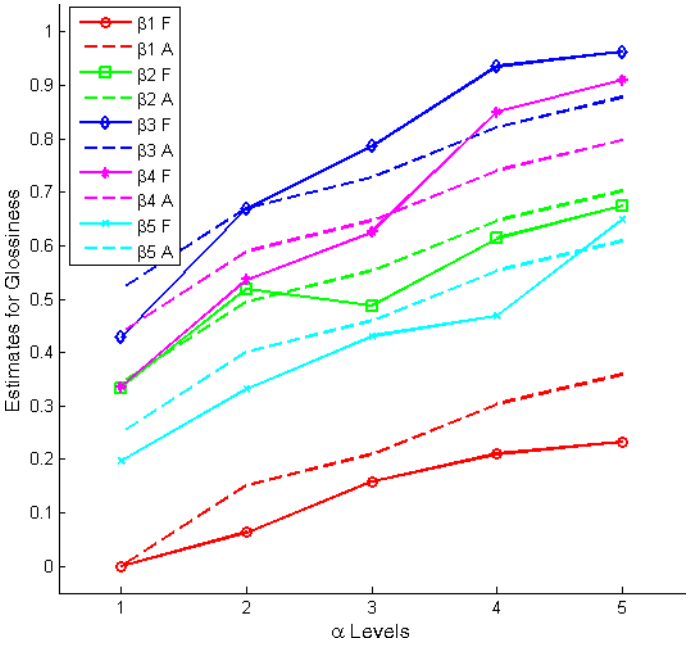

(b)

Figure 8.10: Predictions of the additive model and the full model are shown together for comparison. The full model predictions are plotted in solid lines while the additive model predictions are plotted in dashed lines. (a): gloss is plotted as a function of β level with separate curves denoting different α levels. (b): gloss is plotted as a function of α level with separate lines denoting different β levels. The legend in the plot denotes each curve, where the number next to α and β denotes the level and the letter "F" and "A" denote the full model or additive model respectively.

In Figure 8.10a, the changing pattern of full model curves is that the asymmetry of these curves varies with α. As α level increases, the full model predictions of surfaces with β_1 and β_2 fall below the corresponding additive model predictions; and the full model predictions of surfaces with β_3 and β_4 rise and climb over the corresponding additive model predictions.

To numerically show this asymmetry, we calculated the difference d_i between the full model predictions on the two sides of the peak surface S_{i3} for each α level i in Figure 8.10a as:

$$d_i = [G^{\mathrm{F}}(\alpha_i, \beta_4) + G^{\mathrm{F}}(\alpha_i, \beta_5)] - [G^{\mathrm{F}}(\alpha_i, \beta_1) + G^{\mathrm{F}}(\alpha_i, \beta_2)] \tag{8.6}$$

d_i is plotted in Figure 8.11. The increasing of d_i with α level indicates the increasing asymmetry of full model curves.

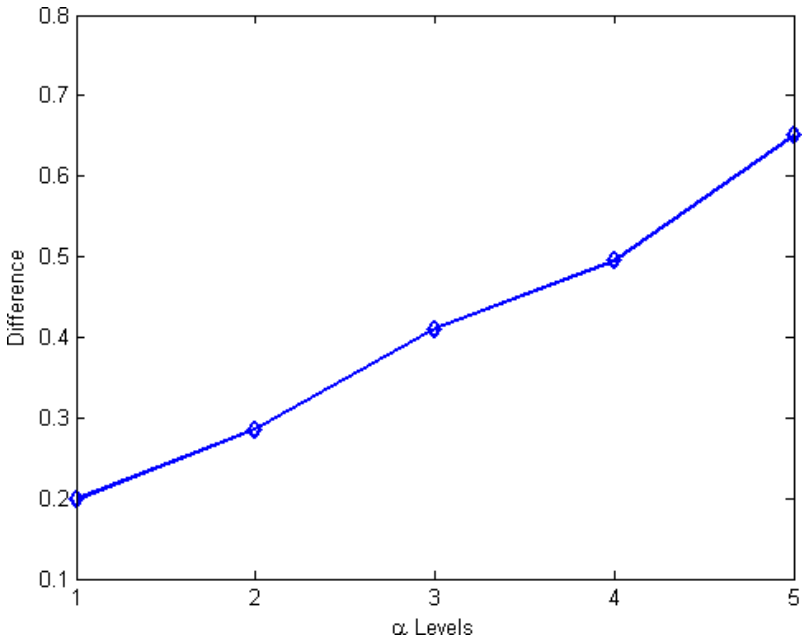

Figure 8.11: The difference between full model parameters on the two sides of the peak (S_{i3}) in Figure 8.10a for each α level.

We also ran t-tests on surface pairs with β level β_2 and β_4 for each α level. The test revealed that for the first two α levels there is no significant difference between surfaces:

- S_{12} and S_{14}: $t(7) = -0.078, p = 0.94$
- S_{22} and S_{24}: $t(7) = -0.384, p = 0.712$

But from α level 3, the difference becomes significant:

- S_{32} and S_{34}: $t(7) = -2.828, p < 0.05$
- S_{42} and S_{44}: $t(7) = -5.829, p < 0.01$
- S_{52} and S_{54}: $t(7) = -3.842, p < 0.01$.

In Figure 8.10b, the difference between the full model and the additive model is presented by the variations in the slopes of regressed lines against α levels. The linear regression of additive model predictions (the dashed parallel lines in Figure 8.10b) has identical slope coefficient 0.0871. Linear regressions of the full model predictions against α levels were conducted for each β level, the resulting coefficients and statistics are shown in Table 8.3. We can see that as β level increases, the slope of the full model increases until β reaches level 4, and slightly decreases for β level 5. Slopes with β level 1 and 2 are lower than that of additive model; slopes with β level 3, 4 and 5 are greater than that of additive model.

Table 8.3: Linear regressions of the full model parameters against α level for each β level. The R^2, F, and p-value of linear regression are also shown.

β level	Coefficients		Linear Regression Stats.		
	slope	intercept	R^2	F	p
1	0.0611	-0.0505	0.96	69.94	< 0.01
2	0.0778	0.2921	0.88	22.99	< 0.05
3	0.1334	0.3562	0.93	42.95	< 0.01
4	0.1464	0.2125	0.97	106.98	< 0.01
5	0.1040	0.1030	0.96	81.90	< 0.01

8.5 Conclusion and Discussion

In this chapter, we investigated how perceived gloss is jointly affected by mesoscale roughness (β) and microscale roughness (α). Our work is related with Ho et al. [2008], who studied 'bumpiness' and glossiness.

The findings are consistent with Ho et al. [2008] in that the microscale roughness exhibits a monotonic relationship with perceived gloss and the mesoscale roughness significantly affects perceived gloss. However, we have two novel findings that are at variance with Ho et al. [2008].

The relationship between perceived gloss and mesoscale roughness is obviously non-monotonic for all microscale roughness levels used in the experiment (consistent with Chapter 7). Ho et al. [2008] also noticed a slight decrease of gloss for their highest bump level surfaces and described it as "the trend was less clearly monotonic". They did not proceed to investigate 'bumpier' surfaces. We examined rougher surfaces and found that perceived gloss decreases for all α levels.

We tested our experimental results against the conjoint measurement models as used by Ho et al. [2008]. They found that the additive model is sufficient to describe the interaction between bumpiness and glossiness, whereas we found the additive model is rejected when compared with the full model for all eight observers in our experiment.

The difference between the full model and the additive model is the nonlinear component. We described this joint effect with a full conjoint measurement model.

Chapter 9

SUMMARY AND CONCLUSIONS

This thesis reports research that has investigated the effects of mesoscale and microscale surface parameters on perceptions of gloss. In this chapter we summarise the thesis argument, present the contribution of the research, and discuss the impact and future work.

9.1 Summary

9.1.1 Thesis Goal, Scope and Strategy

After presenting a survey into perceived and physical gloss it was concluded that little work has been carried out on gloss perception of "rough" surfaces. We therefore chose to investigate both surface geometry and reflection (mesoscale and microscale) factors. The reflection (microscale) factors were modelled using BRDF because of the popularity in literature. After an extended review of previous work concerning surface geometry, $1/f^{\beta}$ noise was chosen as surface mesoscale model because it is parsimonious (having only two parameters) and produces surfaces of natural appearance.

These surface geometry and reflection models were described further in Chapter 3. The RMS height (σ) and magnitude roll-off factor (β) of $1/f^{\beta}$ noise surfaces were

identified as 'mesoscale' roughness parameters [Padilla, 2008]. Four analytical BRDF models were described and three models were chosen to be used in this thesis. The BRDF parameter α was identified as the parameter which corresponds to 'microscale' roughness as it controls the microfacet distribution.

The investigation strategy was then discussed and the experiments were divided into two main stages according to the sophistication of the rendering system.

9.1.2 Experiments

Stage 1

Chapter 4 investigated the apparent gloss of high RMS height Lambertian surfaces reported by Wijntjes and Pont [2010]. Using the simple rendering system (described in Section 4.2), observers reported that gloss increased as surface RMS height was increased, leveling off after RMS height $\sigma > 150$.

Using the same conditions as those described in Chapter 4, Chapter 5 investigated the effect of variations in parameters of the Ward BRDF model on perceived gloss using a moderate RMS height $1/f^{\beta}$ noise surface. We found a monotonic relationship between perceived gloss and the three Ward parameters, which was modelled by a linear function accounting for 83% of the variance. Moreover, we found that moderate RMS height Ward surfaces can produce similar levels of gloss to those produced by the high RMS height Lambertian surfaces described in Chapter 4.

Stage 2

In this stage we modified the rendering system to allow more realistic stimuli to be produced. The improvements included the use of: physically based path tracing, a microfacet BRDF model, an HDR real-world illumination map and rotating surface animations. These improvements were found to remove the apparent gloss observed previously on high RMS height Lambertian surfaces. This illusory gloss is likely to be an artifact of the simple rendering system used in Chapter 4.

To overcome the limitations of manipulating surface RMS roughness [Padilla, 2008], the magnitude roll-off factor β of $1/f^{\beta}$ noise surfaces was varied. The stimuli were

rendered with a constant BRDF model. A subsequent experiment showed that perceived gloss has a non-monotonic relationship with mesoscale roughness (β). Further analysis suggested that perceived gloss is related to the percentage of highlight pixels. A model of highlight pixel behaviour as a function of the distributions of surface absolute slope angle and illumination intensity was proposed.

In Chapter 8, we investigated the joint effect of mesoscale roughness and microscale roughness on perceived gloss by simultaneously varying the roll-off factor (β) and the roughness parameter (α) of the BRDF model. Analysis using conjoint measurement models showed that the additive model was insufficient to describe the response of observers when compared with the full model, which is at variance with the literature. The difference between additive and full models is the nonlinear influence of mesoscale roughness and microscale roughness on perceived gloss.

9.2 Contributions

We believe that the main contributions of this thesis are that it has been shown:

1. that realistic rendering environments are important to the perception of gloss of rough surfaces,
2. that perceived gloss is a non-monotonic function of mesoscale roughness (β) and
3. that the joint effect of mesoscale roughness and microscale roughness on perceived gloss can only be described by a full conjoint model.

Concerning point 1, the use of an HDR environment illumination and physically based rendering described in Chapter 6 shows that realistic rendering is important. In particular, the apparent gloss of high RMS height Lambertian surfaces reported in Chapter 4 was not observed and is likely to be an artifact of the simple rendering system used by Wijntjes and Pont [2010].

Concerning point 2, the use of more realistic stimuli and constant gloss level (BRDF model) showed that there is a non-monotonic relationship between perceived gloss and mesoscale roughness. The literature reported part of this phenomenon (the monotonic increasing phase) but the research reported here shows that this is fol-

lowed by an inverse relationship (perceived gloss falls off rapidly when surface is very rough).

Finally we showed that when surface roughness varies in two categories: mesoscale and microscale, the joint effect is more complicated than that reported previously, and that a full conjoint measurement model is required.

9.3 Discussion and Future Work

Perceptions of textured surfaces have been investigated in terms of separate characteristics which are closely related to surface geometry, such as roughness [Padilla, 2008], directionality [Shah, 2010] and randomness [Emrith et al., 2010], whereas we investigated a perceptual characteristic affected by both surface geometry and reflectance properties. The work reported in this thesis will serve as a progress to discover more systematically how rough, textured surfaces are perceived by humans. The conclusions from this work will provide basis support to investigate more general perceptions of surface textures, such as perceptual texture similarity. For a wider community, the work reported in this thesis would benefit industry fields such as virtual design, manufacturing, cosmetics and cosmetology.

We also would like to address a few open questions about the perceived gloss of rough surfaces and potential investigation in future work.

Metrics for Perceived Gloss

As discussed in the literature survey, measurement of gloss using a gloss meter is a relative value referring to a specific material, which minimises the interference of other factors. In contrast, "perceived gloss" is affected by many factors and Ged et al. [2010] conjectured that the reasoning mechanism that the vision system employs requires rich cues from surface appearance. Perceived gloss as investigated in this thesis is characterised by a relative difference scale obtained under specific conditions. Therefore, deriving a general metric for perceived gloss requires considerable extra work especially concerning the affects of environmental conditions and is outside the scope of this thesis but should be considered for future work.

Illumination Environment

Two illumination conditions (collimated white light and an HDR real-world environment map) were used to render experimental stimuli, but the relationship between the perceived gloss of rough surfaces and the characteristics of illumination was not studied. In future work, this can be investigated using the method of stimuli modelling developed in this study.

DOI Gloss

The DOI cue was deliberately made not obvious in our stimuli. Relatively smooth surfaces at the mesoscale (such as group 1 surfaces in Chapter 7) were rated less glossy than medium rough ones (group 2) by observers. We conjectured that this is caused by the cue of specular highlights. However, these relatively smooth surfaces can exhibit DOI reflection with particular settings of microscale roughness parameter (α). Whether the DOI cue compensates the specular highlight cue would be an interesting question to address.

Predicting Perceived Gloss from Image Features

The investigation of specular highlights conducted in the discussions of Chapter 7 was not experimentally tested in this thesis. Previous work reported in the literature only examined the effect of highlight properties on perceived gloss [Beck and Prazdny, 1981] [Berzhanskaya et al., 2005]. We estimated five properties and found that none of them can satisfactorily explain the behaviour of perceived gloss in our experiments. The perceived gloss seems to be related to hybrid properties of specular highlights. Thus a reliable model based on image features is likely to require several dimensions and the various trends of the properties we observed suggest that a simple linear model may not suffice. Thus a more complicated model of perceived gloss as a function of surface appearance is worth future work. This requires defining computational features of specular highlights and developing novel techniques to precisely extract these features.

References

Adelson, E. H. (2001). On seeing stuff: the perception of materials by humans and machines. In Rogowitz, B. E. and Pappas, T. N., editors, *Human Vision and Electronic Imaging VI*, volume 4299, pages 1–12. SPIE.

Anderson, B. L. and Kim, J. (2009). Image statistics do not explain the perception of gloss and lightness. *Journal of Vision*, 9(11):1–17.

ASTM C346 (2009). Standard test method for 45-deg specular gloss of ceramic materials. ASTM International, West Conshohocken, PA, USA.

ASTM D2457 (2008). Standard test method for specular gloss of plastic films and solid plastics. ASTM International, West Conshohocken, PA, USA.

ASTM D3134 (2008). Standard practice for establishing color and gloss tolerances. ASTM International, West Conshohocken, PA, USA.

ASTM D523 (2008). Standard test method for specular gloss. ASTM International, West Conshohocken, PA, USA.

ASTM D5767 (2004). Standard test methods for instrumental measurement of distinctness-of-image gloss of coating surfaces. ASTM International, West Conshohocken, PA, USA.

ASTM E284 (2009). Standard terminology of appearance. ASTM International, West Conshohocken, PA, USA.

ASTM E430 (2011). Standard test methods for measurement of gloss of high-gloss surfaces by abridged goniophotometry. ASTM International, West Conshohocken, PA, USA.

Barrow, H. G. and Tenenbaum, J. M. (1978). Recovering intrinsic scene charac-

teristics from images. Technical Report 157, AI Center, SRI International, 333 Ravenswood Ave., Menlo Park, CA 94025.

Beck, J. and Prazdny, S. (1981). Highlights and the perception of glossiness. *Attention, Perception, & Psychophysics*, 30:407–410. 10.3758/BF03206160.

Belhumeur, P. N., Kriegman, D. J., and Yuille, A. L. (1999). The bas-relief ambiguity. *International Journal of Computer Vision*, 35:33–44.

Berzhanskaya, J., Swaminathan, G., Beck, J., and Mingolla, E. (2002). Highlights and surface gloss perception. *Journal of Vision*, 2(7):93–93.

Berzhanskaya, J., Swaminathan, G., Beck, J., and Mingolla, E. (2005). Remote effects of highlights on gloss perception. *Perception*, 34(5):565–575.

Billmeyer, F. W. and O'Donnell, F. X. D. (1987). Visual gloss scaling and multidimensional scaling analysis of painted specimens. *Color Research & Application*, 12(6):315–326.

Blake, A. and Bülthoff, H. H. (1990). Does the brain know the physics of specular reflection? *Nature*, 343:165–168.

Blinn, J. F. (1977). Models of light reflection for computer synthesized pictures. *ACM SIGGRAPH Computer Graphics*, 11:192–198.

Brainard, D. and Broussar, C. (2007). Rendertoolbox.

Chantler, M. (1994). *The effect of variation in illuminant direction on texture classification*. PhD thesis, Heriot-Watt University.

CIE Publication 017.4 (1987). International lighting vocabulary. Commission Internationale de l'Éclairage, Vienna, Austria.

CIE Publication 175 (2006). A framework for the measurement of visual appearance. Commission Internationale de l'Éclairage, Vienna, Austria.

Cook, R. L. and Torrance, K. E. (1982). A reflectance model for computer graphics. *ACM Transactions on Graphics*, 1:7–24.

Debevec, P. (1998). Rendering synthetic objects into real scenes: bridging traditional and image-based graphics with global illumination and high dynamic range photography. In *Proceedings of the 25th annual conference on Computer graphics*

and interactive techniques, SIGGRAPH '98, pages 189–198, New York, NY, USA. ACM.

Debevec, P. E. and Malik, J. (1997). Recovering high dynamic range radiance maps from photographs. In *Proceedings of the 24th annual conference on Computer graphics and interactive techniques*, SIGGRAPH '97, pages 369–378, New York, NY, USA. ACM Press/Addison-Wesley Publishing Co.

Dijkstra, T., Cornilleau-Peres, V., Gielen, C., and Droulez, J. (1995). Perception of three-dimensional shape from ego- and object-motion: Comparison between small- and large-field stimuli. *Vision Research*, 35(4):453–462.

DIN 67530 (1982). Reflectometers a means for gloss asssment of plane surfaces of paint coatings and plastics. DIN International Standards, DIN Deutsches Institut für Normung e. V., Berlin, Germany.

Doerschner, K., Boyaci, H., and Maloney, L. T. (2010a). Estimating the glossiness transfer function induced by illumination change and testing its transitivity. *Journal of Vision*, 10(4):1–9.

Doerschner, K., Maloney, L. T., and Boyaci, H. (2010b). Perceived glossiness in high dynamic range scenes. *Journal of Vision*, 10(9).

Dror, R. O., Adelson, E. H., and Willsky, A. S. (2001a). Estimating surface reflectance properties from images under unknown illumination. In *Proceedings SPIE Human Vision and Electronic Imaging IV*, pages 231–242.

Dror, R. O., Adelson, E. H., and Willsky, A. S. (2001b). Surface reflectance estimation and natural illumination statistics. In *Workshop on Statistical and Computational Theories of Vision*.

Dror, R. O., Willsky, A. S., and Adelson, E. H. (2004). Statistical characterization of real-world illumination. *Journal of Vision*, 4(9):821–837.

Ehrenstein, W. and Ehrenstein, A. (1999). Psychophysical methods. *Modern techniques in neuroscience research*, pages 1211–1241.

Emrith, K., Chantler, M. J., Green, P. R., Maloney, L. T., and Clarke, A. D. F. (2010). Measuring perceived differences in surface texture due to changes in higher order statistics. *J. Opt. Soc. Am. A*, 27(5):1232–1244.

Ferwerda, J. and Phillips, J. (2010). Effects of image dynamic range on perceived surface gloss. *Journal of Vision*, 10(7):387.

Ferwerda, J. A., Pellacini, F., and Greenberg, D. P. (2001). A psychophysically-based model of surface gloss perception. In *Proceedings SPIE Human Vision and Electronic Imaging*, pages 291–301.

Fleming, R. W., Dror, R. O., and Adelson, E. H. (2003). Real-world illumination and the perception of surface reflectance properties. *Journal of Vision*, 3(5):347–368.

Fleming, R. W., Jensen, H. W., and Bülthoff, H. H. (2004a). Perceiving translucent materials. In *Proceedings of the 1st Symposium on Applied perception in graphics and visualization*, APGV '04, pages 127–134, New York, NY, USA. ACM.

Fleming, R. W., Torralba, A., and Adelson, E. H. (2004b). Specular reflections and the perception of shape. *Journal of Vision*, 4(9):798–820.

Fleming, W., Dror, R. O., and Adelson, E. H. (2001). How do humans determine reflectance properties under unknown illumination. In *Proceedings of CVPR Workshop on Identifying Objects Across Variations in Lighting: Psychophysics and Computation*, pages 347–368.

Fulvio, J. M., Singh, M., and Maloney, L. T. (2006). Combining achromatic and chromatic cues to transparency. *Journal of Vision*, 6(8).

Ged, G., Obein, G., Silvestri, Z., Le Rohellec, J., and Viénot, F. (2010). Recognizing real materials from their glossy appearance. *Journal of Vision*, 10(9).

Gescheider, G. (1997). *Psychophysics: the fundamentals*. Lawrence Erlbaum.

Gibson, E. J., Gibson, J. J., Smith, O. W., and Flock, H. (1959). Motion parallax as a determinant of perceived depth. *Journal of Experimental Psychology*, 58:40–51.

Han, S. H., Song, M., and Kwahk, J. (1999). A systematic method for analyzing magnitude estimation data. *International Journal of Industrial Ergonomics*, 23(5-6):513 – 524.

Hanson, A. R. (2006). Good practice guide for the measurement of gloss. Guide Measurement Good Practice Guide No. 94, National Physical Liboratory.

Harrison, V. G. W. and Poulter, S. R. C. (1951). Gloss measurement of papers - the effect of luminance factor. *British Journal of Applied Physics*, 2(4):92.

Hartung, B. and Kersten, D. (2002). Distinguishing shiny from matte. *Journal of Vision*, 2(7):551–551.

He, X. D., Torrance, K. E., Sillion, F. X., and Greenberg, D. P. (1991). A comprehensive physical model for light reflection. *SIGGRAPH Comput. Graph.*, 25(4):175–186.

Ho, Y., Landy, M., and Maloney, L. (2008). Conjoint measurement of gloss and surface texture. *Psychological Science*, 19(2):196–204.

Hunter, R. and Harold, R. (1987). *The measurement of appearance*. Wiley-Interscience.

Hutchings, J. (1999). *Food color and appearance*. A Chapman & Hall food science book. Aspen Publishers.

ISO 2813:1994 (1994). Paints and varnishes – determination of specular gloss of non-metallic paint films at 20 degrees, 60 degrees and 85 degrees. International Organization for Standardization, Geneva, Switzerland.

Ji, W., Pointer, M. R., Luo, R. M., and Dakin, J. (2006). Gloss as an aspect of the measurement of appearance. *Journal of the Optical Society of America A*, 23(1):22–33.

Keyf, F. and Etikan, İ. (2004). Evaluation of gloss changes of two denture acrylic resin materials in four different beverages. *Dental Materials*, 20(3):244 – 251.

Kigle-Boeckler, G. (1995). Measurement of gloss and reflection properties of surfaces. *Metal Finishing*, 93(5):28–31.

Kim, J., Marlow, P., and Anderson, B. L. (2011). The perception of gloss depends on highlight congruence with surface shading. *Journal of Vision*, 11(9).

Knoblauch, K. and Maloney, L. T. (2009). Mlcm: Maximum likelihood conjoint measurement. CRAN.

Koenderink, J. J. (1986). Optic flow. *Vision Research*, 26(1):161 – 179.

Koenderink, J. J., Doorn, A. J. V., and Pont, S. C. (2004). Light direction from shadowed random gaussian surfaces. *Perception, special issue: Shadows and Illumination II*, 33(12):1403–1404.

Kurt, M. and Edwards, D. (2009). A survey of brdf models for computer graphics. *ACM SIGGRAPH Computer Graphics*, 43:4:1–4:7.

Lambert, J. H. (1760). *Photometria, sive de Mensura et gradibus luminis, colorum et umbrae*. Ostwald's Klassiker der exakten Wissenschaften, Nr. 31-33. sumptibus viduae E. Klett.

Landy, M. (2007). A gloss on surface properties. *Nature*, 447:158–159.

Leloup, F. B., Pointer, M. R., Dutré, P., and Hanselaer, P. (2011). Luminance-based specular gloss characterization. *J. Opt. Soc. Am. A*, 28(6):1322–1330.

Long, H. and Leow, W. K. (2001). Perceptual texture space improves perceptual consistency of computational features. In *Proceedings of the 17th international joint conference on Artificial intelligence - Volume 2*, IJCAI'01, pages 1391–1396, San Francisco, CA, USA. Morgan Kaufmann Publishers Inc.

LuxRender (2009). Luxrender v0.6.

Maloney, L. T. and Brainard, D. H. (2010). Color and material perception: Achievements and challenges. *Journal of Vision*, 10(9).

Mandelbrot, B. B. (1983). *The Fractal Geometry of Nature*. W. H. Freedman and Co., New York.

Marlow, P., Kim, J., and Anderson, B. L. (2011). The role of brightness and orientation congruence in the perception of surface gloss. *Journal of Vision*, 11(9).

Motoyoshi, I., Nishida, S., Sharan, L., and Adelson, E. (2007). Image statistics and the perception of surface qualities. *Nature*, 447(10):206–209.

Müller, G., Meseth, J., Sattler, M., Sarlette, R., and Klein, R. (2004). Acquisition, synthesis and rendering of bidirectional texture functions. In Schlick, C. and Purgathofer, W., editors, *Eurographics 2004, State of the Art Reports*, pages 69–94. INRIA and Eurographics Association.

Nagata, M., Okajima, K., and Osumi, M. (2007). Quantification of gloss perception as a function of stimulus duration. *Optical Review*, 14(6):406–410.

Nefs, H. T., Koenderink, J. J., and Kappers, A. M. L. (2005). The influence of illumination direction on the pictorial reliefs of lambertian surfaces. *Perception*, 34(3):275–287.

Ng, Y. S., Kuo, C.-H., Wang, C. J., Zeise, E., Mashtare, D., Kessler, J., Maggard, E., and Mehta, P. (2003). Standardization of perceptual based gloss and gloss uniformity for printing systems (incits w1.1). In *PICS*, pages 88–93. IS&T - The Society for Imaging Science and Technology.

Ngan, A., Durand, F., and Matusik, W. (2005). Experimental analysis of brdf models. In *Proceedings of the Eurographics Symposium on Rendering*, pages 117–226. Eurographics Association.

Nishida, S. and Shinya, M. (1998). Use of image-based information in judgments of surface-reflectance properties. *Journal of the Optical Society of America A*, 15(12):2951–2965.

Norman, J. F., Todd, J. T., and Orban, G. A. (2004). Perception of three-dimensional shape from specular highlights, deformations of shading, and other types of visual information. *Psychological Science*, 15(8):565–570.

Obein, G., Knoblauch, K., and Viénot, F. (2004a). Difference scaling of gloss: Nonlinearity, binocularity, and constancy. *Journal of Vision*, 4(9).

Obein, G., Pichereau, T., Harrar, M., Monot, A., Knoblauch, K., and Viénot, F. (2004b). Does binocular vision contribute to gloss perception? *Journal of Vision*, 4(11):73.

Olkkonen, M. and Brainard, D. H. (2010). Perceived glossiness and lightness under real-world illumination. *Journal of Vision*, 10(9).

Olkkonen, M. and Brainard, D. H. (2011). Joint effects of illumination geometry and object shape in the perception of surface reflectance. *i-Perception*, 2(9):1014–1034.

Oren, M. and Nayar, S. K. (1994). Generalization of lambert's reflectance model. In *SIGGRAPH '94: Proceedings of the 21st annual conference on Computer graphics and interactive techniques*, pages 239–246, New York, NY, USA. ACM.

Padilla, S. (2008). *Mathematical models for perceived roughness of three-dimensional surface textures*. PhD thesis, Heriot-Watt University.

Padilla, S., Drbohlav, O., Green, P. R., Spence, A., and Chantler, M. J. (2008). Perceived roughness of $1/f^{\beta}$ noise surfaces. *Vision Research*, 48(17):1791 – 1797.

Pellacini, F., Ferwerda, J. A., and Greenberg, D. P. (2000). Toward a

psychophysically-based light reflection model for image synthesis. In *SIGGRAPH '00: Proceedings of the 27th annual conference on Computer graphics and interactive techniques*, pages 55–64, New York, NY, USA. ACM Press/Addison-Wesley Publishing Co.

Perlin, K. (2002). Improving noise. *ACM Transactions on Graphics*, 21:681–682.

Pfund, A. H. (1930). The measurement of gloss. *J. Opt. Soc. Am.*, 20(1):23–23.

Pharr, M. and Humphreys, G. (2004). *Physically Based Rendering: From Theory to Implementation*. Morgan Kaufmann Publishers Inc., San Francisco, CA, USA.

Phillips, J. and Ferwerda, J. (2009). Effects of image dynamic range on apparent surface gloss. In *Proceedings IS&T 17th Color Imaging Conference*, pages 193–197.

Phillips, J. B., Ferwerda, J. A., and Nunziata, A. (2010). Gloss discrimination and eye movements. In Rogowitz, BE and Pappas, TN, editor, *HUMAN VISION AND ELECTRONIC IMAGING XV*, volume 7527 of *Proceedings of SPIE*. SPIE; IS & T Soc Imaging Sci & Technol; Aptina Imaging Corporat, SPIE-INT SOC OPTICAL ENGINEERING.

Phong, B. T. (1975). Illumination for computer generated pictures. *Communications of the ACM*, 18(6):311–317.

Picard, D. (2006). Partial perceptual equivalence between vision and touch for texture information. *Acta Psychologica*, 121(3):227 – 248.

Pointer, M. R. (2003). Measuring visual appearance - a framework of the future. project 2.3 measurement of appearance. NPL Report COAM 19, November 2003, ISSN: 1475-6684, National Physical Laboratory, British Library Document Supply Centre, Boston Spa, Wetherby, West Yorkshire, LS23 7BQ.

Ramamoorthi, R. and Hanrahan, P. (2001). An efficient representation for irradiance environment maps. *ACM Transactions on Graphics (Proceedings of SIGGRAPH 2001)*, 20(3):497–500.

Ramanarayanan, G., Ferwerda, J., Walter, B., and Bala, K. (2007). Visual equivalence: towards a new standard for image fidelity. *ACM Transactions on Graphics (TOG) - Proceedings of ACM SIGGRAPH 2007*, 26.

Rao, A. R. and Lohse, G. L. (1993). Towards a texture naming system: identifying

relevant dimensions of texture. In *Proceedings of the 4th conference on Visualization '93*, VIS '93, pages 220–227, Washington, DC, USA. IEEE Computer Society.

Sakano, Y. and Ando, H. (2008a). Both head motion and stereo viewing enhance perceived glossiness. *Journal of Vision*, 8(17):80–80.

Sakano, Y. and Ando, H. (2008b). Effects of self-motion on gloss perception. *Perception*, 37 ECVP Abstract Supplement:77.

Sakano, Y. and Ando, H. (2010). Effects of head motion and stereo viewing on perceived glossiness. *Journal of Vision*, 10(9).

Schlick, C. (1994). An inexpensive brdf model for physically-based rendering. *Computer Graphics Forum*, 13(3):233–246.

Schwartz, C., Weinmann, M., Ruiters, R., and Klein, R. (2011). Integrated high-quality acquisition of geometry and appearance for cultural heritage. In *The 12th International Symposium on Virtual Reality, Archeology and Cultural Heritage VAST 2011*. Eurographics Association.

Shah, P. (2010). *A Psychophysically-based Model for the Perceived Directionality of Textured Surfaces*. PhD thesis, School of Mathematical and Computer Sciences, Heriot-Watt University.

Sharan, L., Li, Y., Motoyoshi, I., Nishida, S., and Adelson, E. H. (2008). Image statistics for surface reflectance perception. *Journal of the Optical Society of America. A, Optics, Image Science, and Vision*, 25(4):846–65. PMID: 18382484.

Simoncelli, E. and Olshausen, B. (2001). Natural image statistics and neural representation. *Annual review of neuroscience*, 24(1):1193–1216.

Smith, K. B. (1999). Measuring the perception of glossy surfaces. *Pigment & Resin Technology*, 28(4):217–222.

Stevens, S., Stevens, G., and Marks, L. (1986). *Psychophysics: Introduction to its perceptual, neural, and social prospects*. Transaction Publishers.

Tamura, H., Mori, S., and Yamawaki, T. (1978). Textural features corresponding to visual perception. *IEEE Transactions on Systems, Man and Cybernetics*, 8(6):460 –473.

TAPPI T 480 om-09 (2009). Specular gloss of paper and paperboard at 75 degrees. Technical Association of the Pulp and Paper Industry, Norcross, USA.

te Pas, S. F. and Pont, S. C. (2005). A comparison of material and illumination discrimination performance for real rough, real smooth and computer generated smooth spheres. In *Proceedings of the 2nd symposium on Applied perception in graphics and visualization*, APGV '05, pages 75–81, New York, NY, USA. ACM.

Tighe, B. J. (1978). Subjective and objective assessment of surfaces. In Clark, D. T. and Feast, W. J., editors, *Polymer surfaces*. John Wiley &Sons, Chichester.

Todd, J. T., Norman, J. F., and Mingolla, E. (2004). Lightness constancy in the presence of specular highlights. *Psychological Science*, 15(1):33–39.

Torrance, K. and Sparrow, E. (1967). Theory for off-specular reflection from roughened surfaces. *Journal of the Optical society of America*, 57(9):1105–1114.

Vangorp, P., Laurijssen, J., and Dutré, P. (2007). The influence of shape on the perception of material reflectance. In *SIGGRAPH '07: ACM SIGGRAPH 2007 papers*, page 77, New York, NY, USA. ACM.

Voss, R. F. (1988). Fractals in nature: from characterization to simulation. In Peitgen, H.-O. and Saupe, D., editors, *The Science of Fractal Images*, chapter Fractals in nature: from characterization to simulation, pages 21–70. Springer-Verlag New York, Inc., New York, NY, USA.

Wallach, Hans;O'Connell, D. N. (1953). The kinetic depth effect. *Journal of Experimental Psychology*, 45(4):205–217.

Ward, G. (1992). Measuring and modeling anisotropic reflection. *Computer Graphics*, 26(2).

Ward, G. J. (1994). The radiance lighting simulation and rendering system. In *Proceedings of the 21st annual conference on Computer graphics and interactive techniques*, SIGGRAPH '94, pages 459–472, New York, NY, USA. ACM.

Wendt, G., Faul, F., and Mausfeld, R. (2007). The contribution of binocular cues to gloss perception. *Perception*, 36.

Wendt, G., Faul, F., and Mausfeld, R. (2008). Highlight disparity contributes to the authenticity and strength of perceived glossiness. *Journal of Vision*, 8(1):1–10.

Wijntjes, M. W. A. and Pont, S. C. (2010). Illusory gloss on lambertian surfaces. *Journal of Vision*, 10(9).

Wills, J., Agarwal, S., Kriegman, D., and Belongie, S. (2009). Toward a perceptual space for gloss. *ACM Transactions on Graphics*, 28:103:1–103:15.

Xiao, B. and Brainard, D. H. (2008). Surface gloss and color perception of 3D objects. *Visual Neuroscience*, 25:371–385.

Zchaluk, K. and Foster, D. (2009). Model-free estimation of the psychometric function. *Attention, Perception, & Psychophysics*, 71(6):1414–1425.

Appendices

Appendix A

STIMULI IMAGES USED IN CHAPTER 5

This appendix shows the stimuli images used in the gloss estimation experiment (Exp 1) in Chapter 5. They are listed in five figures (Figures A.1, A.2, A.3, A.4 and A.5), corresponding to the five sampled values of the Ward model parameter α. In each figure, the four columns of images correspond to the four sampled values of k_{d} and the five rows of images correspond to the five sampled values of k_{s}.

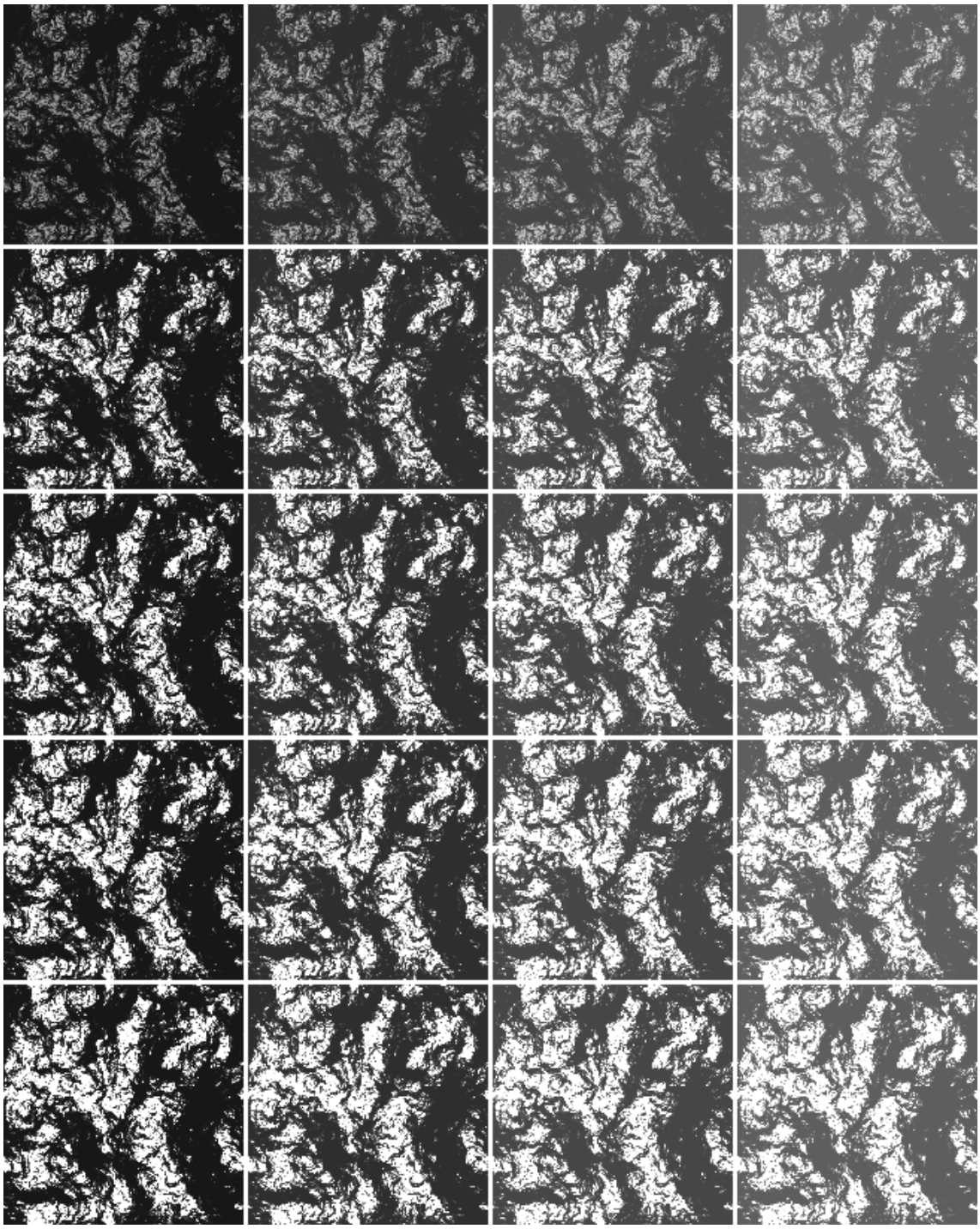

Figure A.1: Stimuli images with α=0.0498. k_{d}=0.285, 0.576, 0.867, 1.157 from left to right; k_{s}=0.0186, 0.051, 0.083, 0.116, 0.148 from top to bottom.

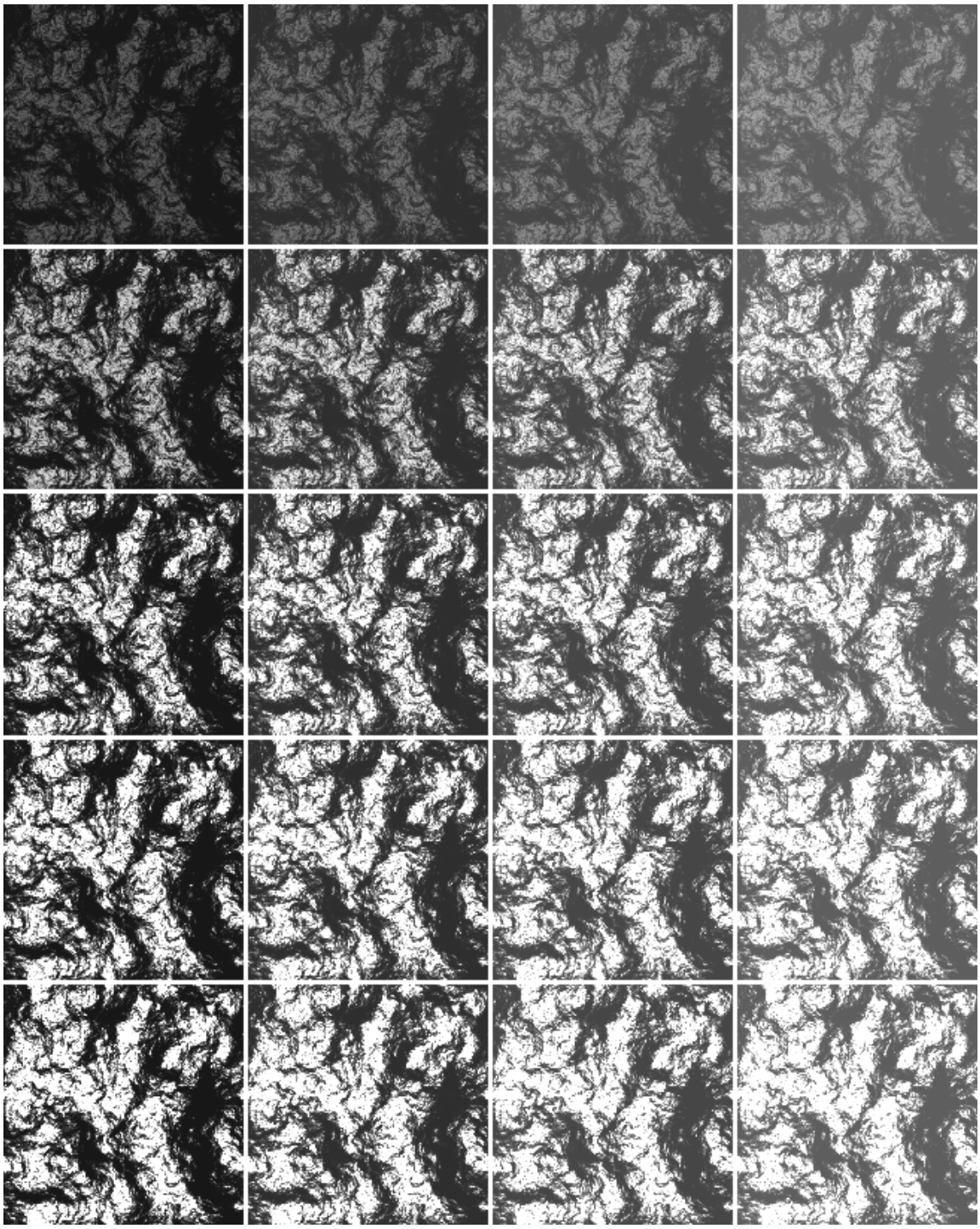

Figure A.2: Stimuli images with $\alpha = 0.0718$. k_{d}=0.285, 0.576, 0.867, 1.157 from left to right; k_{s}=0.0186, 0.051, 0.083, 0.116, 0.148 from top to bottom.

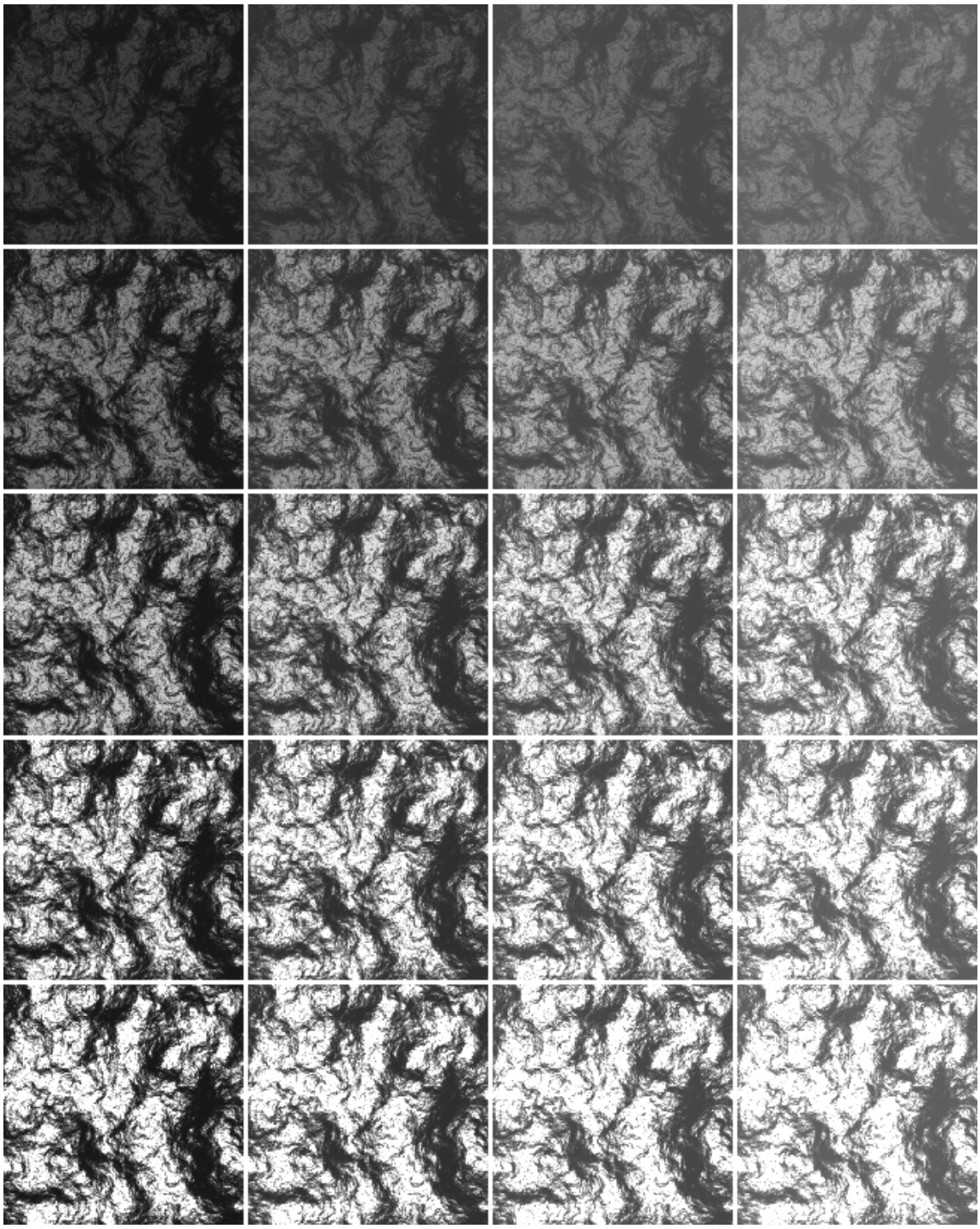

Figure A.3: Stimuli images with $\alpha = 0.0938$. k_{d}=0.285, 0.576, 0.867, 1.157 from left to right; k_{s}=0.0186, 0.051, 0.083, 0.116, 0.148 from top to bottom.

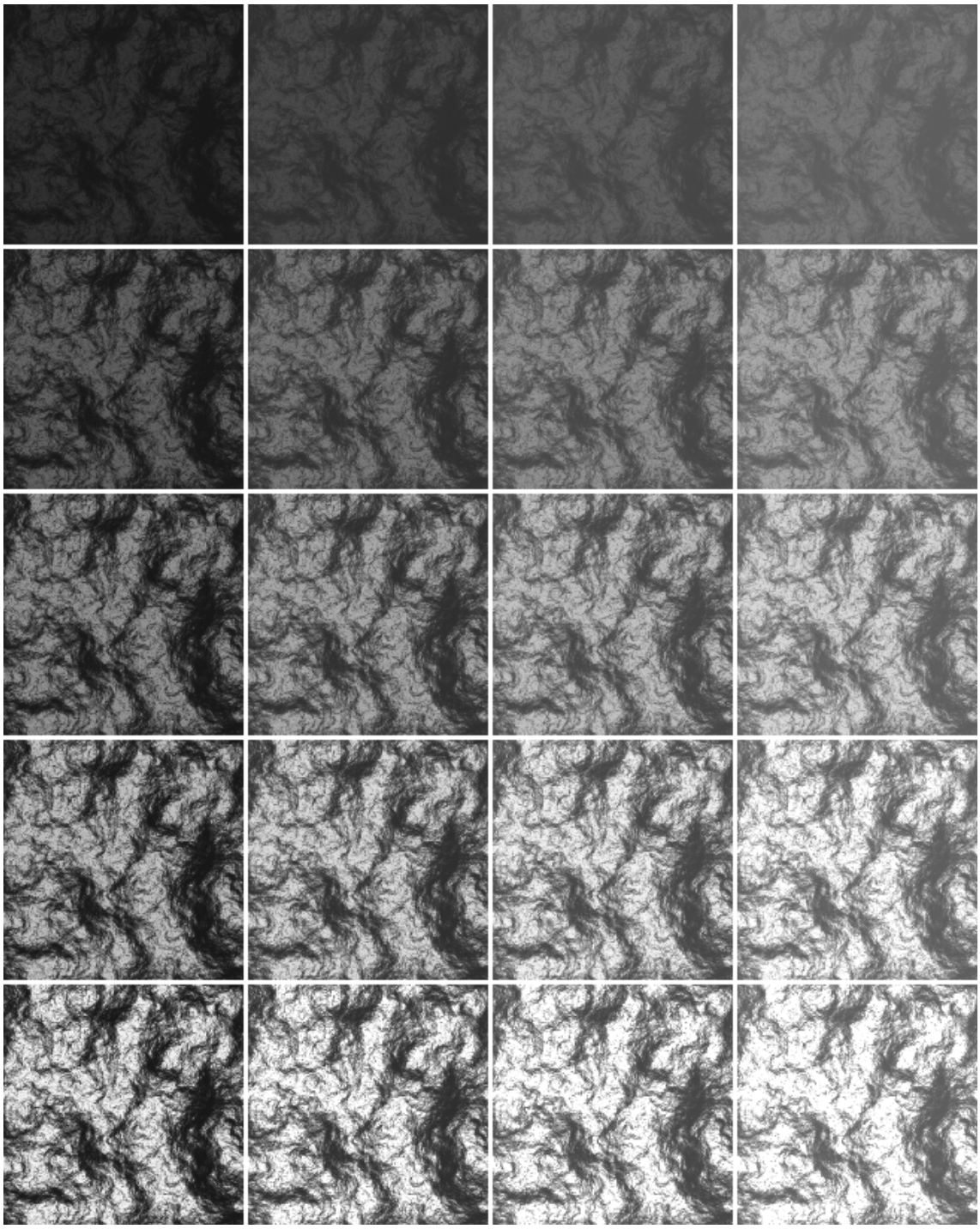

Figure A.4: Stimuli images with $\alpha = 0.116$. k_{d}=0.285, 0.576, 0.867, 1.157 from left to right; k_{s}=0.0186, 0.051, 0.083, 0.116, 0.148 from top to bottom.

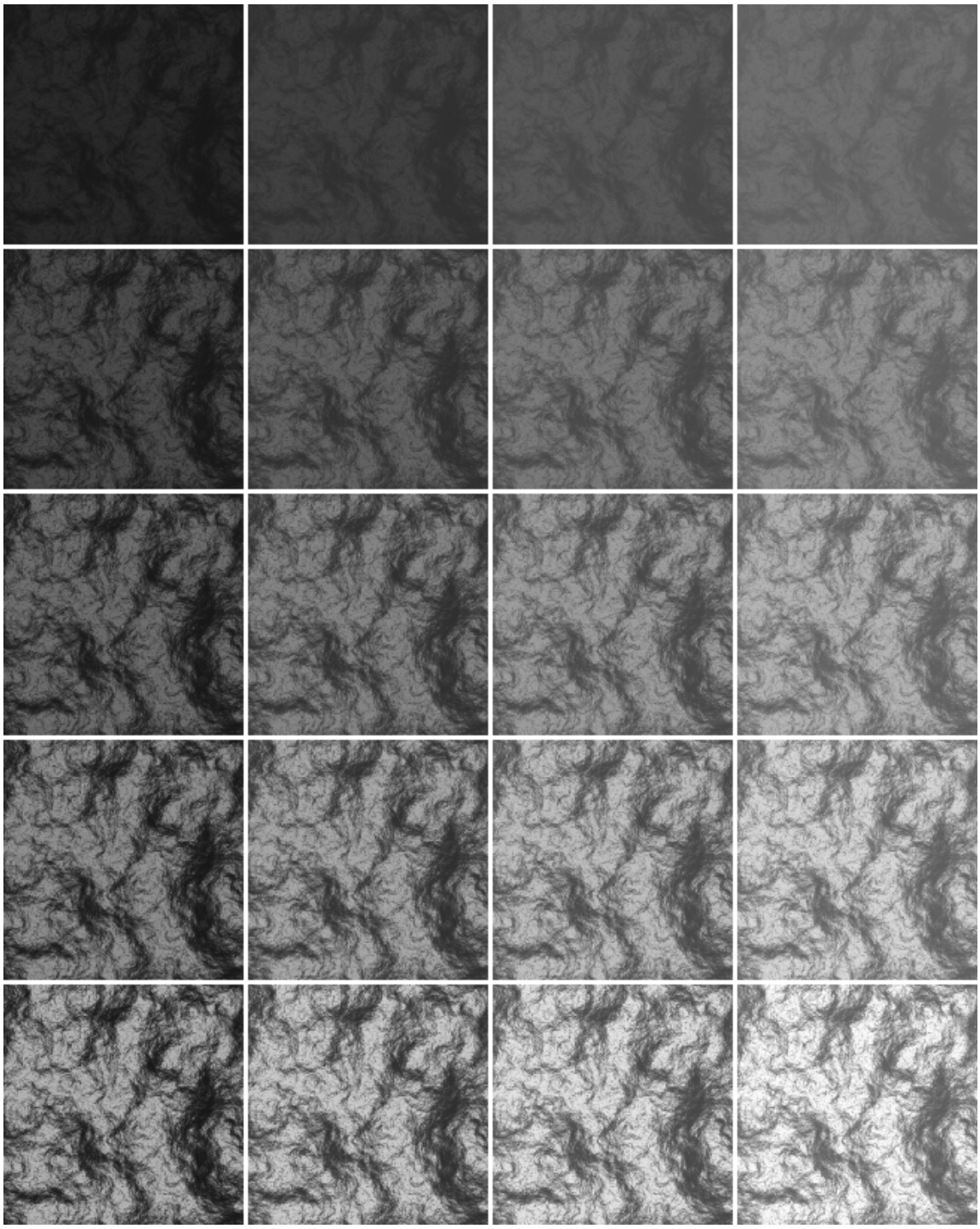

Figure A.5: Stimuli images with $\alpha = 0.138$. k_{d}=0.285, 0.576, 0.867, 1.157 from left to right; k_{s}=0.0186, 0.051, 0.083, 0.116, 0.148 from top to bottom.

Appendix B

EXPERIMENT ON GLOSS TRANSFER FUNCTION BETWEEN ILLUMINATION MAPS

We repeated the experiment conducted by Doerschner et al. [2010a] using $1/f^{\beta}$ noise surfaces. The aim is to investigate whether the perceived gloss transfer functions across illumination maps are also linear and linearly transitive by using rough surfaces as they found by using spheres.

We employed the same experiment and analysis methods as those used by Doerschner et al. [2010b]. The following describes the experiment.

B.1 Stimuli

The surface model was held constant, which was a $1/f^{\beta}$ noise surface with magnitude roll-off factor $\beta = 2.3$, RMS height $\sigma = 22$, random phase seed $\Theta = 0$. The surface was rendered using the method described in Chapter 6 (the Ashikhmin-Shirley model and path tracing). The illumination were varied among three environment maps as those used by Doerschner et al. [2010a] (shown in Figure 6.2). These were two indoor scenes (LF1 and LF3) and one outdoor scene (LF2).

The specular component parameter k_s of the Ashikhmin-Shirley model was equally sampled into 10 levels of gloss (from 0.25 to 0.7 in steps of 0.05). The diffuse component parameter k_d and exponent parameter α were held constant (0.3 and 0.01 respectively). There are totally 30 stimuli images (3 illumination maps $\times$ 10 gloss levels). Example images are shown in Figure B.1.

B.2 Procedure

The staircases comparison method was used to find the equal gloss points [Doerschner et al., 2010a]. Thirty interleaved one-up, one-down staircases were run and each of them was run for 50 trials.

In each staircase, one stimulus of a gloss level under one environment map was shown aside with the test stimulus of gloss level G_n under another environment map. Observers took a Two-Alternative Forced Choice (2AFC) task by indicating which one is glossier. The response decided the next gloss level G_{n+1} shown for the test image. Details about the method was described by Doerschner et al. [2010a].

Four observers participated in the experiment, all of which have normal or corrected to normal vision. Each observer made 1500 comparisons totally, all of them finished in one hour.

B.3 Results

Model-free psychometric functions were fitted and the equal gloss level points were derived by inferencing 50% threshold [Zchaluk and Foster, 2009]. The gloss transfer functions between each pair of environment maps ($\Gamma_{1\to2}(G)$, $\Gamma_{2\to3}(G)$, $\Gamma_{1\to3}(G)$) were expressed by fitting the equal gloss points to linear functions. To examine the transitivity of the transfer functions, we substituted $\Gamma_{2\to3}(G)$ to $\Gamma_{1\to2}(G)$ and obtained the predicted transfer function from LF1 to LF3: $\hat{\Gamma}_{1\to3}(G)$.

Figure B.2 shows the results of two observers (S1 and S2). The equal gloss points are shown as circles, whilst the error bars represent the $\pm$ standard deviation. The fitted linear functions are shown as the solid lines whilst the predicted transfer functions are shown as the dashed line in the bottom plots.

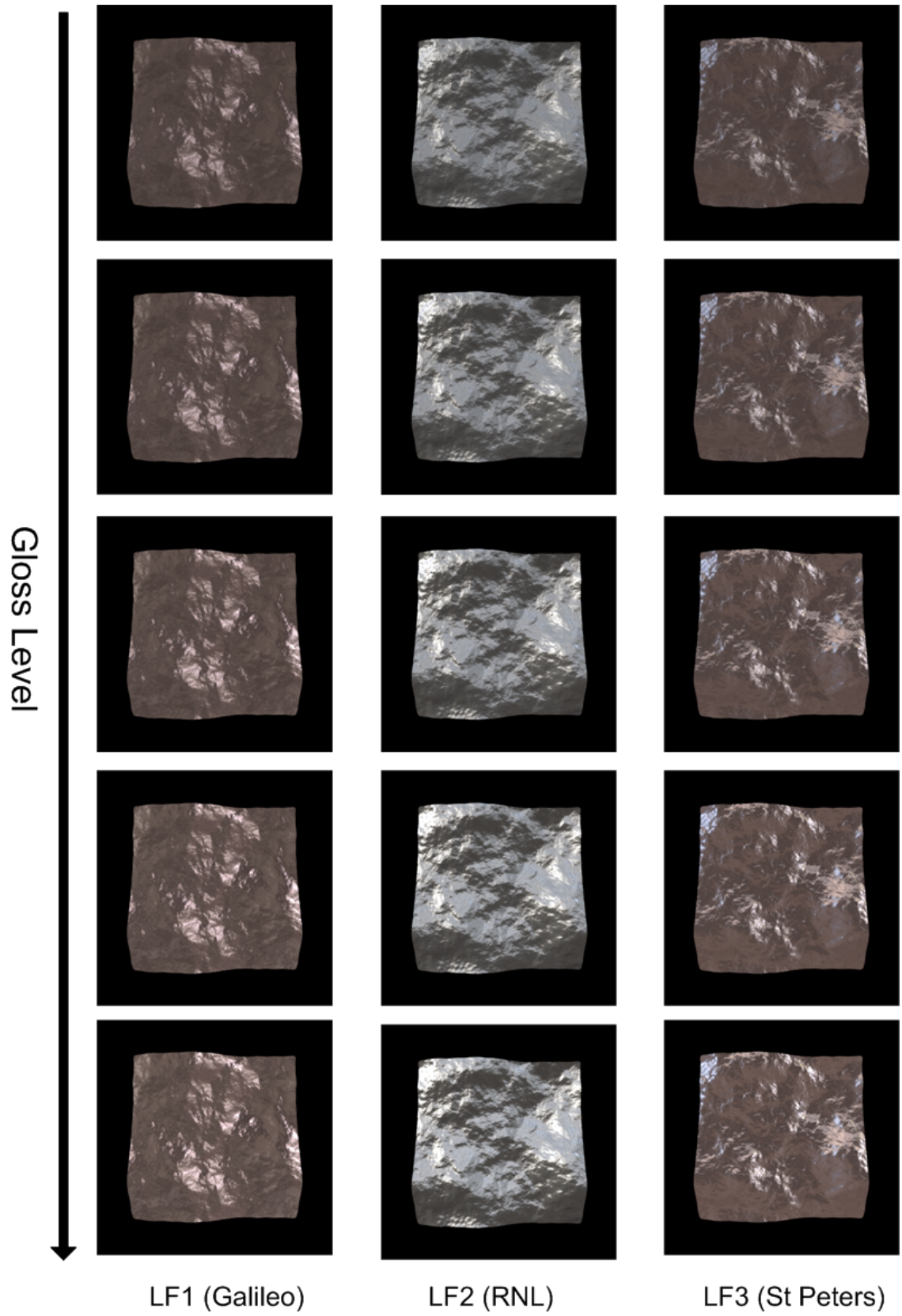

Figure B.1: Five images of surfaces with different gloss level under three environment maps are shown. These images have been adjusted by a nonlinear gamma for display purpose.

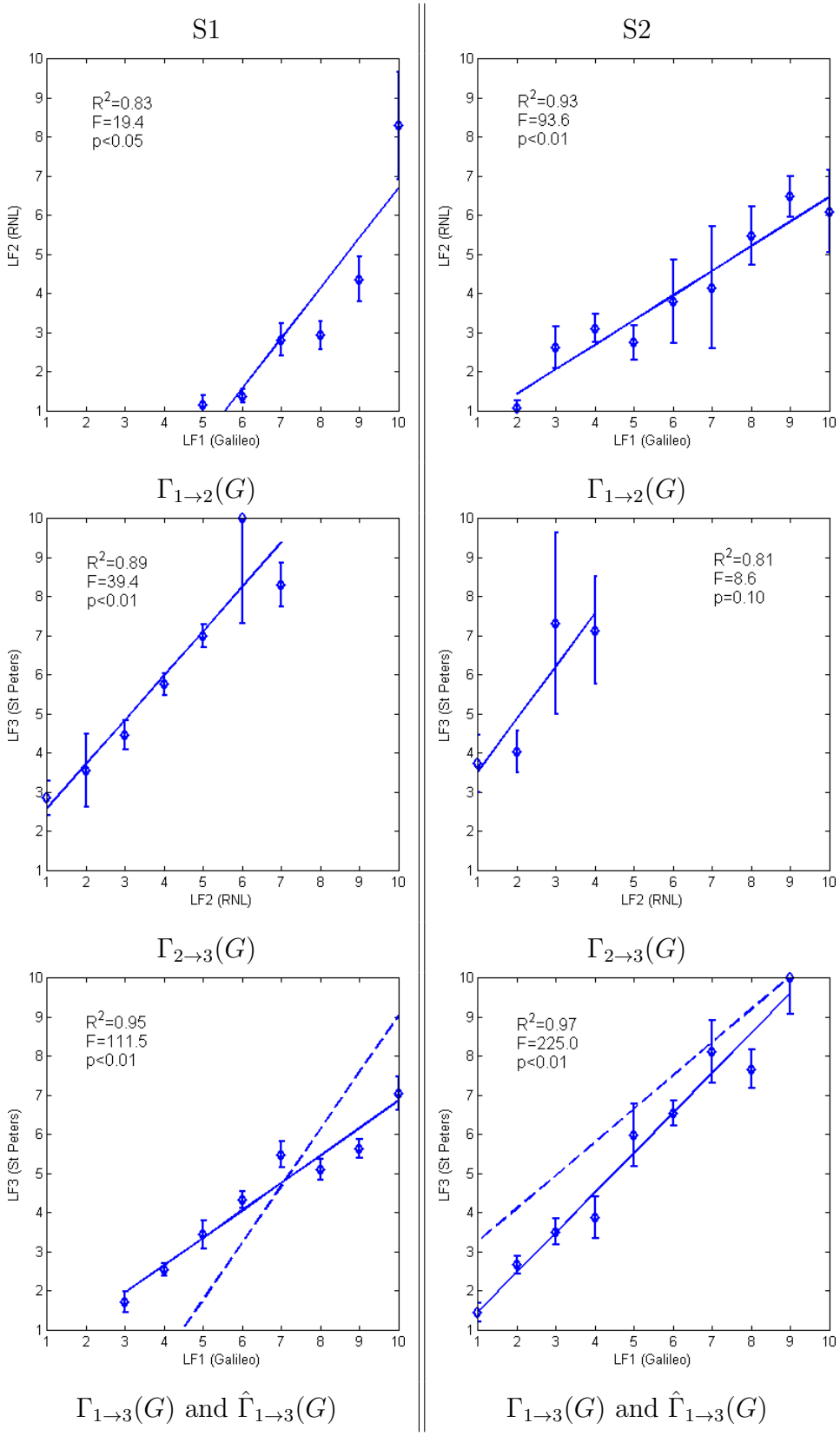

Figure B.2: Gloss transfer functions for observer S1 and S2. Equal gloss levels are represented by circles and the fitted linear functions are plotted in solid lines. The bottom plots show the predicted transfer function of $\Gamma_{1\to2}(\Gamma_{2\to3}(G))$ in dotted line, which is not well consistent with the measured transfer function $\Gamma_{1\to3}(G)$ (solid line).

The results from these two observers show that:

- the transfer functions between any two environment maps can be fitted by a linear function. This agrees with the findings of Doerschner et al. [2010a].
- the predicted transfer function ($\hat{\Gamma}_{1\to3}(G)$) between LF1 and LF3 is obviously not consistent with the measured one ($\Gamma_{1\to3}(G)$). This indicates that the linear transitivity of the transfer functions was not observed.

Inconsistently, the other two observers did not perform as expected and the results did not showed clear trend. No equal gloss level points or transfer functions were obtained.

B.4 Summary

From this repetition experiment we found that: for the rough surfaces as we used here, the linear transfer functions of perceived gloss between illumination maps were not obtained from all observers we used; the linear transitivity of transfer functions was not observed. Perceived gloss of rough surfaces is affected when changing environment maps, but this cannot be modelled or predicted using linear functions as the literature reported.

Appendix C

THE EFFECT OF VARIATION IN RANDOM PHASE SPECTRUM ON PERCEIVED GLOSS

This appendix describes the pilot experiment conducted prior to the main experiment of Chapter 7. The purpose is to examine whether the variation of seed for generating random phase spectrum (Θ) affects the perceived gloss of $1/f^{\beta}$ noise surfaces.

C.1 Experiment

We measured the perceived gloss of $1/f^{\beta}$ noise surfaces generated using a single random phase spectrum and varied random phase spectra. As a pilot experiment, the task and procedure were the same as the main experiment of Chapter 7.

Two groups of stimuli (14 β levels $\times$ 2 conditions of Θ) were produced using the method and parameters as those described in Section 7.1 with modifications in random phase spectra generation. One group used a single seed ($\Theta = 0$), the other group used varied seeds.

Seven observers took part in the pilot experiment. Four observers were shown single

seed stimuli and three observers were shown varied seed stimuli. The raw results were presented in Figure C.1 and Figure C.2 respectively. Figure C.3 shows the arithmetic means of normalized data and geometric means of raw data for the two groups.

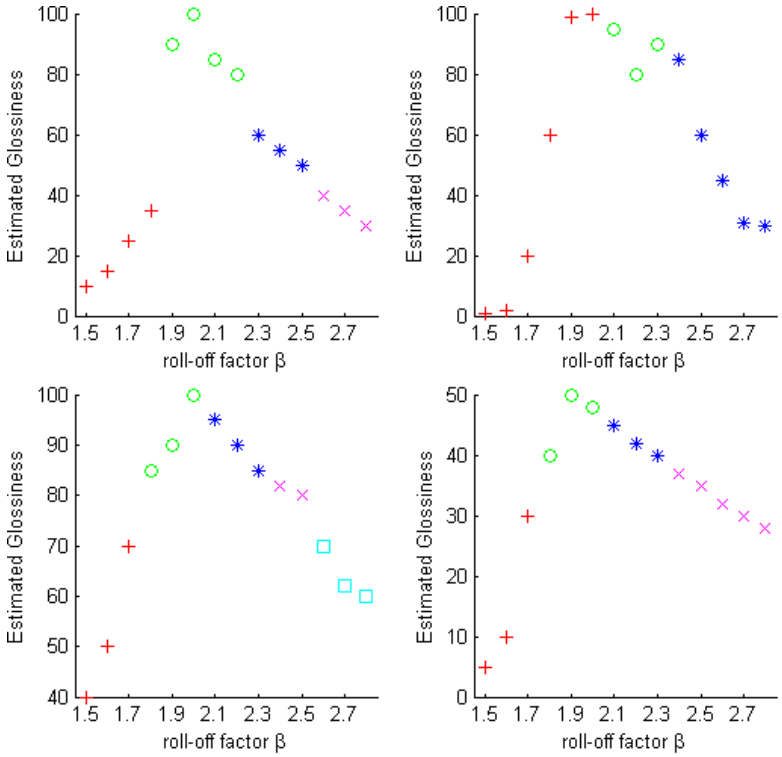

Figure C.1: Experiment results for the four observers who were shown stimuli that were generated using a single random phase spectrum.

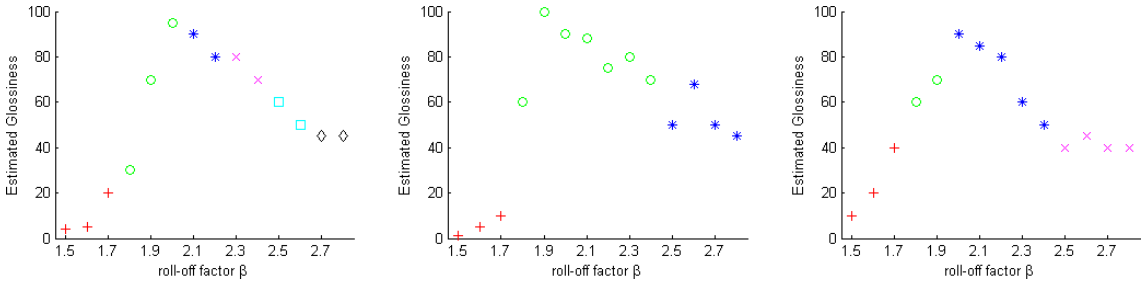

Figure C.2: Experiment results for the three observers who were shown stimuli that were generated using varied seeds for random phase spectra.

A mixed design ANOVA was conducted on the results of these two groups. The statistical test shows that there is no significant effect of the seed for random phase spectrum (Θ) on perceived gloss ($F(1,5) = 0.173 < 1$, $p = 0.694$). This indicates that the perceived gloss of surfaces generated using fixed and varied seeds for random phase spectra was in general the same. The estimated marginal means of perceived

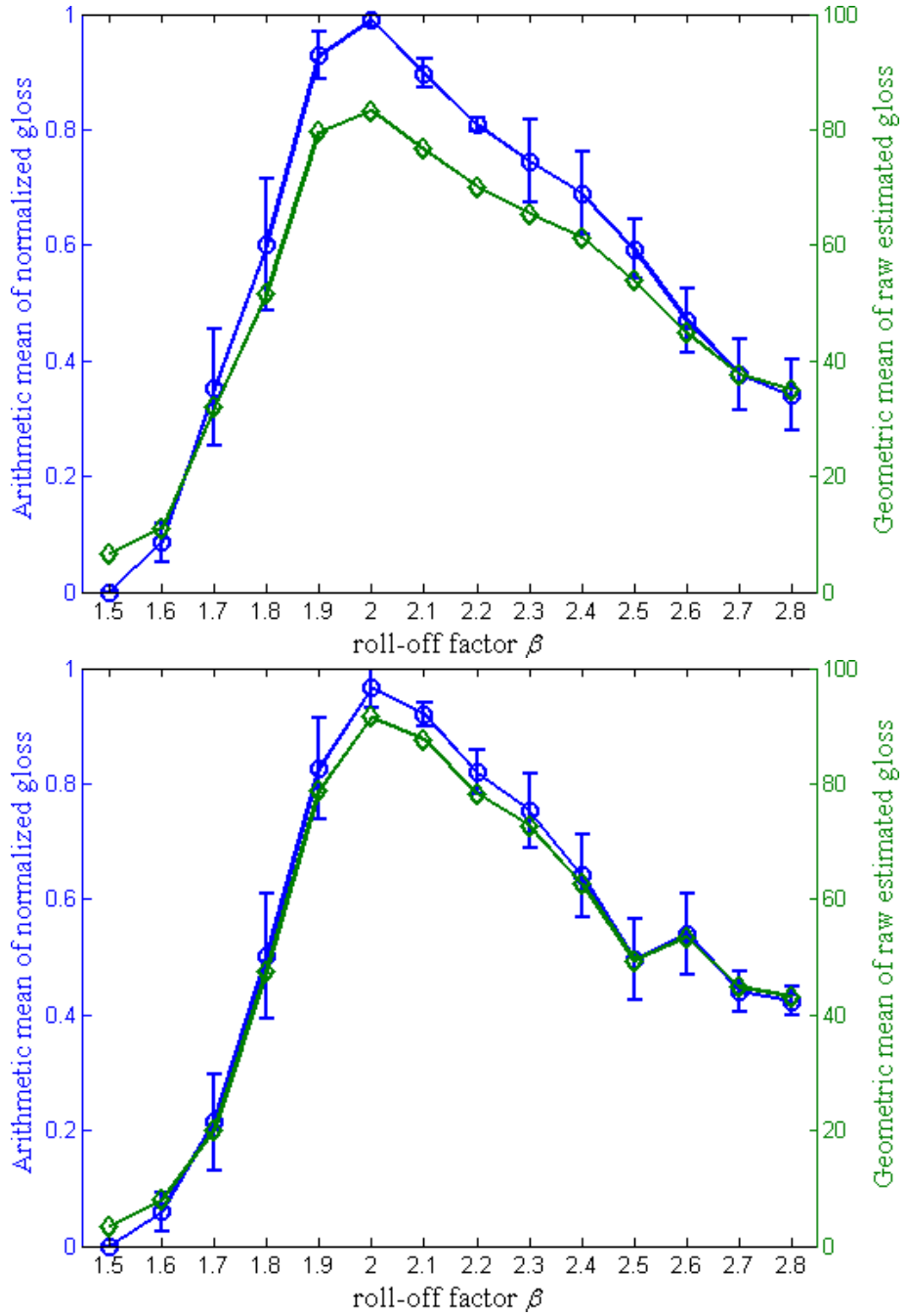

Figure C.3: Mean results of the pilot experiment. The top graph shows the means across the four observers who were shown stimuli generated using fixed seed random phase. The bottom graphs shows the means across the three observers who were shown stimuli generated using varied seed random phase. The arithmetic means of normalised data and geometric means of raw data are plotted against the left and right y-axis respectively.

gloss for random phase spectrum (Θ) are shown in Table C.1 and plotted in a bar chart with 95% confidence intervals in Figure C.4.

Table C.1: Estimated marginal means of perceived gloss of the two groups (fixed seed and varied seed).

Seed for random phase	Mean	Std. Error	95% Confidence Interval	
			Lower Bound	Upper Bound
Single	0.563	0.031	0.482	0.643
Varied	0.543	0.036	0.450	0.635

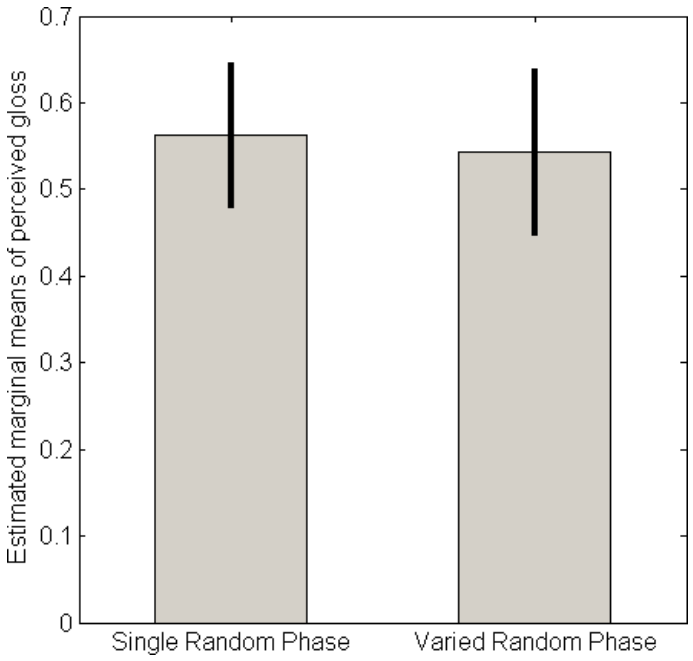

Figure C.4: Estimated marginal means of perceived gloss for random phase spectrum. The error bars denote 95% confidence interval.

C.2 Conclusion

This pilot experiment indicates that the seed for generating random phase spectrum does not significantly affect perceived gloss of $1/f^{\beta}$ noise surface. Therefore, the constraint of using a fixed seed for generating random phase spectrum imposed in the experiments of Chapters 4, 5 and 6 was relaxed to using varied seeds in later experiments.

Appendix D

FITTED PARAMETERS OF CONJOINT MEASUREMENT MODELS

This appendix shows the fitted parameters of conjoint measurement models for the eight observers in the experiment of Chapter 8. These are listed in five figures. Figure D.1 and Figure D.2 show the fitted parameters of the two independent models (G^{I_α} and G^{I_β}) respectively. Figure D.3 shows the fitted parameters of the additive model (G^{A}). Figure D.4 and Figure D.5 show the fitted parameters of the full model (G^{F}), which are separately plotted against levels of β and α.

These results were used to calculate the means and standard errors across all eight observers, resulting the plots in Figure 8.3, Figure 8.5 and Figure 8.7.

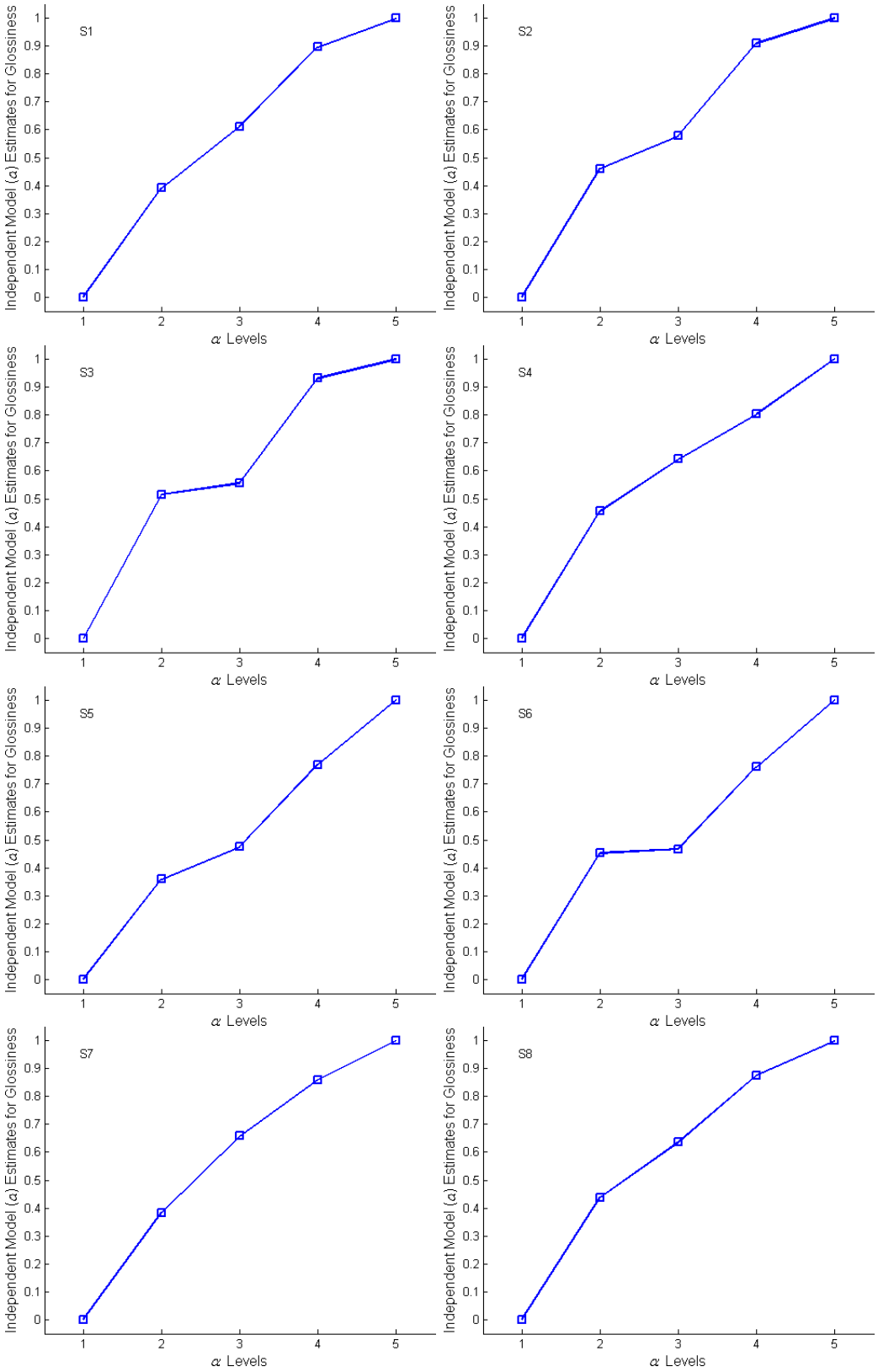

Figure D.1: Fitted parameters for the independent model G^{I_α}.

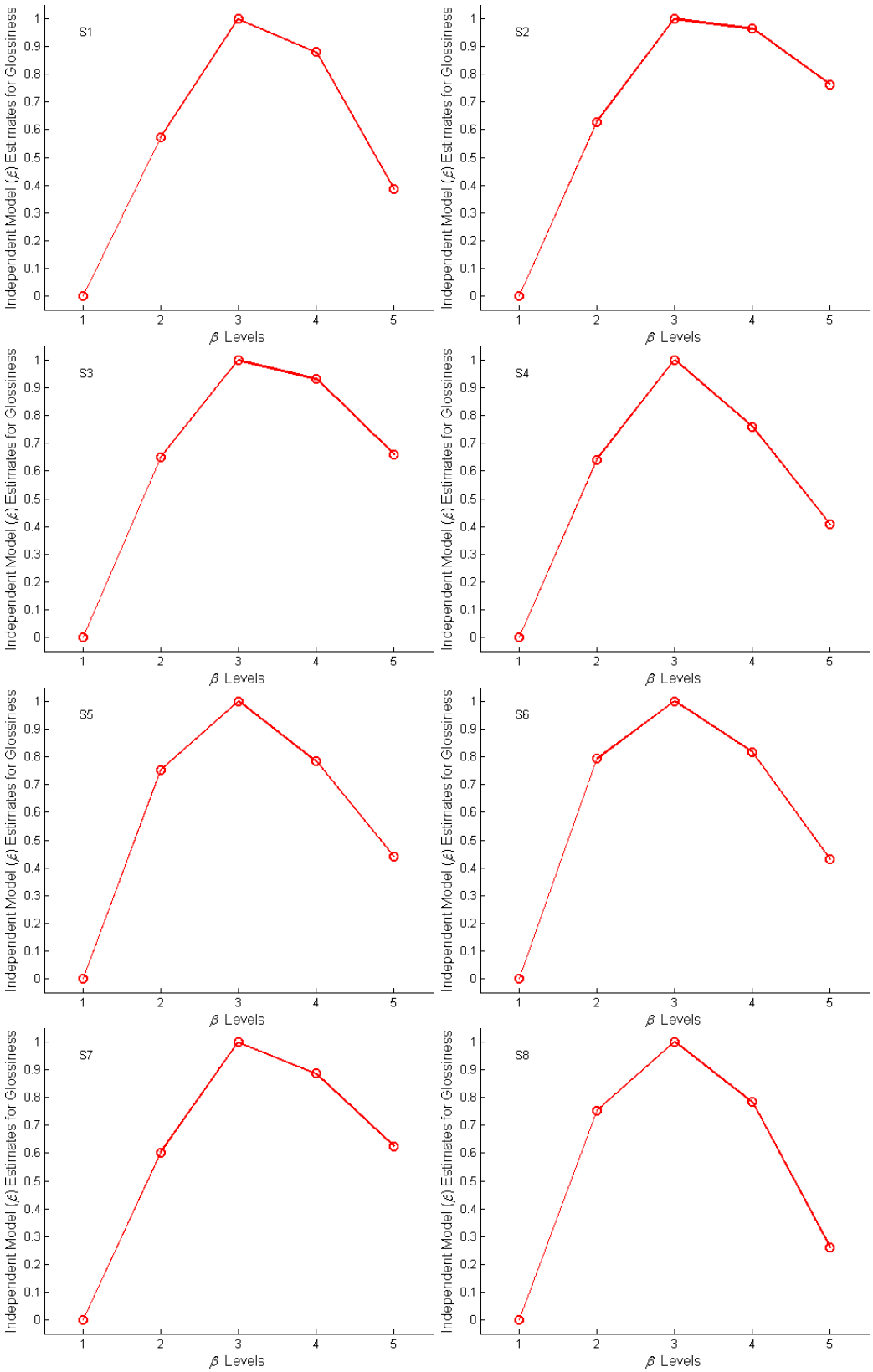

Figure D.2: Fitted parameters for the independent model G^{I_β}.

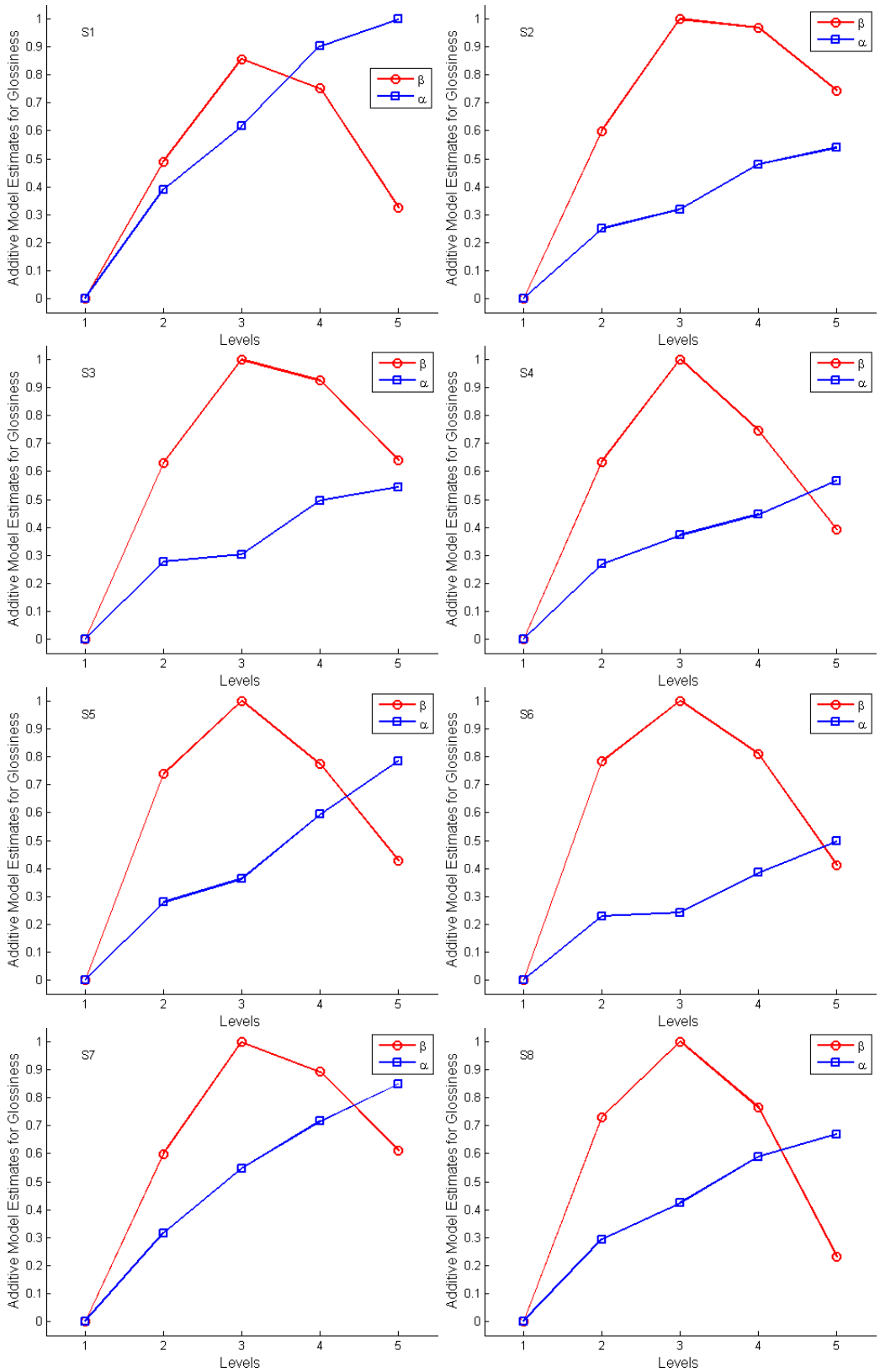

Figure D.3: Fitted parameters for the additive model G^{A}.

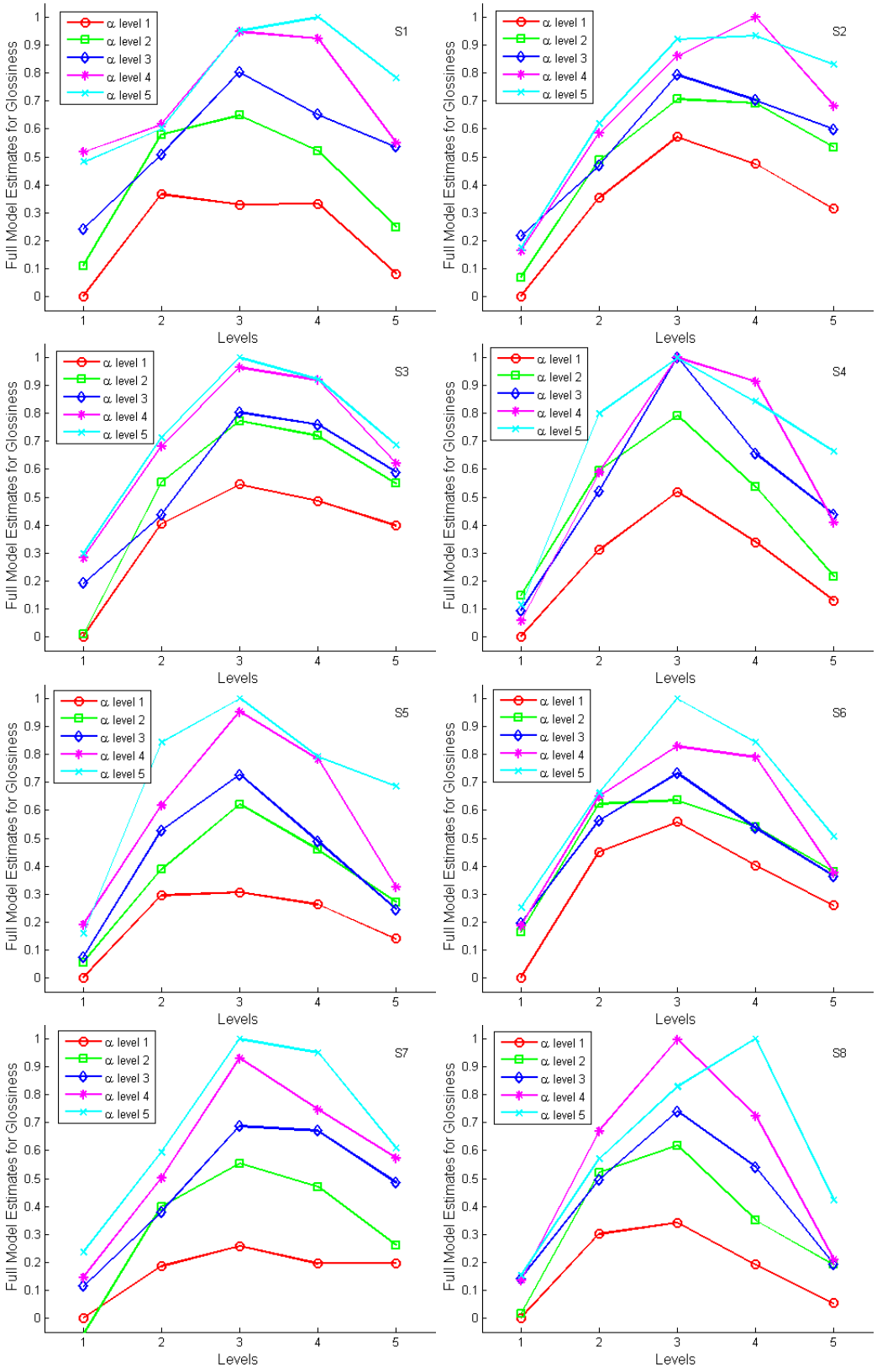

Figure D.4: Fitted parameters for the full model G^{F}. These are plotted against β levels. Different curves denote α levels.

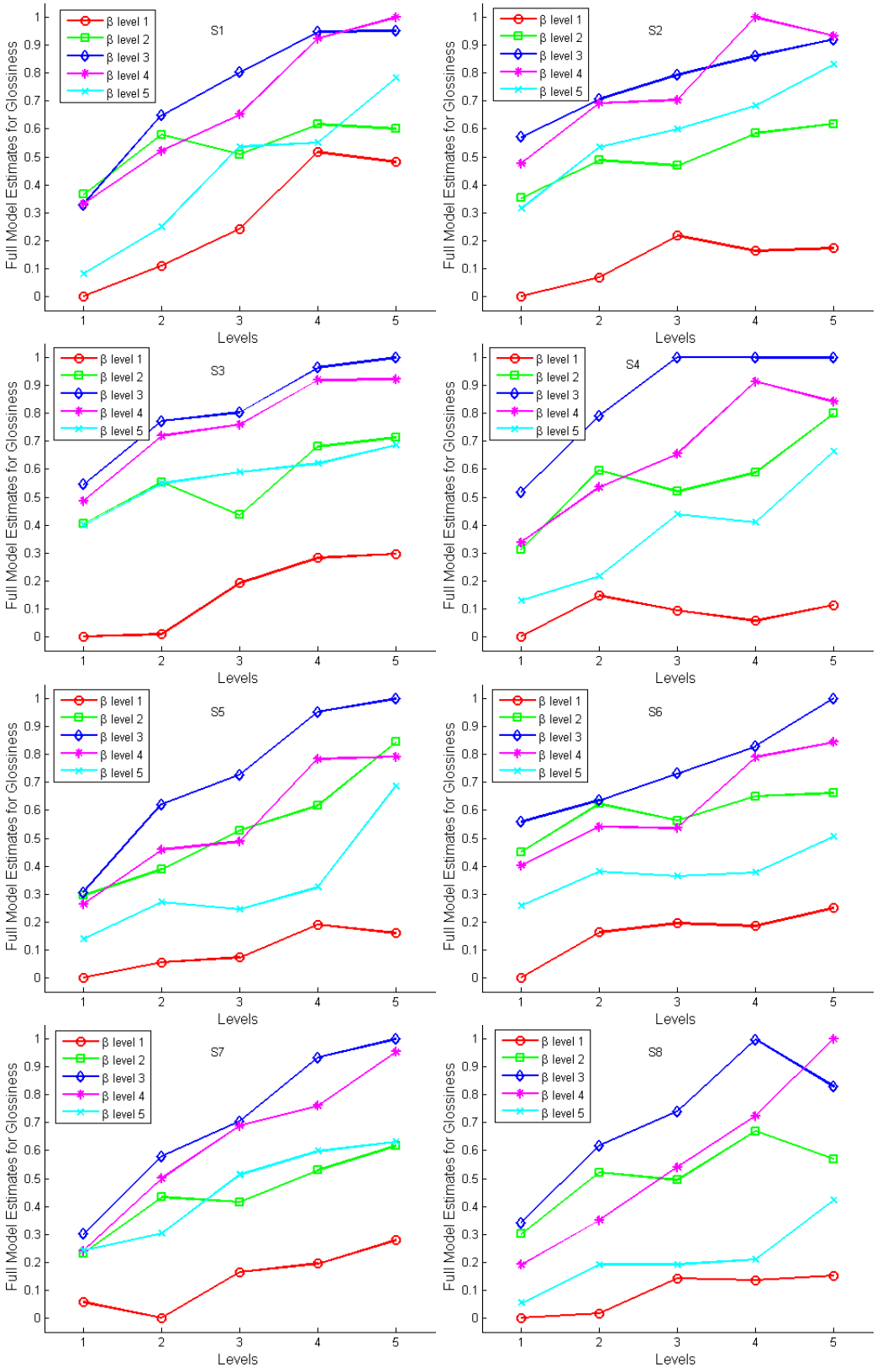

Figure D.5: Fitted parameters for the full model G^{F}. These are plotted against α levels. Different curves denote β levels.

Appendix E

EXPERIMENT RESULTS

Table E.1: The gloss estimation experiment results of Chapter 4. The left column denotes the ten Lambertian surfaces with different RMS height (σ) used in the experiment of Chapter 4. The numbers are the index i of surface S_{σ_i}. The other columns show the results from the ten observers.

S_{σ_i}	s1	s2	s3	s4	s5	s6	s7	s8	s9	s10
1	0.30	0.19	0.53	0.36	0.39	0.56	0.50	0.41	0.40	0.26
2	0.25	0.25	0.44	0.35	0.44	0.55	0.52	0.32	0.47	0.35
3	0.33	0.20	0.46	0.43	0.59	0.60	0.50	0.36	0.48	0.21
4	0.38	0.30	0.47	0.49	0.59	0.60	0.55	0.45	0.43	0.34
5	0.40	0.32	0.64	0.75	0.51	0.80	0.57	0.44	0.47	0.48
6	0.35	0.35	0.64	0.80	0.68	0.62	0.54	0.43	0.50	0.65
7	0.29	0.50	0.70	0.80	0.55	0.76	0.59	0.44	0.53	0.57
8	0.35	0.53	0.60	0.58	0.58	0.78	0.59	0.55	0.66	0.21
9	0.38	0.71	0.73	0.58	0.67	0.81	0.58	0.61	0.66	0.35
10	0.32	0.60	0.59	0.77	0.71	0.88	0.62	0.56	0.53	0.24

Table E.2: The gloss estimation experiment results of Chapter 5 (Exp 1). The left three columns denote the 100 stimuli which are represented by the combinations of the three Ward model parameters (k_d, k_s and α) used in the experiment. The other columns show the results from the ten observers.

k_d	k_s	α	s1	s2	s3	s4	s5	s6	s7	s8	s9	s10
0.29	0.02	0.05	0.14	0.94	0.72	0.48	0.30	0.92	0.60	0.36	0.72	0.33
0.29	0.02	0.07	0.04	0.39	0.34	0.10	0.09	0.90	0.59	0.19	0.59	0.41
0.29	0.02	0.09	0.03	0.40	0.16	0.00	0.16	0.48	0.24	0.10	0.16	0.59
0.29	0.02	0.12	0.00	0.40	0.19	0.00	0.04	0.43	0.15	0.07	0.56	0.65
0.29	0.02	0.14	0.00	0.05	0.05	0.00	0.04	0.04	0.27	0.07	0.46	0.39
0.29	0.05	0.05	0.76	0.75	0.88	0.93	0.84	1.00	0.96	0.88	0.98	0.73
0.29	0.05	0.07	0.42	0.76	0.65	0.75	0.61	0.72	0.62	0.40	0.80	0.52
0.29	0.05	0.09	0.20	0.58	0.23	0.20	0.20	0.90	0.39	0.32	0.55	0.29
0.29	0.05	0.12	0.15	0.34	0.43	0.35	0.10	0.62	0.29	0.14	0.65	0.37
0.29	0.05	0.14	0.11	0.15	0.22	0.07	0.28	0.22	0.55	0.16	0.56	0.36
0.29	0.08	0.05	0.61	0.76	0.91	1.00	0.96	0.99	0.99	0.96	0.92	0.63
0.29	0.08	0.07	0.76	0.69	0.88	0.93	0.96	0.93	0.84	0.61	0.96	0.51
0.29	0.08	0.09	0.34	0.62	0.48	0.33	0.54	0.82	0.48	0.39	0.71	0.35
0.29	0.08	0.12	0.21	0.59	0.32	0.27	0.34	0.60	0.54	0.16	0.51	0.66
0.29	0.08	0.14	0.13	0.61	0.39	0.00	0.30	0.50	0.34	0.12	0.27	0.58
0.29	0.12	0.05	0.91	0.91	0.96	1.00	1.00	1.00	0.92	0.95	0.96	0.90
0.29	0.12	0.07	0.95	0.66	0.85	0.99	1.00	0.99	0.90	0.93	0.85	0.59
0.29	0.12	0.09	0.75	0.55	0.82	0.84	0.85	0.99	0.82	0.58	0.70	0.74
0.29	0.12	0.12	0.21	0.51	0.51	0.53	0.25	0.97	0.56	0.22	0.77	0.47
0.29	0.12	0.14	0.11	0.50	0.41	0.33	0.53	0.50	0.54	0.31	0.41	0.36
0.29	0.15	0.05	0.96	0.91	0.96	1.00	1.00	1.00	1.00	0.98	0.98	0.38
0.29	0.15	0.07	0.94	0.59	0.88	0.96	0.99	0.97	0.86	0.93	0.90	0.79
0.29	0.15	0.09	0.93	0.62	0.70	0.91	1.00	0.84	0.88	0.77	0.89	0.56
0.29	0.15	0.12	0.76	0.68	0.67	0.71	0.83	0.78	0.61	0.65	0.76	0.84
0.29	0.15	0.14	0.10	0.34	0.44	0.44	0.32	0.47	0.53	0.43	0.69	0.13
0.58	0.02	0.05	0.02	0.36	0.46	0.39	0.39	0.69	0.60	0.16	0.59	0.36

Continued on Next Page...

Table E.2 – continued from previous page

k_d	k_s	α	s1	s2	s3	s4	s5	s6	s7	s8	s9	s10
0.58	0.02	0.07	0.10	0.11	0.15	0.04	0.20	0.60	0.17	0.30	0.57	0.17
0.58	0.02	0.09	0.00	0.27	0.09	0.01	0.11	0.18	0.08	0.07	0.37	0.78
0.58	0.02	0.12	0.01	0.10	0.14	0.00	0.14	0.08	0.12	0.07	0.32	0.59
0.58	0.02	0.14	0.00	0.02	0.12	0.00	0.09	0.20	0.08	0.03	0.31	0.26
0.58	0.05	0.05	0.54	0.60	0.61	0.92	0.68	0.96	0.64	0.41	0.86	0.36
0.58	0.05	0.07	0.30	0.32	0.45	0.82	0.62	0.82	0.70	0.33	0.71	0.37
0.58	0.05	0.09	0.15	0.31	0.33	0.10	0.32	0.53	0.25	0.09	0.71	0.23
0.58	0.05	0.12	0.06	0.27	0.32	0.35	0.12	0.44	0.24	0.27	0.37	0.17
0.58	0.05	0.14	0.09	0.08	0.15	0.38	0.06	0.22	0.11	0.12	0.47	0.35
0.58	0.08	0.05	0.85	0.75	0.54	0.89	0.53	0.94	0.72	0.42	0.78	0.64
0.58	0.08	0.07	0.81	0.47	0.65	0.70	0.67	0.95	0.59	0.57	0.95	0.44
0.58	0.08	0.09	0.52	0.38	0.65	0.41	0.51	0.65	0.71	0.50	0.57	0.36
0.58	0.08	0.12	0.16	0.08	0.39	0.26	0.19	0.53	0.40	0.30	0.51	0.30
0.58	0.08	0.14	0.08	0.30	0.27	0.05	0.08	0.45	0.43	0.07	0.61	0.05
0.58	0.12	0.05	0.73	0.47	0.68	0.68	0.75	0.91	0.53	0.53	0.90	0.40
0.58	0.12	0.07	0.81	0.47	0.59	0.81	0.68	0.96	0.70	0.56	0.75	0.17
0.58	0.12	0.09	0.64	0.38	0.44	0.77	0.76	0.76	0.58	0.26	0.62	0.66
0.58	0.12	0.12	0.33	0.34	0.52	0.67	0.82	0.34	0.33	0.24	0.51	0.38
0.58	0.12	0.14	0.12	0.33	0.53	0.41	0.21	0.50	0.34	0.13	0.42	0.22
0.58	0.15	0.05	0.70	0.65	0.61	0.82	0.73	0.96	0.75	0.73	0.80	0.27
0.58	0.15	0.07	0.91	0.68	0.50	0.94	0.79	0.82	0.61	0.61	0.95	0.17
0.58	0.15	0.09	0.89	0.36	0.65	0.65	0.59	0.81	0.76	0.43	0.82	0.67
0.58	0.15	0.12	0.56	0.36	0.49	0.79	0.70	0.88	0.45	0.38	0.52	0.67
0.58	0.15	0.14	0.36	0.26	0.40	0.47	0.21	0.54	0.37	0.19	0.35	0.50
0.87	0.02	0.05	0.08	0.37	0.21	0.40	0.24	0.59	0.38	0.09	0.51	0.33
0.87	0.02	0.07	0.09	0.03	0.09	0.03	0.26	0.16	0.19	0.04	0.29	0.49
0.87	0.02	0.09	0.05	0.30	0.19	0.01	0.04	0.22	0.09	0.18	0.40	0.41
0.87	0.02	0.12	0.00	0.07	0.08	0.06	0.07	0.01	0.03	0.02	0.30	0.19
0.87	0.02	0.14	0.00	0.00	0.05	0.00	0.00	0.01	0.00	0.02	0.19	0.20
0.87	0.05	0.05	0.62	0.40	0.47	0.76	0.30	0.69	0.62	0.10	0.57	0.37

Continued on Next Page...

Table E.2 – continued from previous page

k_d	k_s	α	s1	s2	s3	s4	s5	s6	s7	s8	s9	s10
0.87	0.05	0.07	0.37	0.27	0.49	0.74	0.76	0.47	0.41	0.36	0.73	0.31
0.87	0.05	0.09	0.04	0.28	0.16	0.18	0.13	0.16	0.22	0.10	0.29	0.46
0.87	0.05	0.12	0.10	0.30	0.18	0.20	0.07	0.01	0.21	0.25	0.10	0.38
0.87	0.05	0.14	0.01	0.11	0.10	0.00	0.00	0.11	0.00	0.01	0.24	0.11
0.87	0.08	0.05	0.59	0.23	0.39	0.76	0.65	0.92	0.42	0.41	0.63	0.33
0.87	0.08	0.07	0.72	0.26	0.39	0.58	0.66	0.59	0.41	0.50	0.64	0.67
0.87	0.08	0.09	0.46	0.30	0.46	0.74	0.33	0.78	0.57	0.16	0.57	0.47
0.87	0.08	0.12	0.11	0.28	0.28	0.21	0.29	0.44	0.31	0.20	0.16	0.11
0.87	0.08	0.14	0.17	0.04	0.21	0.01	0.13	0.44	0.08	0.04	0.34	0.11
0.87	0.12	0.05	0.52	0.47	0.44	0.45	0.81	0.71	0.41	0.41	0.77	0.29
0.87	0.12	0.07	0.76	0.44	0.52	0.54	0.31	0.71	0.41	0.32	0.82	0.43
0.87	0.12	0.09	0.50	0.39	0.42	0.76	0.72	0.85	0.42	0.28	0.54	0.49
0.87	0.12	0.12	0.34	0.07	0.65	0.41	0.62	0.72	0.40	0.16	0.42	0.61
0.87	0.12	0.14	0.16	0.01	0.23	0.31	0.61	0.47	0.27	0.14	0.17	0.49
0.87	0.15	0.05	0.59	0.30	0.45	0.65	0.48	0.84	0.45	0.46	0.47	0.06
0.87	0.15	0.07	0.67	0.08	0.47	0.83	0.67	0.88	0.45	0.38	0.79	0.13
0.87	0.15	0.09	0.76	0.33	0.29	0.59	0.67	0.88	0.39	0.41	0.51	0.96
0.87	0.15	0.12	0.57	0.38	0.47	0.51	0.67	0.78	0.44	0.20	0.51	0.10
0.87	0.15	0.14	0.41	0.05	0.38	0.59	0.37	0.48	0.56	0.34	0.36	0.21
1.16	0.02	0.05	0.13	0.10	0.14	0.13	0.29	0.49	0.18	0.17	0.56	0.58
1.16	0.02	0.07	0.04	0.25	0.22	0.07	0.09	0.22	0.07	0.03	0.49	0.65
1.16	0.02	0.09	0.07	0.00	0.10	0.00	0.03	0.09	0.02	0.03	0.23	0.03
1.16	0.02	0.12	0.01	0.00	0.00	0.00	0.00	0.00	0.00	0.00	0.21	0.53
1.16	0.02	0.14	0.00	0.00	0.00	0.00	0.00	0.00	0.00	0.01	0.17	0.06
1.16	0.05	0.05	0.46	0.15	0.24	0.70	0.69	0.68	0.36	0.34	0.46	0.03
1.16	0.05	0.07	0.33	0.29	0.18	0.51	0.37	0.47	0.54	0.31	0.28	0.42
1.16	0.05	0.09	0.09	0.19	0.30	0.43	0.20	0.21	0.32	0.05	0.71	0.43
1.16	0.05	0.12	0.09	0.01	0.15	0.03	0.12	0.07	0.24	0.03	0.21	0.14
1.16	0.05	0.14	0.11	0.06	0.16	0.21	0.09	0.16	0.12	0.01	0.31	0.21
1.16	0.08	0.05	0.41	0.08	0.23	0.54	0.39	0.61	0.47	0.30	0.14	0.56

Continued on Next Page...

Table E.2 – continued from previous page

k_d	k_s	α	s1	s2	s3	s4	s5	s6	s7	s8	s9	s10
1.16	0.08	0.07	0.52	0.15	0.47	0.64	0.54	0.79	0.60	0.34	0.51	0.88
1.16	0.08	0.09	0.40	0.08	0.39	0.61	0.60	0.52	0.36	0.44	0.54	0.68
1.16	0.08	0.12	0.21	0.33	0.17	0.27	0.77	0.32	0.17	0.13	0.50	0.51
1.16	0.08	0.14	0.16	0.19	0.23	0.34	0.51	0.16	0.19	0.08	0.21	0.21
1.16	0.12	0.05	0.41	0.07	0.36	0.59	0.88	0.51	0.43	0.54	0.50	0.01
1.16	0.12	0.07	0.33	0.15	0.41	0.68	0.76	0.63	0.41	0.35	0.51	0.62
1.16	0.12	0.09	0.42	0.01	0.34	0.79	0.77	0.85	0.33	0.36	0.41	0.65
1.16	0.12	0.12	0.43	0.11	0.40	0.41	0.67	0.76	0.50	0.27	0.44	0.43
1.16	0.12	0.14	0.23	0.08	0.31	0.34	0.57	0.38	0.48	0.06	0.45	0.49
1.16	0.15	0.05	0.35	0.35	0.32	0.72	0.75	0.72	0.41	0.40	0.49	0.61
1.16	0.15	0.07	0.55	0.11	0.31	0.84	0.66	0.55	0.49	0.50	0.33	0.14
1.16	0.15	0.09	0.45	0.09	0.31	0.65	0.79	0.48	0.41	0.42	0.56	0.64
1.16	0.15	0.12	0.41	0.19	0.45	0.52	0.53	0.75	0.44	0.48	0.52	0.89
1.16	0.15	0.14	0.34	0.21	0.36	0.74	0.47	0.22	0.35	0.40	0.59	0.33

Table E.3: Results of the adjustment experiment in Chapter 5 for k_d. The first column denotes the ten reference Lambertian surfaces with different RMS height (σ). The other columns are the adjusted k_d from the ten observers.

S_{σ_i}	s1	s2	s3	s4	s5	s6	s7	s8	s9	s10
1	1.26	1.30	1.19	1.10	1.29	1.17	1.22	1.22	1.38	1.21
2	1.14	1.06	1.01	1.07	1.10	1.09	1.01	1.08	1.16	1.06
3	0.97	0.97	0.89	1.02	1.00	0.95	0.78	0.95	1.08	1.02
4	0.81	0.77	0.81	0.85	0.89	0.88	0.70	0.87	0.96	0.85
5	0.73	0.87	0.74	0.76	0.70	0.79	0.68	0.76	0.85	0.63
6	0.71	0.65	0.70	0.60	0.70	0.68	0.66	0.71	0.67	0.74
7	0.57	0.46	0.60	0.51	0.61	0.60	0.58	0.58	0.76	0.54
8	0.48	0.39	0.54	0.45	0.53	0.56	0.44	0.50	0.63	0.42
9	0.46	0.48	0.39	0.41	0.43	0.47	0.42	0.51	0.55	0.20
10	0.34	0.36	0.35	0.36	0.34	0.46	0.40	0.48	0.50	0.27

Table E.4: Results of the adjustment experiment in Chapter 5 for k_{s}. The first column denotes the ten reference Lambertian surfaces with different RMS height (σ). The other columns are the adjusted k_{s} from the ten observers.

S_{σ_i}	s1	s2	s3	s4	s5	s6	s7	s8	s9	s10
1	0.13	0.12	0.13	0.14	0.11	0.12	0.12	0.12	0.13	0.10
2	0.12	0.12	0.12	0.13	0.11	0.12	0.12	0.11	0.12	0.13
3	0.10	0.09	0.14	0.11	0.11	0.11	0.12	0.10	0.11	0.10
4	0.09	0.08	0.10	0.09	0.10	0.10	0.11	0.09	0.10	0.13
5	0.08	0.07	0.10	0.09	0.09	0.08	0.09	0.08	0.09	0.11
6	0.07	0.07	0.06	0.07	0.08	0.06	0.08	0.07	0.07	0.09
7	0.05	0.07	0.07	0.06	0.08	0.06	0.07	0.06	0.08	0.07
8	0.04	0.05	0.06	0.04	0.08	0.05	0.05	0.05	0.06	0.08
9	0.04	0.04	0.05	0.03	0.06	0.03	0.05	0.05	0.06	0.08
10	0.03	0.03	0.04	0.02	0.06	0.03	0.04	0.04	0.04	0.06

Table E.5: Results of the adjustment experiment in Chapter 5 for α. The first column denotes the ten reference Lambertian surfaces with different RMS height (σ). The other columns are the adjusted α from the ten observers.

S_{σ_i}	s1	s2	s3	s4	s5	s6	s7	s8	s9	s10
1	0.14	0.13	0.12	0.13	0.12	0.13	0.13	0.13	0.13	0.12
2	0.13	0.12	0.12	0.13	0.12	0.12	0.13	0.12	0.12	0.12
3	0.11	0.11	0.13	0.11	0.11	0.11	0.12	0.11	0.11	0.11
4	0.10	0.10	0.11	0.10	0.10	0.11	0.12	0.10	0.11	0.11
5	0.09	0.09	0.11	0.10	0.09	0.09	0.11	0.09	0.10	0.12
6	0.08	0.09	0.08	0.08	0.09	0.09	0.10	0.08	0.08	0.10
7	0.07	0.09	0.08	0.08	0.09	0.08	0.08	0.08	0.08	0.10
8	0.07	0.07	0.07	0.06	0.08	0.07	0.08	0.07	0.07	0.09
9	0.07	0.06	0.07	0.06	0.08	0.06	0.07	0.06	0.06	0.09
10	0.06	0.06	0.07	0.05	0.08	0.06	0.07	0.06	0.06	0.08

Table E.6: Perceived gloss from the experiment in Chapter 7. The first column denotes the 14 stimuli with different β. The other columns are the perceived gloss (raw data from magnitude estimation) from the nine observers.

β	s1	s2	s3	s4	s5	s6	s7	s8	s9
1.5	10	0.5	26	40	0.1	2	1	1	1
1.6	20	1	28	60	1	2	1	20	1
1.7	40	1	30	70	5.5	3	3	40	4
1.8	80	2	50	85	9.8	5	8	60	8
1.9	85	1.5	52	90	9.8	5	10	100	8
2.0	100	2	80	90	9.8	5.5	10	95	7.5
2.1	96	4	85	80	10	5	9	90	6.5
2.2	95	4	90	80	10	5	8	80	7
2.3	75	3.5	70	75	7.5	4	6	70	7
2.4	70	3	65	70	9.5	4	6	60	7
2.5	60	2.5	55	60	5	3.5	5	25	7
2.6	60	2.5	54	60	6	3.5	5	30	6.5
2.7	65	2.5	55	65	5	3.5	5	35	6.5
2.8	50	2	54	60	4.5	3.5	5	30	6.5

Table E.7: The pair comparison experiment results of Chapter 8. The left four columns are the full 300 pair combinations of the 25 stimuli denoted using the roughness levels (subscripts) of surface S_{ij} and surface S_{kl}, where i and k denote α levels and j and l denote β levels. The other columns show the results from the eight observers, which are the times that surface S_{kl} was judged to be glossier than surface S_{ij}. Note that each pair was shown three times, thus the maximum number is three.

α_i	β_j	α_k	β_l	s1	s2	s3	s4	s5	s6	s7	s8
1	1	1	2	3	3	3	3	3	3	3	3
1	1	1	3	3	3	3	2	3	3	2	3
1	1	1	4	3	3	3	3	3	3	3	3
1	1	1	5	3	3	3	3	2	3	3	3
1	1	2	1	1	3	1	2	1	3	0	2
1	1	2	2	3	3	3	3	3	3	3	3
1	1	2	3	3	3	3	3	2	3	3	3
1	1	2	4	3	3	3	2	3	3	3	2
1	1	2	5	3	3	3	3	3	3	1	3
1	1	3	1	2	3	3	2	3	2	2	3
1	1	3	2	3	2	3	3	3	3	3	3
1	1	3	3	3	3	3	3	3	3	3	3
1	1	3	4	2	3	3	2	3	3	3	2
1	1	3	5	3	3	3	3	3	3	3	3
1	1	4	1	3	3	3	3	3	3	3	3
1	1	4	2	3	3	3	3	3	3	3	3
1	1	4	3	2	3	3	3	3	3	3	3
1	1	4	4	3	3	3	2	2	3	3	2
1	1	4	5	3	3	3	3	3	3	3	3
1	1	5	1	3	2	3	1	3	3	3	3
1	1	5	2	3	3	3	3	3	3	3	1
1	1	5	3	3	3	3	3	3	3	3	3
1	1	5	4	3	3	3	3	3	3	3	3

Continued on Next Page...

Table E.7 – continued from previous page

α_i	β_j	α_k	β_l	s1	s2	s3	s4	s5	s6	s7	s8
1	1	5	5	3	3	3	2	3	3	3	3
1	2	1	3	2	3	3	3	2	3	2	3
1	2	1	4	1	2	2	2	0	2	2	0
1	2	1	5	1	2	3	0	2	0	2	1
1	2	2	1	0	0	0	0	0	1	1	0
1	2	2	2	2	3	2	3	3	2	3	2
1	2	2	3	2	3	3	3	3	3	3	3
1	2	2	4	2	3	3	3	3	1	3	2
1	2	2	5	1	3	3	0	1	0	1	0
1	2	3	1	1	0	0	1	0	0	0	0
1	2	3	2	2	2	3	3	3	3	3	2
1	2	3	3	3	3	3	3	3	3	2	3
1	2	3	4	3	3	3	2	3	2	3	3
1	2	3	5	2	3	2	2	1	0	3	1
1	2	4	1	1	0	0	0	1	0	1	0
1	2	4	2	3	3	3	3	3	3	3	3
1	2	4	3	3	3	3	3	2	3	3	3
1	2	4	4	2	3	3	3	3	3	3	3
1	2	4	5	2	3	2	1	2	0	2	1
1	2	5	1	3	0	0	1	0	0	3	1
1	2	5	2	3	2	3	3	3	3	3	3
1	2	5	3	3	3	3	3	3	3	3	3
1	2	5	4	3	3	3	2	3	3	3	3
1	2	5	5	3	3	3	3	3	3	3	3
1	3	1	4	3	1	0	0	1	1	1	0
1	3	1	5	1	0	0	0	0	0	0	0
1	3	2	1	0	0	0	1	1	0	0	0
1	3	2	2	2	0	3	2	2	2	2	3
1	3	2	3	3	3	3	3	3	2	3	3
1	3	2	4	2	3	3	3	3	2	3	3

Continued on Next Page...

Table E.7 – continued from previous page

α_i	β_j	α_k	β_l	s1	s2	s3	s4	s5	s6	s7	s8
1	3	2	5	1	2	2	0	1	0	2	3
1	3	3	1	1	0	0	0	0	0	0	0
1	3	3	2	3	0	0	2	3	3	3	2
1	3	3	3	3	2	3	3	3	2	3	3
1	3	3	4	3	3	2	3	3	0	3	2
1	3	3	5	0	1	2	0	0	0	2	0
1	3	4	1	2	0	0	1	0	0	1	0
1	3	4	2	3	2	3	3	3	2	3	3
1	3	4	3	3	3	3	3	3	2	3	3
1	3	4	4	3	3	3	3	3	3	3	3
1	3	4	5	2	2	3	0	0	0	3	0
1	3	5	1	2	0	0	0	3	0	0	1
1	3	5	2	3	2	3	1	3	3	3	3
1	3	5	3	3	3	3	3	3	3	3	3
1	3	5	4	3	3	3	2	3	3	3	3
1	3	5	5	3	3	2	1	3	3	3	2
1	4	1	5	1	0	0	0	1	0	1	0
1	4	2	1	3	0	0	0	0	0	1	0
1	4	2	2	3	2	2	3	1	3	2	3
1	4	2	3	3	3	3	3	3	3	3	3
1	4	2	4	3	3	3	2	3	2	3	3
1	4	2	5	0	1	2	1	1	2	3	1
1	4	3	1	1	0	0	1	1	0	0	1
1	4	3	2	1	2	1	3	3	3	3	3
1	4	3	3	3	3	3	2	2	3	2	3
1	4	3	4	3	3	3	3	3	3	3	3
1	4	3	5	2	2	3	2	1	0	3	2
1	4	4	1	2	0	0	1	1	0	2	0
1	4	4	2	2	2	3	3	3	3	3	3
1	4	4	3	3	3	3	3	3	3	3	3

Continued on Next Page...

Table E.7 – continued from previous page

α_i	β_j	α_k	β_l	s1	s2	s3	s4	s5	s6	s7	s8
1	4	4	4	2	3	3	2	3	3	3	3
1	4	4	5	3	3	1	2	2	2	3	1
1	4	5	1	1	0	0	0	1	1	1	2
1	4	5	2	3	2	3	3	3	3	3	3
1	4	5	3	3	3	3	3	3	3	3	3
1	4	5	4	3	3	3	3	3	3	3	3
1	4	5	5	3	3	3	2	3	3	3	2
1	5	2	1	2	0	0	0	2	0	0	1
1	5	2	2	3	3	3	3	2	3	2	3
1	5	2	3	3	3	3	2	3	3	3	3
1	5	2	4	3	3	3	3	3	3	3	3
1	5	2	5	3	3	3	3	3	3	3	2
1	5	3	1	2	0	1	0	1	0	0	1
1	5	3	2	3	3	2	3	2	3	3	3
1	5	3	3	3	3	3	3	3	3	3	3
1	5	3	4	2	3	3	3	2	3	3	3
1	5	3	5	3	3	3	3	3	3	3	2
1	5	4	1	3	0	0	0	2	0	1	2
1	5	4	2	3	3	2	3	3	3	3	3
1	5	4	3	3	3	3	3	3	3	3	3
1	5	4	4	3	3	3	3	3	3	3	3
1	5	4	5	3	3	3	3	3	3	3	3
1	5	5	1	3	0	0	0	1	1	1	2
1	5	5	2	3	3	3	3	3	3	3	3
1	5	5	3	3	3	3	3	3	3	3	3
1	5	5	4	3	3	3	3	3	3	3	3
1	5	5	5	3	3	3	3	3	3	2	3
2	1	2	2	3	3	3	2	3	3	3	3
2	1	2	3	3	3	3	3	3	3	3	3
2	1	2	4	3	3	3	2	3	3	3	3

Continued on Next Page...

Table E.7 – continued from previous page

α_i	β_j	α_k	β_l	s1	s2	s3	s4	s5	s6	s7	s8
2	1	2	5	2	3	3	3	3	3	3	3
2	1	3	1	3	2	2	2	1	2	3	3
2	1	3	2	3	3	3	2	3	3	3	3
2	1	3	3	3	3	3	3	3	3	3	2
2	1	3	4	3	3	3	2	2	3	3	3
2	1	3	5	3	3	3	2	3	3	2	3
2	1	4	1	3	2	3	2	3	1	2	3
2	1	4	2	3	3	3	3	3	3	3	3
2	1	4	3	3	3	3	1	3	3	3	3
2	1	4	4	3	3	3	1	3	3	3	2
2	1	4	5	2	3	3	3	3	3	3	2
2	1	5	1	2	3	3	3	3	3	3	1
2	1	5	2	2	3	3	3	2	3	3	3
2	1	5	3	3	3	3	3	3	3	3	3
2	1	5	4	3	3	3	3	3	3	3	3
2	1	5	5	3	3	3	3	3	3	3	3
2	2	2	3	1	3	3	2	3	2	3	1
2	2	2	4	0	3	3	2	2	1	2	0
2	2	2	5	1	3	2	0	0	0	1	0
2	2	3	1	0	1	0	0	0	0	0	0
2	2	3	2	1	0	0	2	2	1	2	2
2	2	3	3	2	3	3	3	3	2	2	3
2	2	3	4	2	2	2	3	2	1	3	3
2	2	3	5	1	1	2	1	1	0	1	0
2	2	4	1	1	0	0	0	0	0	1	0
2	2	4	2	3	3	3	2	3	2	3	2
2	2	4	3	2	3	3	3	3	2	3	3
2	2	4	4	3	3	3	3	3	3	2	3
2	2	4	5	2	2	3	0	1	0	3	0
2	2	5	1	1	0	0	0	0	0	0	1

Continued on Next Page...

Table E.7 – continued from previous page

α_i	β_j	α_k	β_l	s1	s2	s3	s4	s5	s6	s7	s8
2	2	5	2	3	3	3	2	3	2	1	1
2	2	5	3	3	3	3	3	3	3	3	3
2	2	5	4	3	3	3	1	3	3	3	3
2	2	5	5	2	3	2	2	3	0	3	1
2	3	2	4	1	1	0	0	0	1	1	0
2	3	2	5	0	0	0	0	0	0	0	0
2	3	3	1	0	0	0	0	0	0	0	0
2	3	3	2	1	0	0	0	0	0	1	0
2	3	3	3	3	2	3	2	3	2	3	3
2	3	3	4	1	2	2	1	0	1	2	1
2	3	3	5	0	1	0	1	0	1	1	0
2	3	4	1	0	0	0	0	0	0	0	0
2	3	4	2	1	0	1	1	0	2	1	1
2	3	4	3	3	3	3	2	3	3	3	3
2	3	4	4	3	3	3	3	3	3	3	3
2	3	4	5	0	2	0	1	0	0	2	0
2	3	5	1	2	0	0	0	0	0	0	0
2	3	5	2	1	1	0	1	3	1	2	1
2	3	5	3	3	3	3	3	3	3	3	3
2	3	5	4	3	3	3	2	3	3	3	3
2	3	5	5	3	3	1	1	3	0	2	1
2	4	2	5	1	0	0	1	0	1	0	0
2	4	3	1	0	0	0	0	0	0	1	0
2	4	3	2	1	1	0	1	2	2	0	2
2	4	3	3	2	2	2	3	3	3	3	3
2	4	3	4	3	1	2	3	3	1	3	3
2	4	3	5	1	0	0	1	1	0	3	1
2	4	4	1	1	0	0	0	0	0	0	1
2	4	4	2	2	1	2	2	2	2	1	3
2	4	4	3	3	3	3	2	3	3	3	3

Continued on Next Page...

Table E.7 – continued from previous page

α_i	β_j	α_k	β_l	s1	s2	s3	s4	s5	s6	s7	s8
2	4	4	4	3	3	3	3	3	3	3	3
2	4	4	5	2	0	0	1	1	0	2	1
2	4	5	1	0	0	0	0	0	0	0	0
2	4	5	2	3	3	1	3	3	3	3	3
2	4	5	3	3	3	3	3	3	3	3	3
2	4	5	4	3	3	3	3	3	3	3	3
2	4	5	5	2	3	2	1	3	0	2	2
2	5	3	1	2	0	1	1	1	1	1	1
2	5	3	2	2	0	1	3	3	3	2	3
2	5	3	3	3	3	3	3	3	3	3	3
2	5	3	4	3	3	3	3	3	3	3	3
2	5	3	5	2	1	2	3	1	1	2	1
2	5	4	1	2	0	0	0	1	0	1	2
2	5	4	2	2	2	2	3	3	3	2	3
2	5	4	3	3	3	3	3	2	3	3	3
2	5	4	4	3	3	3	3	3	3	3	3
2	5	4	5	3	3	1	1	2	1	2	1
2	5	5	1	3	0	1	2	0	1	2	1
2	5	5	2	3	3	3	3	3	3	3	3
2	5	5	3	3	3	3	3	3	3	3	3
2	5	5	4	3	3	2	2	3	3	3	3
2	5	5	5	3	3	3	3	3	2	3	3
3	1	3	2	3	3	3	3	3	3	2	3
3	1	3	3	3	3	3	3	2	3	2	3
3	1	3	4	3	3	3	3	3	3	3	2
3	1	3	5	3	3	3	3	3	3	3	2
3	1	4	1	2	2	3	3	3	1	1	2
3	1	4	2	3	3	3	2	2	3	3	3
3	1	4	3	3	2	3	3	3	3	3	2
3	1	4	4	3	3	3	2	3	3	3	3

Continued on Next Page...

Table E.7 – continued from previous page

α_i	β_j	α_k	β_l	s1	s2	s3	s4	s5	s6	s7	s8
3	1	4	5	3	3	3	3	3	3	3	2
3	1	5	1	3	1	3	3	3	2	2	1
3	1	5	2	2	3	3	3	3	3	3	3
3	1	5	3	3	3	3	1	3	3	3	3
3	1	5	4	2	3	3	2	3	3	3	3
3	1	5	5	2	3	3	3	3	2	3	3
3	2	3	3	3	3	3	3	3	3	3	3
3	2	3	4	2	2	3	2	1	0	3	1
3	2	3	5	3	3	3	0	0	0	2	0
3	2	4	1	1	0	0	0	0	1	1	0
3	2	4	2	1	1	3	2	3	2	3	3
3	2	4	3	3	3	3	3	3	3	3	3
3	2	4	4	3	3	3	3	2	3	3	3
3	2	4	5	1	3	3	1	0	0	2	0
3	2	5	1	1	0	0	1	0	0	1	0
3	2	5	2	2	2	3	3	3	2	2	2
3	2	5	3	2	3	3	3	3	3	3	3
3	2	5	4	3	2	3	3	3	3	3	3
3	2	5	5	3	3	3	3	2	3	3	1
3	3	3	4	0	1	0	0	0	0	0	2
3	3	3	5	1	0	0	0	0	0	1	0
3	3	4	1	0	0	0	0	0	0	0	0
3	3	4	2	1	0	0	0	0	0	0	0
3	3	4	3	1	3	3	2	3	1	2	3
3	3	4	4	1	2	3	3	2	2	3	2
3	3	4	5	1	1	0	0	0	0	1	0
3	3	5	1	2	0	1	0	0	0	0	0
3	3	5	2	1	0	0	1	2	2	0	1
3	3	5	3	3	3	3	0	3	3	3	1
3	3	5	4	3	2	3	2	2	3	2	3

Continued on Next Page...

Table E.7 – continued from previous page

α_i	β_j	α_k	β_l	s1	s2	s3	s4	s5	s6	s7	s8
3	3	5	5	2	2	1	1	1	0	0	0
3	4	3	5	1	1	0	1	0	0	0	0
3	4	4	1	1	0	0	0	1	0	0	0
3	4	4	2	3	1	2	1	1	3	1	1
3	4	4	3	3	3	3	3	3	3	3	3
3	4	4	4	3	3	2	3	3	3	3	3
3	4	4	5	0	0	0	2	0	0	0	1
3	4	5	1	2	0	0	0	0	0	0	0
3	4	5	2	0	2	1	2	3	1	2	2
3	4	5	3	2	2	3	2	3	3	3	3
3	4	5	4	3	3	2	2	3	3	3	3
3	4	5	5	0	2	0	2	3	1	0	1
3	5	4	1	2	0	0	0	2	0	0	2
3	5	4	2	0	0	3	2	3	3	0	3
3	5	4	3	3	3	2	3	3	3	3	3
3	5	4	4	3	3	3	2	3	3	2	3
3	5	4	5	2	3	2	0	2	0	3	0
3	5	5	1	0	0	0	2	0	1	0	2
3	5	5	2	1	1	3	3	3	3	3	3
3	5	5	3	2	2	3	3	3	3	3	3
3	5	5	4	3	3	3	3	3	3	2	3
3	5	5	5	3	2	2	2	3	3	3	2
4	1	4	2	2	3	3	3	3	3	3	3
4	1	4	3	3	3	3	3	3	3	3	3
4	1	4	4	1	3	3	3	3	3	3	3
4	1	4	5	1	3	3	3	3	3	3	2
4	1	5	1	2	1	0	0	2	1	2	3
4	1	5	2	2	3	3	3	3	3	3	3
4	1	5	3	1	3	3	3	3	3	3	3
4	1	5	4	3	3	3	3	3	3	3	3

Continued on Next Page...

Table E.7 – continued from previous page

α_i	β_j	α_k	β_l	s1	s2	s3	s4	s5	s6	s7	s8
4	1	5	5	2	3	3	3	3	3	3	2
4	2	4	3	3	2	3	3	3	3	3	3
4	2	4	4	3	3	3	3	3	1	3	1
4	2	4	5	1	3	2	1	0	1	2	0
4	2	5	1	0	0	0	1	0	0	0	0
4	2	5	2	1	0	2	3	2	2	2	0
4	2	5	3	3	3	3	3	2	3	3	3
4	2	5	4	3	3	3	3	2	3	3	3
4	2	5	5	3	3	2	2	1	0	2	0
4	3	4	4	2	3	0	1	0	1	1	0
4	3	4	5	0	0	0	0	0	0	0	0
4	3	5	1	0	1	0	0	0	0	0	0
4	3	5	2	0	0	0	0	0	0	0	0
4	3	5	3	2	1	3	3	2	2	1	0
4	3	5	4	1	2	1	0	0	0	2	2
4	3	5	5	1	0	0	1	0	0	1	0
4	4	4	5	0	0	0	1	0	0	1	0
4	4	5	1	0	0	0	0	0	0	2	0
4	4	5	2	0	1	1	0	2	0	1	1
4	4	5	3	0	0	1	1	3	3	2	1
4	4	5	4	2	2	2	2	1	2	3	3
4	4	5	5	2	0	0	0	0	0	0	0
4	5	5	1	1	0	0	1	0	0	0	0
4	5	5	2	1	0	1	2	3	3	1	3
4	5	5	3	3	3	3	3	3	3	3	3
4	5	5	4	2	3	3	3	3	3	3	2
4	5	5	5	2	3	1	2	3	2	2	3
5	1	5	2	3	3	3	3	3	3	3	3
5	1	5	3	3	3	3	3	3	3	3	3
5	1	5	4	3	3	3	3	3	3	3	3

Continued on Next Page...

Table E.7 – continued from previous page

α_i	β_j	α_k	β_l	s1	s2	s3	s4	s5	s6	s7	s8
5	1	5	5	2	3	3	3	3	3	3	3
5	2	5	3	3	3	3	3	1	3	3	2
5	2	5	4	3	3	2	1	0	3	3	3
5	2	5	5	2	3	2	1	1	0	2	0
5	3	5	4	1	1	2	1	0	0	1	2
5	3	5	5	0	0	0	1	0	0	0	0
5	4	5	5	1	1	0	0	0	0	0	0

List of publications by the author during PhD

Qi, L., Chantler, M. J., Siebert, J. P., and Dong, J. (2010). The Effect of Mesoscale Surface Roughness on Perceived Gloss. In *Proceedings of 2nd CIE Expert Symposium on Appearance*, pages 83-85, Gent, Belgium.

Qi, L., Chantler, M. J., Siebert, J. P., and Dong, J. (2011). How Mesoscale and Microscale Roughness Affect Perceived Gloss. *AVA, AVA/BMVA SPRING (AGM) MEETING 2011.*

Qi, L., Chantler, M. J., Siebert, J. P., and Dong, J. (2012). How Mesoscale and Microscale Roughness Affect Perceived Gloss. In *Proceedings of Predicting Perceptions: The 3rd International Conference on Appearance*, Page: 48-51, Edinburgh, UK. Conference Proceedings Publication ISBN: 978-1-4716-6869-2.

Sun, Y., Dong, J., Qi, L., and Chantler, M. J. (2012). Automatic Cooking of Porridge Based on Human Visual Perception. In *Proceedings of Predicting Perceptions: The 3rd International Conference on Appearance*, Pages 104-107, Edinburgh, UK. Conference Proceedings Publication ISBN: 978-1-4716-6869-2.

Ji, P., Dong, J., Qi, L. and Chantler, M. J. (2012). Perceived Directionality of Random-phase Fractal Surfaces Based on Mojette Transform. In *Proceedings of Predicting Perceptions: The 3rd International Conference on Appearance*, Pages 39-42, Edinburgh, UK. Conference Proceedings Publication ISBN: 978-1-4716-6869-2.

The major work of this thesis will be submitted to related journals.